Finite Element Modelling of Shielded Metal Arc Welding

By

M Cronje

Thesis presented at the University of Stellenbosch in partial fulfilment of the requirements for the degree of

Master of Science in Mechanical Engineering

Department of Mechanical Engineering
Stellenbosch University
Private Bag X1, 7602 Matieland, South Africa

Study leader: Mr K. van der Westhuizen
Dr A.B. Taylor

December 2005

DECLARATION

I, the undersigned, hereby declare that the work contained in this thesis is my own work and that I have not previously in its entirety or in part submitted it at any university for a degree.

Signature:……..

M. Cronje

Date:……..

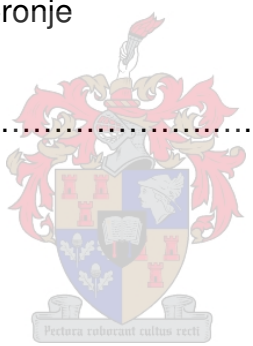

ABSTRACT

Finite Element Modelling of Shielded Metal Arc Welding

M. Cronje

Department of Mechanical Engineering

Stellenbosch University

Private Bag X1, 7602 Matieland, South Africa

Thesis: MScEng (Mech) December 2005

This study involved the modelling and verification of the Shielded Metal Arc Welding of mild steel with the focus on displacement and temperature distribution prediction of welded plates.

The project was divided into three phases namely; the literature survey into finite element modelling of welding processes, the modelling of a welding process and verification of the modelling with experimental results.

A working welding model was created using a commercial finite element software package with the capabilities to model welding processes. The welding model was systematically developed from a two-dimensional model into a three-dimensional full physics process model. Experimental measured welding heat input parameters were applied in the model, temperature dependent material properties were applied and actual structural restraints from the experiments were modelled.

Displacement and temperature distributions were measured on mild steel plates welded with the Shielded Metal Arc Welding process. The plate temperature was measured at various locations with K-type thermocouples spot welded onto the plates. Plate deformation was measured at various stages of the manufacturing process. Tendencies in plate displacement were investigated with a change in certain welding parameters. The finite element model was verified and good correlations were found, especially for the temperature distribution in the welded plates.

UITREKSEL

Eindige Element Modellering van Geskermde Metaal Vonk Sweis

M. Cronje

Departement Meganiese Ingenieurswese

Universiteit van Stellenbosch

Privaatsak X1, 7602 Matieland, Suid-Afrika

Tesis: MScIng (Meg) Desember 2005

Hierdie studie behels die modellering en verifiëring van Geskermde Metaal Vonk Sweis van sagte staal met die fokus gemik op die verplasing en temperatuur verspreiding van gesweiste plate.

Die projek was opgedeel in drie fases naamlik; die literatuurstudie van die eindige element modellering van sweisprosesse, die modellering van ‘n sweisproses en die verifiëring van die model met eksperimentele resultate.

’n Werkende model was geskep met die gebruik van ‘n kommersiële eindige element pakket met die vermoë om sweisprosesse te modelleer. Die sweis model was sistematies ontwikkel vanaf ’n twee-dimensionele model na ’n volledige-proses drie-dimensionele model. Eksperimentele gemete sweis hitte-inset parameters was toegepas in die model, temperatuur afhanklike materiaal eienskappe en die strukturele beperkings van die eksperiment was gemodelleer.

Verplasing en temperatuur verspreiding van sagte staal plate, gesweis met die Geskermde Metaal Vonk Sweisproses, was gemeet. Die plaat temperatuur was gemeet by verskeie liggings met K-tipe termokoppels wat gepuntsweis is op die plaat. Plaat verplasing was gemeet by verskillende stadiums van die vervaardigingsproses. Tendense in plaat verplasing was ondersoek met verandering in sekere sweis veranderlikes. Die resultate van die eindige element metode was geverifieer en goeie korrelasie was gevind, veral vir die temperatuur verspreiding in gesweiste plate.

ACKNOWLEDGEMENTS

First of all, I would like to thank Dr Taylor and Mr Van der Westhuizen for their persistent motivation, visionary guidance and continual support. You believed in this project where others doubted. Your inspiration made this project possible.

Many thanks to the modelling teams of Stellenbosch Automotive Engineering (CAE) and IMEC (Belgium) who were always nearby and willing to assist in the many challenges faced in this project. The free advice and support you have given cannot be valued and I will always be in your debt.

The staff and artisans at SMD for all the mechanical services and performing of the experiments, especially Mr Van der Vinne and Van der Berg for their patience, support and advise which were unmistakably the backbone of the project. Mr Cobus Zietsman who made everything possible and was never to busy to give a helping hand.

Many friends, co-students and colleagues for their support and understanding.

Lastly, my family who provided continuous support, love and motivation and a very special lady friend, Hannelie, for the support and motivation during the project.

DEDICATIONS

I dedicate this to my father, you made this all possible.

TABLE OF CONTENTS

LIST OF FIGURES

LIST OF TABLES

NOMENCLATURE

c	-	specific heat [J/kg.℃]
d	-	weld bead width [m]
E	-	Young's modulus [GPa]
E_l	-	energy per unit length [J/mm]
g	-	gravitational acceleration [m/s²]
h	-	plate thickness [mm]
h_c	-	convection heat transfer coefficient [W/m².℃]
h_r	-	radiation heat transfer coefficient [W/m².℃]
I	-	electric current [A]
k	-	thermal conductivity [W/m.℃]
L	-	characteristic length [mm]
Nu	-	Nusselt number
P	-	power [W]
Ra	-	Rayleigh number
T	-	temperature [℃]
T_m	-	melting point temperature [℃]
t	-	time [s]
V	-	voltage [V]
v	-	welding speed [m/s]
Q	-	heat input [W]
q	-	heat flux [W/m²]
x,y,z	-	spatial coordinates [m]
α	-	thermal diffusivity [m²/s]
β	-	thermal coefficient of volume expansion [K^{-1}]

η_{arc}	-	arc efficiency
ρ	-	density [kg/m³]
ν	-	kinematic viscosity [m²/s]

LIST OF ABBREVIATIONS

AC	-	Alternating current
DC	-	Direct current
EMF	-	Electromotive force
FE	-	Finite element
FEA	-	Finite element analysis
FEM	-	Finite element method
GMAW	-	Gas metal arc welding
GTA	-	Gas tungsten arc
HAZ	-	Heat affected zone
MIG	-	Metal inert gas
MSC	-	Macneal-Schwendler Corporation
NASA	-	National Aeronautical and Space Administration
NASTRAN	-	NASA Structural Analysis Program
SMAW	-	Shielded metal arc welding
TIG	-	Tungsten inert gas

1 INTRODUCTION

South Africa's automotive component manufacturing industry is renowned internationally for its expertise, flexibility and rapid growth in production. The country has vast resources and already counts among the twenty largest vehicle manufacturers in the world and is fast increasing its vehicle-manufacturing capacity. However, South Africa is not at the leading edge of technological development of manufacturing in the automotive industry (Lourens, 2002). South Africa competes against the world: whether it is Mexico, China or Australia. Therefore it is critical to improve and develop manufacturing technology that will, if properly applied, improve productivity, add value to products and reduce waste.

The implementation of numerical techniques to model manufacturing processes has the advantage of improving the product, perfecting the process, reducing scrap rates, reducing product realization costs and improves the efficiency of the manufacturing process. The graphical display of the modelling software available also gives insight to the mechanics of the manufacturing process.

Modelling can be used as a tool in many stages of the life of a product: from a concept evaluation tool to manufacturing analysis tool. There is a big market for this kind of analysis in an industry where there are still heavily relied on extensive testing and development. This primitive approach to production is not only expensive but also time consuming.

The complex nature of the welding process causes difficulty in analysing and modelling by numerical methods. These complexities include: temperature dependent material properties, non-linear boundary conditions, moving heat sources, phase changes and transformations, complex residual stress states and the difficulties of making experimental measurements at high temperatures. In addition to these complexities, finite element modelling of the weld process must

include complex thermo-mechanical interactions, filler metal deposit and moving heat sources.

The objectives for the thesis could be summarised as:

- Create a thermal-mechanical finite element analysis of the welding process.
- Perform welding experiments to determine the plate deflections and temperature distribution in mild steel plates during shielded metal arc welding (SMAW).
- Evaluate the verification of experimental and numerical results.
- Determine the parameters necessary for an accurate and effective weld simulation and the sensitivity of modelling parameters on the results.

In Chapter 2 and 3 the literature survey done on welding and the application of the finite element method (FEM) in weld modelling are discussed. The modelling assumptions and techniques used by previous researchers used in the thesis are discussed in Chapter 3. The experimental setup and results are discussed in Chapter 4 with all the experimental results in Appendix B and C. The description of the weld modelling is in Chapter 5 and the verification of numerical results with experimental results is in Chapter 6. Conclusions and recommendations are made in Chapter 7.

2 WELDING

2.1 Background of Welding

Although welding is considered a relatively new process as practiced today, its origins can be traced to ancient times. Around 1000 B.C. the Egyptians and others in the Mediterranean area learned to accomplish forge welding. Blacksmiths from the Middle Ages developed the art of welding by hammering metals to a high level of maturity.

It was not until the 1800s that the technological foundations of modern welding were established when the electric arc and acetylene gas was discovered. The development of electrical generators in the mid 1800s made electrical power became available in amounts sufficient to sustain arc welding. At the turn of the 19th century, carbon arc welding had become a popular commercial process for joining metals, but the process was still limited. Welding with a metal electrode was developed and had the unique feature that the electrode added filler metal to the welding joint (Groover, 1999).

Arc welding with a fusible electrode, the most important of the fusion processes, was more complex in character and developed more slowly. In the early stages of this development fusion welding was used primarily as a means of repairing worn or damaged metal parts, but during the First World War, research was initiated into the acceptability of the technique as a primary means of joining steel plate and prototype structure were made.

Welding has been employed at an increasing rate for its advantages in design flexibility, cost savings, reduced overall weight and enhanced structural performance.

2.2 Physics of Welding

There are two main categories for welding: fusion and solid phase welding processes. In fusion welding, two edges or surfaces to be joined are heated to the melting point and, where necessary, molten filler metal is added to fill the joint gap. For solid phase welding, two clean, solid metal surfaces are brought into sufficiently close contact for a metallic bond to be formed. Solid phase welding can be accomplished at temperatures as low as room temperature.

By using a heat source with sufficient power it is possible to fuse through a complete section of very thick plate. The weld pool produced is difficult to control and the heat affected zone (HAZ) of such welds has a relatively coarse grain, adversely affecting the mechanical properties of the steel (Lancaster, 1965).

2.2.1 Heat Transfer

An understanding of the nature of heat transfer is essential for the proper appreciation of the heat effect of fusion welding. Heat transfer theory can indicate the minimum heat input rate to form a weld of any given width, and the essential variables which govern the heating rate and cooling rate in the heat affected zone and the weld metal.

The electric arc heat source is known as a surface heat source, which applies heat over a small area on the metal surface. In most fusion welding a continuous moving source is used. The continuous moving source has a special characteristic: once steady conditions have been achieved, the temperature distribution relative to the heat source is stationary. This condition is known as the quasi-stationary state and in most cases it is convenient in developing equations regarding the source as stationary and the heat flow medium (the work piece) as moving. Equation 2-1 shows the conduction of heat in a homogeneous isotropic solid in terms of rectangular co-ordinates (Lancaster, 1965):

$$\frac{\partial^2 T}{\partial x^2}+\frac{\partial^2 T}{\partial y^2}+\frac{\partial^2 T}{\partial z^2}-\frac{1}{\alpha}\frac{\partial T}{\partial t}=0 \qquad \text{Equation 2-1}$$

The power of the welding process is the product of the current I and voltage V passing through the arc. The power is converted to heat, but due to convection, conduction, radiation and spatter, heat losses occur. The temperature attainable in an arc is limited by heat leakage rather than by a theoretical limit (Phillips, 1968). The effect of heat losses is expressed by the arc efficiency coefficient, η_{arc}, in the calculation of the welding power.

$$P=\eta_{arc} VI \qquad \text{Equation 2-2}$$

Welding arcs are usually maintained between an electrode and a plate work piece. Such an arc is constricted at the rod and spreads out towards the plate. The column temperature is highest where it is most constricted, in this instance near the electrode. Having a clear understanding of the temperature and heat flux distribution in an arc is very important for the load application in weld modelling. An accurate representation of the thermal flux in the finite element method (FEM) software package will help with more accurate and reliable results.

2.3 Welding Processes

Arc welding is a fusion process in which coalescence of the metals is achieved by the heat from an electric arc between an electrode and the work. Filler metal is added in most welding processes to increase the volume and strength of the weld joint. A pool of molten metal, consisting of base and filler metal is formed near the tip of the electrode. As the electrode is moved along the joint, the molten metal solidifies in its wake. In this section some of the common arc welding processes that use consumable electrodes will be discussed.

2.3.1 Shielded Metal Arc Welding

Shielded metal arc welding (SMAW) use an electrode consisting of a filler metal rod coated with chemicals that provide flux and shielding (Figure 2-1). The filler metal used in the rods must be compatible with the metal to be welded, the composition usually close to that of the base metal. Currents typically used in SMAW range between 30 and 300 A at voltages from 15 to 45 V. Selection of the power parameters depends on the metals being welded, electrode type and length, and depth of penetration.

Shielded metal arc welding is performed manually and the equipment is portable and low cost, making SMAW highly versatile. Base metals that could be welded with SMAW include steels, stainless steels, cast irons and certain non-ferrous alloys. The disadvantage of SMAW is the use of consumable electrode sticks and needs to be replaced at regular intervals. The level of the current used is also a limitation because the electrode length varies during the operation and affects the heat resistance of the electrode.

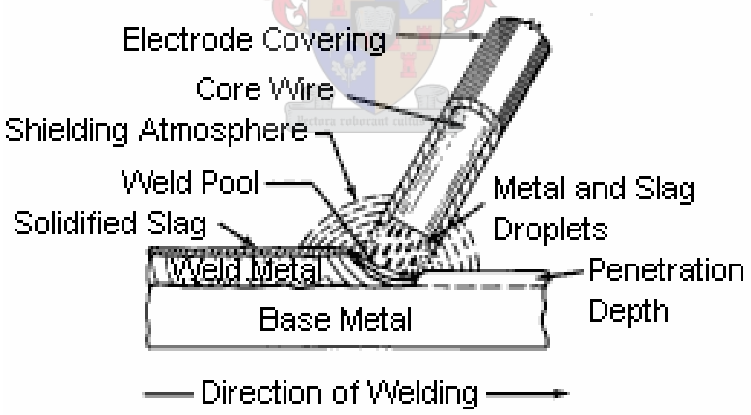

Figure 2-1: Shielded metal arc welding (SMAW)

2.3.2 Gas Metal Arc Welding

Gas metal arc welding (GMAW) is an arc welding process in which the electrode is a consumable bare wire and shielding is accomplished by flooding the arc with a gas. The bare wire is fed continuously from a spool through the welding gun.

The GMAW have various advantages over SMAW, which make it popular in fabrication operations. The combination of bare electrode wire and shielding gas eliminates the formation of slag on the weld bead and thus precludes the use of manual cleaning after welding. This makes GMAW popular for multi-pass welding. Because GMAW is continuously wire fed, the electrode do not need replacing at regular intervals such as in the case of SMAW, making this process suitable for automated welding. The utilization of electrode material is higher than with SMAW.

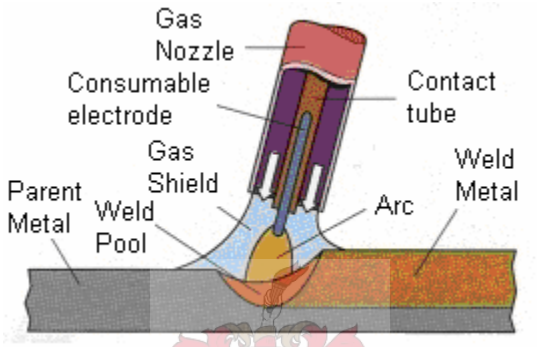

Figure 2-2: Gas metal arc welding (GMAW).

2.3.3 Gas Tungsten Arc Welding

Gas tungsten arc welding is an arc welding process that uses a non-consumable tungsten electrode and an inert gas for arc shielding (Figure 2-3). The term TIG (tungsten inert gas) welding and WIG (W is the chemical symbol for tungsten) welding are often applied to this process. The GTAW can be implemented with or without filler metal. When filler metal is used, it is added to the weld pool from a separate rod or wire. The typical shielding gases used are argon, helium or a mixture of these gases.

Advantages of GTAW in the applications to which it is suited includes high-quality welds, no weld spatter because no filler metal is transferred across the arc and little or no post weld cleaning because no flux is used. The welding costs of GTAW are higher than SMAW or GMAW because specialized equipment is

used, lower manual speed and the use of an inert gas. GTAW will be typically applied where a technical advantage is needed (Lancaster, 1965).

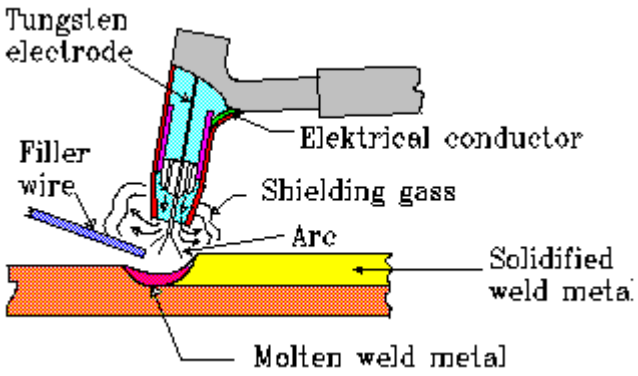

Figure 2-3: Gas tungsten arc welding (GTAW).

2.4 Welding Distortions

Welding distortions due to a weld in a plate arise primarily because the strip of material which has been melted contracts on cooling down from melting point to room temperature. Welding distortions can be separated into three types of distortions: angular, longitudinal and transverse distortion.

The contraction of weld metal as it cools after deposition causes shrinkage that takes place simultaneously in all directions, and therefore it causes several types of distortion as illustrated in Figure 2-4. The levels of welding distortions depend mostly on the heat input and the material thickness (Luo, Ishiyama, Murakawa, 1999). Material type also determines the extent of welding deformation.

If the contraction of the weld was unhindered, the longitudinal contraction of the weld would be equal to αT_m where α is the thermal expansion and T_m the melting temperature. Assuming only elastic deformation the corresponding stress would be $E\alpha T_m$ where E is the Young's modulus of the material. The value of $E\alpha T_m$ is greater than the elastic limit, so that plastic deformation of the weld takes place during cooling and the residual stress in the weld exceeds the elastic limit.

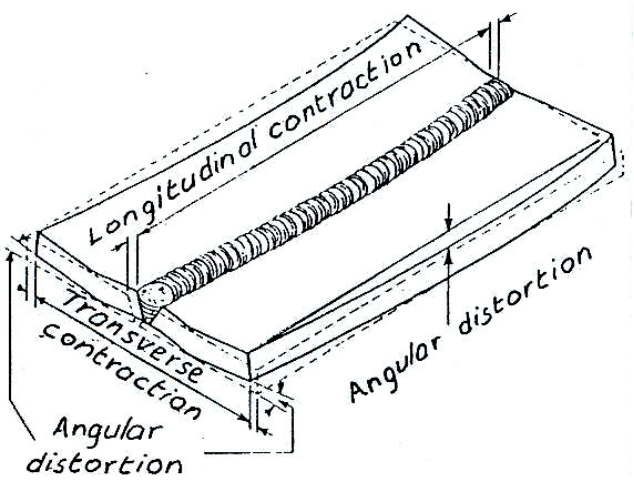

Figure 2-4: Welded plate distortions (Faure, undated)

In multi-pass welding, the first run in a butt weld pulls the plates together when shrinkage occurs (Figure 2-5). The second run is restrained by the first, which has to be compressed before plates can move together. The pull at the top and the push at the bottom of the weld give rise to angular distortion. A number of superimposed runs trying to contract, along with the initial shrinkage of the first run, cause a transverse shrinkage of the joint. Similar forces act along the length of the joint, thus producing lengthwise distortion and longitudinal shrinkage.

2.4.1 Control of Welding Distortions

Distortion due to welding has been regarded as a critical issue and has led to the development of various techniques and guidelines to minimize these distortions. In general, most of the distortion mitigation techniques have been developed according to theoretical, mathematical and generally accepted knowledge from experience or analogy. Faure had suggested three rules for the prevention and control of distortions (Faure, undated):

- Reduce the effective shrinkage force.
- Utilise shrinkage forces to reduce distortion.
- Balance shrinkage forces with other forces.

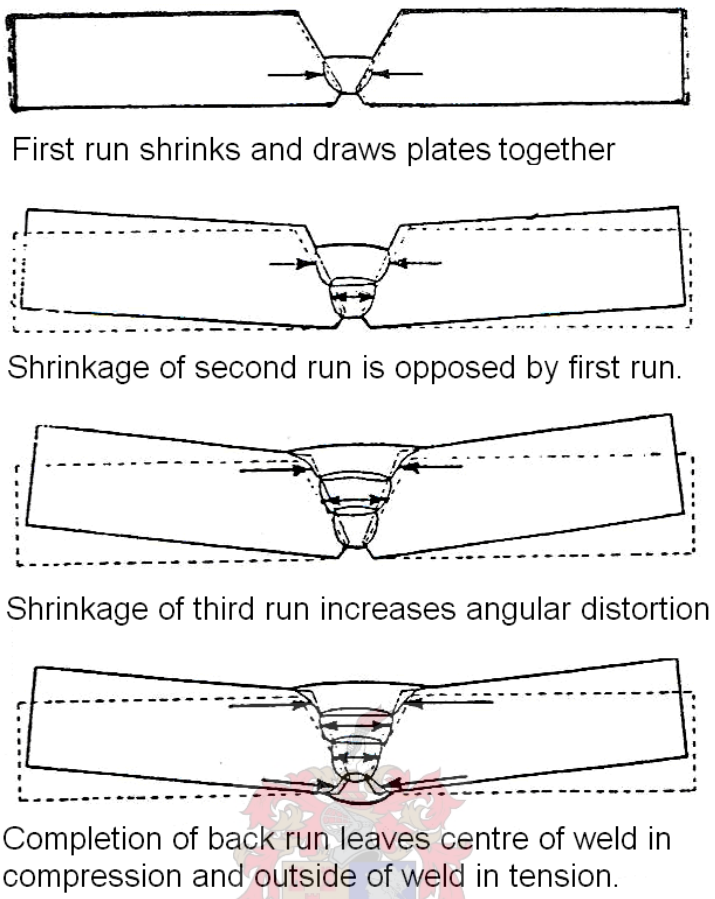

Figure 2-5: Welding distortion in multiple-run welding (Faure, undated)

The effective shrinkage force can be reduced with the use of fewer runs, proper edge penetration, placing of weld near the neutral axis, intermittent welds, use of correct welding sequences like the back-step method (Figure 2-6) and welding thin plates at a 45° angle.

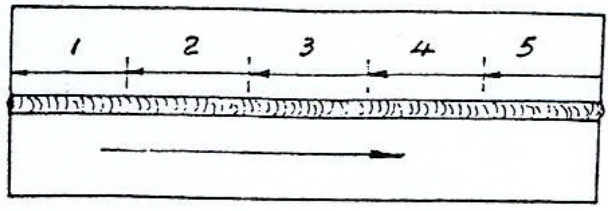

Figure 2-6: The back-step method (Faure, undated).

The distortions can be reduced by utilising the shrinkage forces by spacing the parts to allow for shrinkage and presetting parts to counter distortion. To balance

shrinkage forces with other forces, a proper welding sequence can be used to counter shrinkage force (Figure 2-7). Other techniques to reduce distortion and residual stresses are tack welding to prevent movement of parts, peening for stress relieving, using of heat to straighten parts, use of jigs and fixtures, machining and stress-relieving heat treatment.

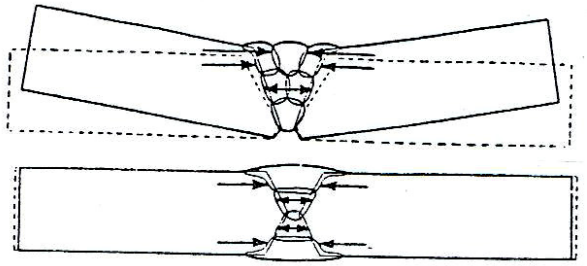

Figure 2-7: Angular distortion control with symmetrical welds (Faure, undated).

The use of optimised welding sequences changes the distribution of the residual stresses but does not change the maximum residual stress. High residual stress is formed in a region around the weld line irrespective of the welding sequence, however, the welding sequence mainly effect the distortions in the weldment (Kadivar, Jafarpur, Baradaran, 2000).

Distortion control becomes more difficult the larger and more complex the structure becomes. It is advisable to attack the overall accuracy control problem by starting at the end of the fabrication sequence and working backwards. Current procedures to reduce welding distortion can be divided according to the three stages at which it takes place:

- Pre-welding strategies such as fix devices, etc.
- In-process corrections such as speed adjustments, change of planned weld sequence, etc.
- Post-welding adjustments such as flame heating.

It was suggested that better control of certain welding variables would eliminate the conditions that promoted distortion (Tsai, Park, Cheng, 1999). This included

the reduction of fillet welds size and length, high speed welds, low heat input welding process, intermittent welds, back stepping (Figure 2-6) and balancing heat about the plate's neutral axis in butt joint welding.

Thermal management techniques have been applied for distortion control of welded plates. Two common techniques investigated (Figure 2-8) were the gas tungsten arc (GTA) and heat sinking (Jung, Tsai, 2004) procedures. The GTA increased the HAZ by preheating. Heat sinking reduced the HAZ by applying a cooling chamber beneath the welding area (Figure 2-9).

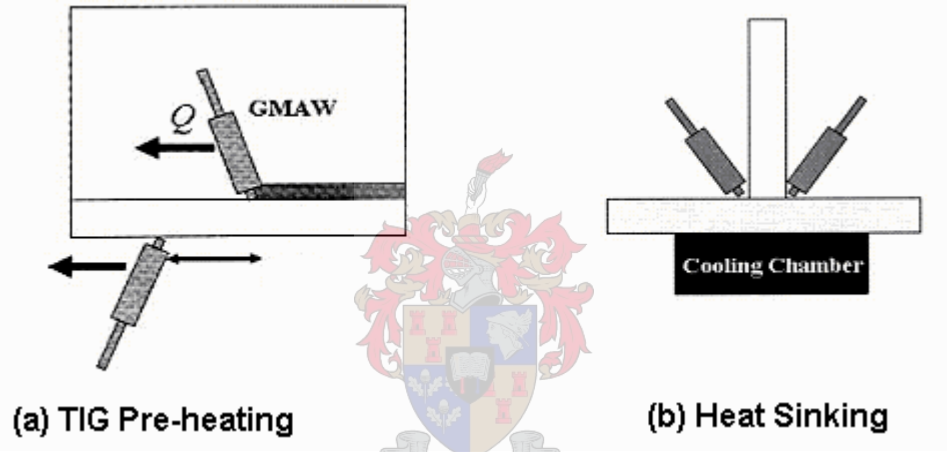

Figure 2-8: Thermal management techniques applied to welding.

Jung and Tsai used plasticity-based distortion analysis (PDA) and elastic-plastic analysis to obtain stress and strains results in welded T-joints. It was found that the heat sinking increased angular distortion and that GTA preheating reduced it. A combination of GTA preheating and external restraining effectively reduced the angular distortion. The reduction of angular distortion during GTA preheating was not fully understood, since there was little difference between the results from GTA preheating and no thermal management.

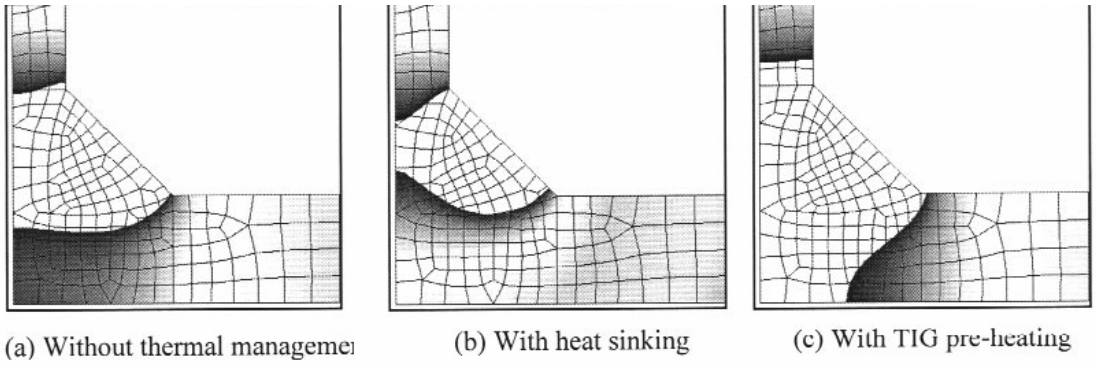

Figure 2-9: Effect of thermal management techniques on HAZ (Jung, 2004).

2.4.2 Calculation of Welding Distortions

Welding deformation reduces the accuracy of manufacturing and decreases productivity due to the need for correction work. The minimization of distortions from as early as the design stage will lead to higher quality of products as well as higher productivity. Prediction of welding distortions through analytical and numerical methods like empirical equations and FEA form an essential part in manufacturing.

With the use of more expensive steels or other metals, like stainless steel, larger welding deformations can occur due to the materials' properties. It is important to foresee forthcoming welding deformations and its extent to prevent costly repairs of inaccurate welds. The methods for analytical approaches for determination of welding deformations of several researchers had been investigated.

It was found that the welding deformations calculation methods of Okerblom, Walter, Horst Pflug, Sparagen–Etinger and Blodgett, applied to calculate deformations of welded samples, gave results that differ greatly (cited by Audronis and Bendikas, 2003). Their studies looked at the results for longitudinal contraction, longitudinal deflection on the plate's plane, transversal contraction and transversal deflection. These results were compared with FEA results.

The calculations proposed by the abovementioned researchers must be used with caution. These formulas are capable of reliable predictions within the limitations upon which it is based. Any change of parameters, which has not been included, can lead to a calculation error. In many cases these calculations may serve the purpose of predicting no more than the order of the magnitude of welding distortions. The formulas are however not suitable for predicting distortions of large structures (Moshaiov, Eagar, 1990).

A method based on the inherent strain theory combined with FEM for the prediction of welding deformations was proposed by various researchers (Luo, et al., 1999 and Jang, Lee, 2003). The equivalent forces and moments that would result in the same deformations as in welding could be obtained by using the inherent strain method. Using the obtained equivalent nodal loads, the welding deformation could be calculated by elastic FE analysis.

2.5 Metallurgy of Welding

Welding has the ability to join various metals, both similar and dissimilar. The joining bond is metallurgical rather than just mechanical, as with riveting and bolting. Due to the intense heating and fast cooling of the weld material the microstructure of the metal undergoes considerably changes.

This region is termed the heat affected zone (HAZ). In cold worked metals the HAZ may have experienced recrystallization and grain growth and thus a diminishment of strength, hardness and toughness. Upon cooling residual stresses may form in this region, which weakens the joint (Callister, 1997).

2.5.1 Low Carbon Steels

The metal most widely used in welded fabrication is carbon steel containing up to about 0.3% carbon (mild steel). This material undergoes only minor hardening in the heat-affected zone of fusion welds and normally is welded without any pre- or post welding heat treatment. Higher carbon steels are more difficult to weld,

except in the form of thin sheet or bar, because hardening of the weld and heat affected zone may result in embrittlement and cracking. One undesirable feature common to all ferrous materials welded is grain growth in the region near the fusion boundary.

A welded joint consists out of a molten pool zone (MPZ), a fusion zone (FZ) and a heat affected zone (HAZ). The HAZ is defined as the part of the metal that has not been melted but whose material properties or microstructure has been altered by the heat of the welding. This zone is indicated by region 4 to 1 in Figure 2-10.

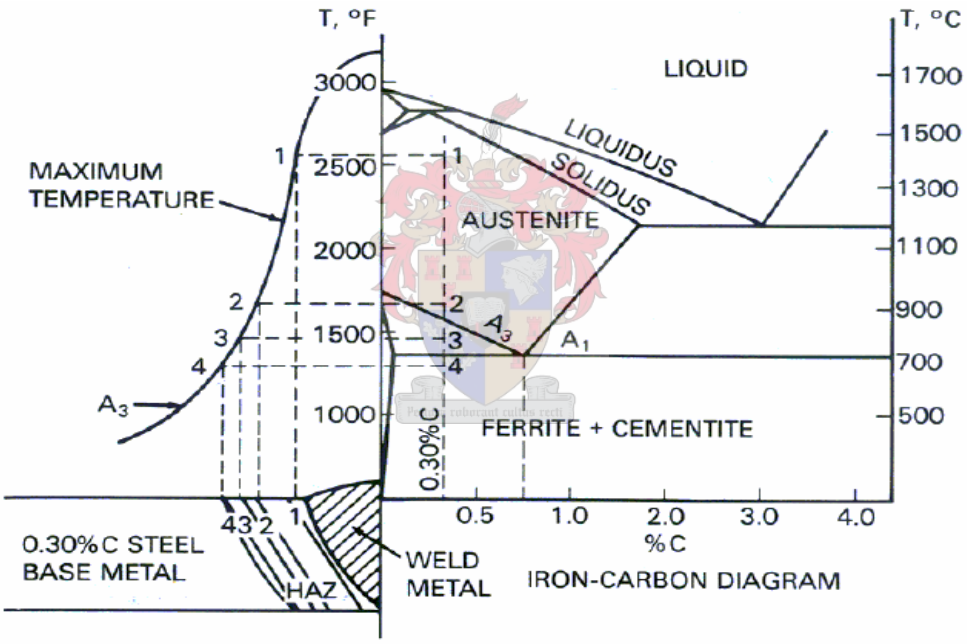

Figure 2-10: Phase diagram for carbon steel during welding.

In region 1 the temperatures were close to melting point. The heat treatment has refined the grain structure and austenitic grain growth takes place. There is an improvement in toughness of the mild steel. If the cooling rate is high, the microstructure can readily change to martensite.

The heat from the welding process has raised the temperature in region 2 to just above the lower critical point. At this temperature the ferrite remains unchanged, but the pearlite is dissolved to austenite. Upon cooling, the carbon is precipitated in the form of small globules of cementite in ferrite. This type of structure is acceptable as it produces softness and good ductility. In region 3 the metal was heated to just above 600 ℃ and consists of newly formed fine equiaxed grains of ferrite and pearlite. This temperature region undergoes relieving of residual stress. Temperatures below 450 ℃ remain unchanged.

2.6 Conclusion

A literature study was carried out to gather information on the welding process and the mechanics of plate deformation during welding. Sequence welding and thermal management techniques used in distortion control and prevention in welded plates were discussed. The use of optimised welding sequences helps to control welding distortion during welding but have no effect on the maximum stress values. Thermal management techniques can be used to control the size of the HAZ and reduce residual stresses through stress relieving.

Theoretical equations were obtained to be used in first order derivatives of the experimental and modelling results. In these first order derivatives the experimental and modelling results were compared with the theoretical results to insure the validity of the results. The use of thermal management techniques and other welding mitigation techniques were not studied in depth in the literature survey and can be looked into in future studies. The causes and control of welding fracture can also be investigated in future welding research.

3 FINITE ELEMENT METHOD: APPLICATION TO WELDING

3.1 Introduction

The finite element method (FEM) is a computational technique used to obtain approximate solutions of boundary value problems in engineering. The finite element method is a way of getting a numerical answer to a specific problem. A simple description of FEM is the cutting of a structure into several elements, describing the behaviour of each element in a simple way, reconnecting the elements at ”nodes” as if it were pins or drops of glue that held the elements together.

A literature survey was done to look at the development and history of the finite element method, the role of FEM in welding analysis and the effect of welding and modelling parameters on the results. The survey focused on temperature field estimation and welding deformation. Weld modelling guidelines on element mesh, boundary conditions and material properties from the survey were applied in the thesis.

3.2 Finite Element Analysis of Welding

The numerical modelling of welding can be used as design tool or manufacturing analysis tool. As a design tool, FEM can be used to evaluate the feasibility of designs as early as the concept phase. As a manufacturing analysis tool, for fixed designs, different welding processes and sequences can be evaluated to minimize welding distortion (Michelaris, DeBiccari, 1996).

Despite the success that had been demonstrated by researchers over the past few decades of conduction heat flow models in predicting fusion weld sizes, base

metal temperatures and processing requirements, FEA application in the welding manufacturing world is still uncommon (Fuerschbach, Eisler, 2002).

Welding distortion prediction is still done empirically, results taken from experiments done under various conditions. The results are used to develop correlations parametrizing the effects of various welding and geometrical conditions. These experimentally derived formulations are only applicable to the conditions it is tested to.

For the past twenty years, the finite element method (FEM) was used for the prediction of welding induced residual stresses and distortions. More recently researchers focused on improving the earlier FEM models of welding by looking at the effect of the welding on the whole structure (Michaleris, et al., 1996). Other complexities that are also involved in the FEA of welding is temperature and history dependent material properties, high gradients of temperature, stress and strain fields with respect to both time and spatial coordinates, large deformations in thin structures, phase transformation and creep phenomena.

3.2.1 Two-dimensional vs. Three-dimensional Modelling

A full three-dimensional model with a sufficiently fine mesh can model the heat flow as accurately as the errors in the material properties, geometry, heat input, convection and radiation parameters permit (Goldak, Bibby, Moore, House, Patel, 1986). The reason that three-dimensional analysis has not been standard procedure for the thermal analysis of welds is that it is time consuming and resource intensive.

In choosing proper models for weld analysis, the analyst must balance accuracy against cost. In two-dimensional (2D) cross-sectional models (Figure 3-1), heat flow is constrained in the plane of the plate. These 2D models can achieve accurate results for thin plates. Assuming heat transfer only in the cross-sectional

plane can provide a useful and economical approximation for many welding situations. The results from a low cost cross-sectional analysis could be used in designing an efficient mesh for more complex models (Michelaris, et al., 1996).

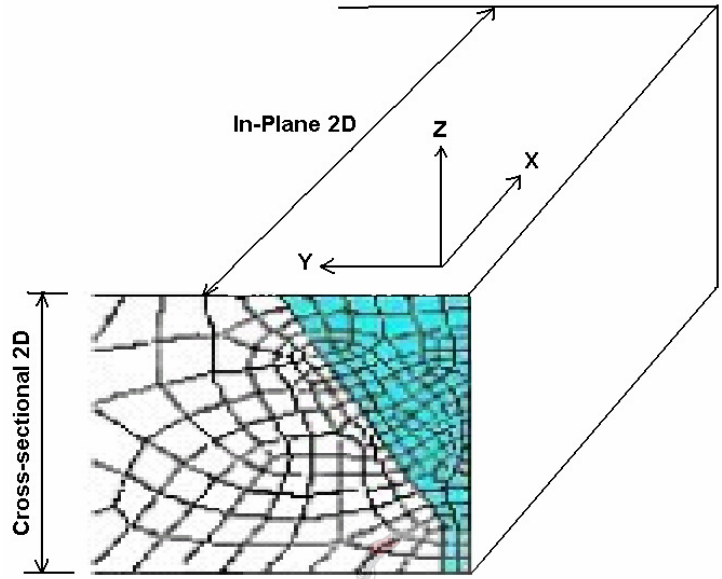

Figure 3-1: Illustration of the 2D planes in the modelling of welded plates.

Cross-sectional 2D offered accurate results for predicting residual stresses. Large structures may buckle due to residual stresses parallel to the welding direction. These 2D models cannot represent buckling caused by longitudinal stresses. A fully three-dimensional thermo-mechanical simulation of a large structure can represent this distortion mode (Bonifaz, 2000).

Earlier studies on weld response were limited to cross-sectional 2D modelling. Studies had shown that good correlations were observed between numerical predictions and experimental results for these models. Residual stress predictions in 2D modelling provided accurate estimations comparable to 3D analyses, since the stress field exhibits a uniform distribution through the length of the work piece (Deo, Michelaris, Sun, 2002). These models have been particularly useful for its high efficiency and accuracy in determining the solution in the analysis plane and reduced computational requirements. Two-dimensional analysis does create inaccurate results where tack welding or fixturing allow out-

of-plane movement. Longitudinal heat transfer, instability aspects and end effects cannot be realized in cross sectional two-dimensional formulations.

Michaleris (1996) presented a numerical analysis technique for the prediction of welding distortion by combining the in-plane 2D (Figure 3-1) welding simulation with 3D structural analysis in a decoupled analysis approach. First, a 2D welding simulation of the portion to be welded had to be performed to determine the residual stress distribution. Then a 3D structural (elastic) analysis can be performed on the whole structure, using the residual distribution of the welding simulation as loading.

If temperature gradients through the thickness of the plates are minimal in the 3D analysis then shell elements can be used to model the thermal welding process. The advantage of the decoupled approach is computational simplicity and efficiency. This approach allowed for the evaluation of the initial design and following modifications without the need of performing any additional welding simulations.

Weavar assumed full penetration welds at every joint using 2D shell elements (Weaver, 1999). Goldak assumed that the temperature gradient through the thickness, $\partial T/\partial z$, of the plate was zero. The error in the model grows as the $\partial T/\partial z$ grows and more heat flows in the z direction. Goldak assured that in sufficiently thin plates, the 2D analysis does provide useful data away from the weld. It permits variations in geometry and heat source to be analysed accurately and economically (Goldak, et al., 1986). These assumptions are valid for the experiments investigated in this thesis.

A 2D thermal analysis was initially used in the thesis to establish a working welding model. The procedure for the 2D analysis was used as a basis to design and perform a 3D analysis. Using a simple 2D model helped to identify and solve

problems that would have occurred in the 3D models. The 3D model proved to be time consuming and shell elements was used for full process weld modelling.

3.2.2 Thermal and Structural Analysis

MSC.Marc (MSC.Marc Manual, 2005) is capable of performing a coupled thermal-structural analysis. The definition of coupled systems includes the multiple domains and independent or dependent variables describing different physical systems. In the situation with multiple domains, the solution for both domains is obtained simultaneously. In a coupled welding analysis the temperature distribution and the thermal strains caused by the intense heat source are calculated simultaneously.

Thermal and mechanical analysis were performed separately to simplify the welding simulation and to make it more computationally efficient (Michelaris, et al., 1997). The nodal temperature results from a thermal analysis were applied as a boundary condition in the structural analysis. The advantages of decoupled welding analyses was that shorter multiple analysis were run, making it quicker to identify errors. More detail was applied to each individual analysis, making the model more realistic and accurate. The effect of mechanical response on the thermal behaviour was assumed negligible in uncoupled thermal and structural analyses (Deo, et al., 2002).

3.2.3 Prediction of Welding Distortion

Distortions induced by welding have been regarded as a critical issue in terms of performance, quality and productivity. Various welding mitigation and distortion control techniques have been developed (Jung, et al., 2004). These methods include external restraining, preheating, auxiliary side heating, heat sinking, etc. To assess the effects of welding on structures efficiently, and in turn to implement various distortion mitigation techniques, a validated method for predicting welding induced distortion is necessary.

Warping is a common problem experienced in the welding fabrication of thin-walled panel structures. This causes a loss of dimensional control and structural integrity and increased fabrication costs due to poor fit between panels. Correction work done to highly distorted plates can be expensive and can cause more damage to the plates.

3.2.4 Modelling Assumptions

In the modelling of the welding process certain assumptions were made to simplify the model. Parent metal and welded metal had the same mechanical properties, i.e. softening of material was neglected. The deformation process was rate independent, and an elastic-plastic constitutive model with kinematic hardening assumed for the material. Mechanical properties are depended on temperature, which meant the plasticization area was temperature-dependent (Bonifaz, 2000).

The following assumptions were made: the weld pool is a zone of zero deviatoric stress, as well as the regions where the temperatures exceed the melting temperatures for the material. This was because a fluid could not resist shear stress with resulting fluid motion if a shear stress is applied. Along the un-welded portion of the joint, a stress-free condition was assumed. The residual stresses in rolled plates were assumed negligible. The only significant stresses that could be found in the plates were the stresses caused by the cutting process of the plates. Any stresses that were in the plate before welding was relieved during the heat process of the welding.

Michelaris and DeBicarri (1996) did not consider phase transformations in two-dimensional thermo-mechanical welding simulations. The temperature dependent material property data for a steel (SAE 1020) similar to the structural steel AH-36 used by Michelaris in the experiments was used. It was assumed that a little change in chemical composition had no significant effect on the

thermal properties of the steel. Section 3.3 discuses the material models and assumptions used in the models.

3.2.5 Applied Heat Source

In 1946 Rosenthal presented a solution for the temperature distribution of a travelling point source of heat. This had formed the basis for most subsequent studies in heat flow. Experimental results indicated that Rosenthal's equation (Equation 3-1) gave good agreement with the actual weld size, but it did not provide information on the shape of the weld pool.

$$T - T_0 = \frac{q}{2\pi kr} e^{\frac{-v(r-x)}{2\alpha}} \qquad \text{Equation 3-1}$$

Rosenthal's equation tends to over predict the weld depth and under estimate the weld width at high process parameters. This was due to the point heat source assumption that was made by Rosenthal. A point heat source gave infinite high heat input near the heat source point. The solution also gave unrealistic representations of the HAZ of the material.

Eagar and Tsai (1983) presented a solution for a travelling heat source on a semi-infinite plate (Equation 3-2). This distributed heat source theory provided the first estimate of weld pool geometry based on fundamentals of heat transfer. The same assumptions that Rosenthal made was used: the absence of convective and radiative heat losses, constant thermal properties and a quasi-steady state semi-infinite medium. The only difference was the Gaussian distributed representation of the heat source.

$$Q(x,y) = \frac{q}{2\pi\sigma^2} e^{\frac{-(x^2+y^2)}{2\alpha}} \qquad \text{Equation 3-2}$$

The theory provided gave good correlation with experiments done on carbon steel, stainless steel, aluminium and titanium. Only weld depth did not have good correlation with the experiments. An enhancement factor that estimated the temperature profile of finite thickness plates proposed by Myers (cited by Eagar, et al., 1983) gave much better agreement.

The maximum power generated during welding can be determined with the power equation for electric current given in $P = \eta VI$. This represented the net heat input in equations. The heat loss due to radiation, conduction through the electrode and heat consumed towards burning of flux and melting of electrode was accounted for by the arc efficiency parameter η (Adak, Mandal, 2003).

Tsai and Eagar (1985) measured the arc efficiency for gas tungsten arc (GTA) welding on a water-cooled copper anode. The arc efficiency was determined by measuring the heat that arrived at the copper anode and divided it by the total heat produced by the arc. The heat was calculated to be 80% of the heat generated in the arc. This arc efficiency was much higher than the arc efficiency of normal welding when a molten pool was presented.

Tsai also investigated the effects of arc lengths and proved to be the primary parameter governing the heat distributions while the current dominated the magnitude of the heat flux. A change in arc length influenced the heat distribution parameter, σ. From Equation 3-2 it could be seen that the heat flux would drop rapidly with a smaller σ. The heat distribution parameter is shown in Figure 3-2.

Jeong and Cheo introduced a similar 2D Gaussian heat source for a fillet weld joint but with distribution parameters in the X and Y coordinate directions (cited by Nguyen, Ohta, Matsuoka, Suzuki, Maeda, 1999). The conformal mapping technique was used for the solution of the temperature field in the plate of finite thickness for the fillet-welded joint. Even though the available solutions using the Gaussian heat sources could predict the temperature at regions close to the heat

source, it was still limited by the shortcoming of the 2D heat source itself with no effect of penetration.

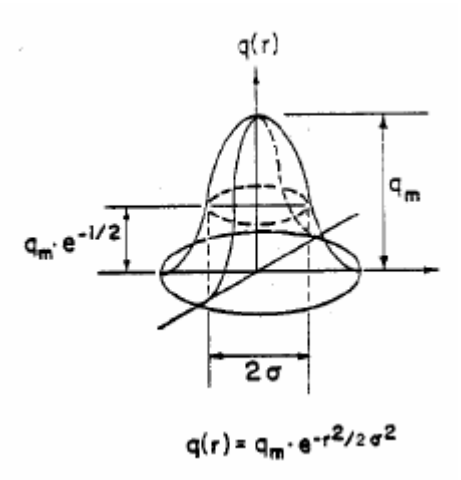

Figure 3-2: Gaussian distributed volume heat source (Eagar, et al., 1983).

Goldak (1983) first introduced the three-dimensional (3D) double ellipsoidal moving heat source. Finite element modelling (FEM) was used to calculate the temperature field of a bead-on-plate and showed that this 3D heat source could overcome the shortcoming of the previous 2D Gaussian model to predict the temperature of the welded joints with much deeper penetration.

$$Q(x,y,z) = \frac{6\sqrt{3}r\,Q}{a\;b\;c\;\pi\sqrt{\pi}} exp(-\frac{3x^2}{c^2} - \frac{3y^2}{a^2} - \frac{3z^2}{b^2}) \qquad \text{Equation 3-3}$$

Goldak initially proposed a semi-ellipsoidal heat source in which heat flux was distributed in a Gaussian manner throughout the heat source's volume (Equation 3-3). This heat source predicted the temperature gradients in front of the arc less steep than experimentally observed and steeper behind the arc. A double ellipsoidal heat source was proposed to overcome that problem.

The heat source consisted out of two different semi-ellipsoidal volumes that were combined to give the new heat flux (Figure 3-3). An equation for a semi-ellipsoidal in front and in back had to be specified where the source parameters are a, b, c_r and c_f as described in Figure 3-3. Values for the source parameters were obtained by the measurement of the weld pool geometry (Nguyen, et al., 1999) or from measuring weld surface rippling effects. In the absence of better data the distance in front of the heat source equal one half the weld width and the distance behind the heat source equal twice the width (Goldak, Chakravarti, Bibby, 1984).

The cost of preparing a fine mesh for FEA is relatively low compared to the computing costs. It is more difficult to prepare a carefully graded mesh to achieve the desired accuracy with low computing costs. Goldak (1986) presented guidelines: the mesh had to be sufficiently fine to model the heat source with adequate accuracy. Goldak stated that four quadratic elements be used along each axis to capture the inflection of the Gaussian distribution.

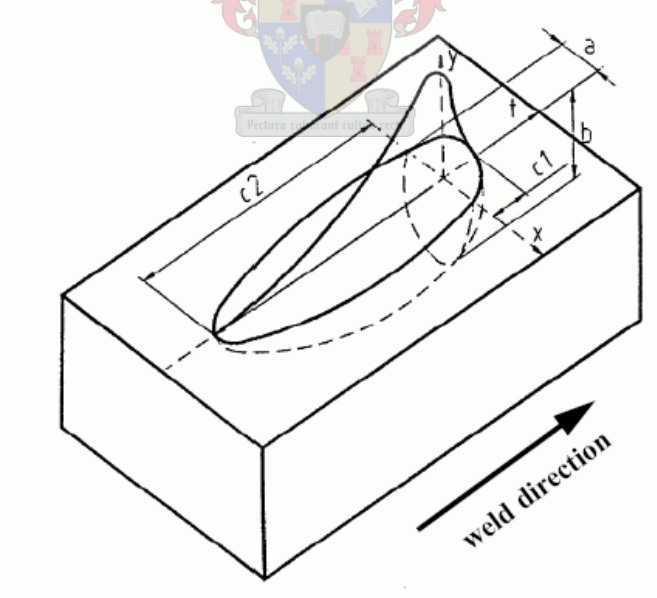

Figure 3-3: Double ellipsoidal density heat source (Francis, 2002).

The length of the time step influenced the accuracy of the heat source model. Goldak proposed that the heat source might move approximately one-half of a weld pool length in one time step for in-plane and three-dimensional models (Goldak, et al., 1986). The calculation of an optimised time step is described in the next section.

3.2.6 Time Step Estimate

In non-linear heat transfer analysis, negative temperature values below absolute zero can be calculated, which is not physically possible (Figure 3-4). This effect is caused if the time step is too small and inaccurate FEM approximations are obtained. When a too small time step or too large element is used in the welding analysis, the energy of the element is not calculated at all the nodes of the element. This results in an increase in heat flux at the nodes where it is applied and a negative flux to cancel this effect out, leading to negative temperature calculations. This is rectified if the time step is increased, mesh refined or lumped heat capacity matrix (linear elements) is used.

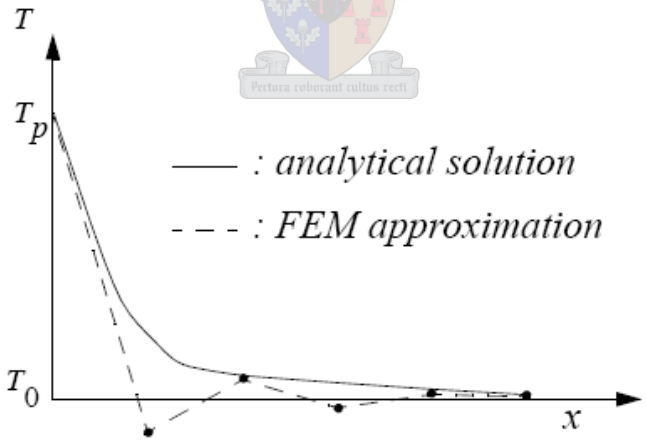

Figure 3-4: Negative temperature effect due to small initial time step estimate (MSC.Marc Manual, 2005).

To avoid inaccurate results or unstable solutions, the proper choice of the initial time step was required. A responsible initial time step was dependent on a number of factors, including the spatial size of the element mesh and the thermal

diffusivity of the material. Consider the heat conduction equation for an isotropic material with constant thermal conductivity, no internal heat generation and heat transfer in one direction only (Equation 3-4). For the same change in temperature, Equation 3-5 can be used to estimate the relationship between the spatial and time increments.

$$\rho c_p \frac{\partial T}{\partial t} = k \frac{\partial^2 T}{\partial X^2} \qquad \text{Equation 3-4}$$

$$\Delta t = \Delta x^2 \frac{\rho c_p}{k} \qquad \text{Equation 3-5}$$

The length of the time step influenced the accuracy of the heat source model. Goldak (1986) proposed that the heat source might move approximately one-half of a weld pool length in one time step for in-plane and three-dimensional models.

Time integration is a numerical method used for the solving of the equations used in the FEA. The default time integration method in MSC.Marc was the Single Step Houbolt method. This method proved to be the best for the welding analysis. The Single Step Houbolt procedure is unconditionally stable, second order accurate and asymptotically annihilating.

In Msc.Marc both fixed and adaptive time stepping schemes were available for transient heat transfer analysis. In fixed time stepping scheme, the program is forced to step through the transient with a fixed time step that is user specified. The convergence control of maximum allowed error in temperature estimate used for property evaluation for an increment is used with the fixed time stepping scheme. For the adaptive time stepping scheme the maximum allowable nodal temperature change is used for time step estimation (Msc.Marc, 2005).

The fixed time stepping used less computation time than the adaptive time stepping but with an accuracy penalty. The accuracy of results was dependent on the time step used in the fixed time stepping. It was decided to use the

adaptive time stepping that gave more accurate results but were more time consuming.

3.2.7 Boundary Heat Loss Conditions

Many researchers used a combined convective and radiation heat transfer coefficient (Bonifaz, 2000). This allowed the use of one heat loss boundary condition instead of two. Rykalin proposed a heat transfer coefficient in Equation 3-6 (cited by Goldak, et al., 1983).

$$h_{comb} = 24.1\times10^{-4}\,\varepsilon T^{1.61} \qquad \text{Equation 3-6}$$

Goldak reported that this equation was not as accurate as applying both Newton's equations for cooling and the Stefan – Boltzmann equation for radiation with appropriate coefficients. Radiation heat transfer is proportional to the fourth power of the temperature difference and only becomes significant at very high temperatures (> 800 °C). Preston ignored the radiation heat losses from the plates since it had no influence on the residual stress results and incorporated it into the arc efficiency (cited by Francis, 2002).

The combined heat transfer coefficient used in this thesis was calculated by adding the convective and radiation heat transfer coefficients (Equation 3-7). The convection heat transfer coefficient (Equation 3-8) was derived from the Nusselt number for natural flow from a heated plate. See Appendix A for derivation of Equation 3-8. The radiation heat transfer coefficient (Equation 3-9) was derived from the linearization of the Stefan – Boltzman equation.

$$h = \overline{h}_c + h_r \qquad \text{Equation 3-7}$$

$$h_c = \frac{0.14\,k\left(\frac{\Delta\rho}{\rho}\right)^{\frac{1}{3}}}{\left(\frac{v\alpha}{g}\right)^{\frac{1}{3}}}$$ Equation 3-8

$$h_r = \sigma\varepsilon\left(T^2 + T_e^2\right)\left(T + T_e\right)$$ Equation 3-9

3.3 Material Properties

For the past couple of decades the thermal properties in welding analysis had been assumed constant. Rosenthal's equation could not be extended to include non-linear properties since the final solution applied was only valid for linear equations. The error caused by assuming constant thermal properties was proved by Goldak (1986) to be substantial. Values for conductivity were usually chosen to obtain best agreement with welding experiments: 25 W/m.℃ for 3D heat flow and 41 W/m.℃ for 2D heat flow, for low carbon steel.

Since the error in heat flux for a given temperature gradient was directly proportional to the error in the conductivity, it was desirable to use the best data available. Unfortunately, it was seldom possible to find the data needed and thus unsuitable data was often used in calculations (Louhenkilpi, Markku, Kytonen, Vapalathi, 2003). The temperature dependent material property data used in this thesis was obtained from the internet and other published material data. In cases where non-linear properties for a specific material were not available, data of similar materials were used.

3.3.1 Conductivity

Weld pool convection is a complex phenomenon that is difficult to simulate. This convection is therefore simulated by multiplying the conductivity with a factor when the temperature exceeds the liquidus temperature. Values between eight and ten had been proposed in the literature (Ericsson, 2003). The Msc.Marc Manual proposed that conductivity must be increased to a high value at a

temperature just below the melting point (~1500 ℃ for steel) to account for increased conductivity due to stirring effect in molten metal (Msc.Marc Manual, 2005). Goldak (1984) assumed a thermal conductivity of 120 W/m.℃ in the liquid range for low carbon steel. The model for the conductivity for low carbon steel is shown in Figure 3-5. For this thesis, the value of the conductivity in the liquid zone was assumed to be 120 W/m.℃.

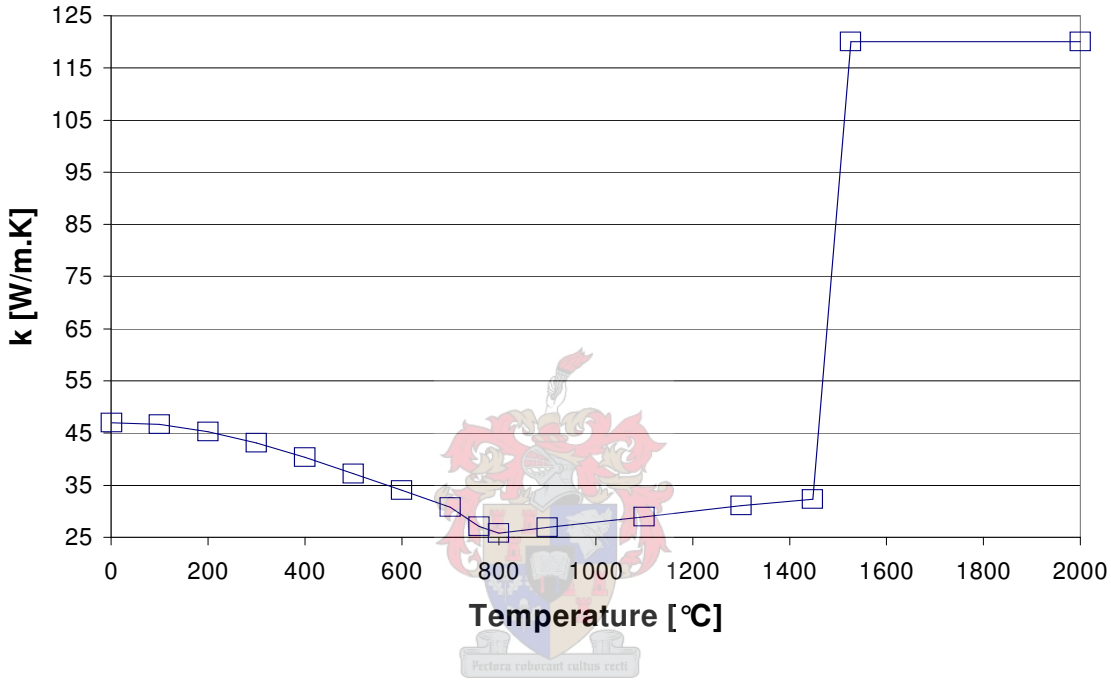

Figure 3-5: Temperature dependant thermal conductivity for mild steel (Goldak, et al., 1984).

3.3.2 Specific Heat

Heat capacity is the property that indicates the ability of the material to absorb heat from the external surroundings. The specific heat represents the heat capacity per unit mass. Zhu and Chao (2002) suggested the use of the constant room temperature value for specific heat, while other authors put emphasis on the use of temperature dependent material properties in welding simulations (Goldak, et al., 1983 and Audronis, et al., 2003). The specific heat for low carbon steel, similar in chemical content as SABS 1431 300 WA is shown in Figure 3-6.

A small change in chemical content has negligible influence on the thermal properties of the materials. This assumption was used to obtain material data at high temperatures.

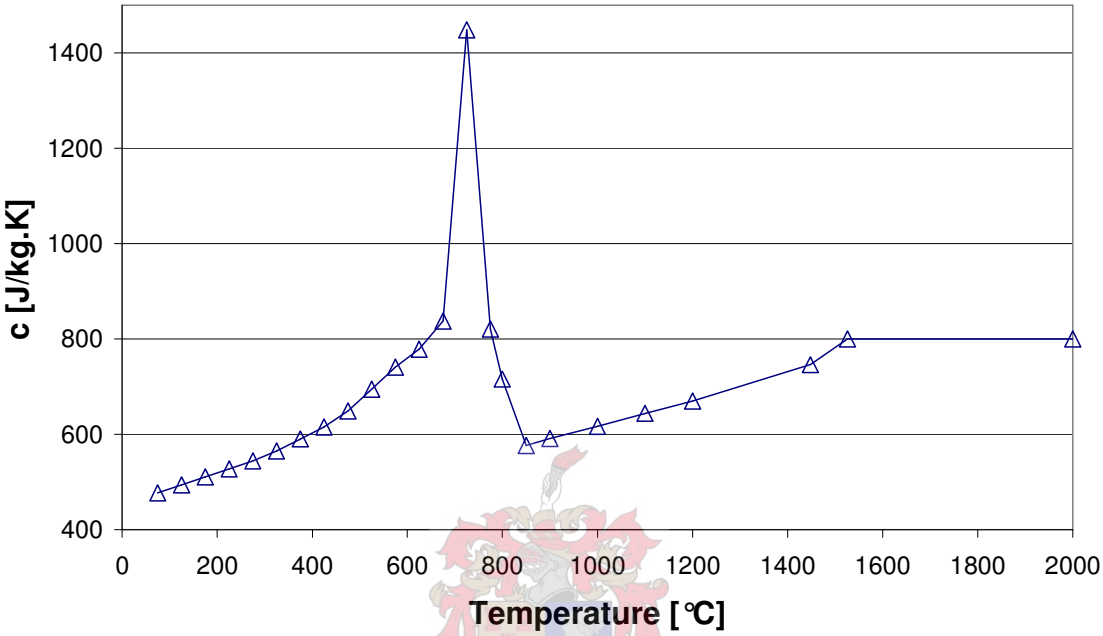

Figure 3-6: Specific heat for mild steel (British Iron and Steel Research Association Metallurgy, 1953).

Latent heat can be induced because of a phase change that can be characterized as solid-to-solid, solid-to-fluid, fluid-to-solid, depending on the nature of the process. The effect of latent heat can be specified in the material properties menu. The basic assumption of the latent heat option in MSC.Marc is that the latent heat is uniformly released in a temperature range between the solidus and liquidus temperatures of the materials. The latent heat can be specified by varying the specific heat as a highly non-linear function of temperature (MSC.Marc Manual, 2005).

A latent heat of fusion of 260 kJ/kg was specified for mild steel. Sufficient experimental data for the solid-to-solid phase transformation in carbon steel was

available and a direct input of temperature dependent specific heat was used (Figure 3-6). Conflicting reports on the use of latent heats were found. Bonifaz (2000) considered latent heat in his models while Wu reported that the solid to liquid phase latent heat had an insignificant effect on temperature results (Wu, Syngellakis, Mellor, 2001).

3.3.3 Yield Strength

It was assumed that little change in chemical composition had negligible effect on the thermal and mechanical properties of the material. In the case where no non-linear data was available, an engineering approach proposed by Zhu and Choa (2002) was used.

Zhu showed that previous researchers had looked at the effects of non-linear material properties. Not only was temperature dependent properties difficult to obtain but the use of these properties in FEM modelling were also computer resource consuming. Zhu and Chao suggested an engineering approach using simplified properties constituted by a piece-wise linear function with temperature for the yield stress and constant room-temperature values of all the other properties for computational weld simulation.

It was assumed that the yield stress for the material took the room temperature value when $0 < T < 100$ ℃, 5% of the room temperature value when $T > T_1 = 2/3$ of the melting temperature and a linear function of temperature in between i.e. 100 ℃ $< T < T_1$ (Zhu, et al., 2002). Zhu and Chao investigated an aluminium alloy, 5052-H32, and obtained results within 10% accuracy (Figure 3-7).

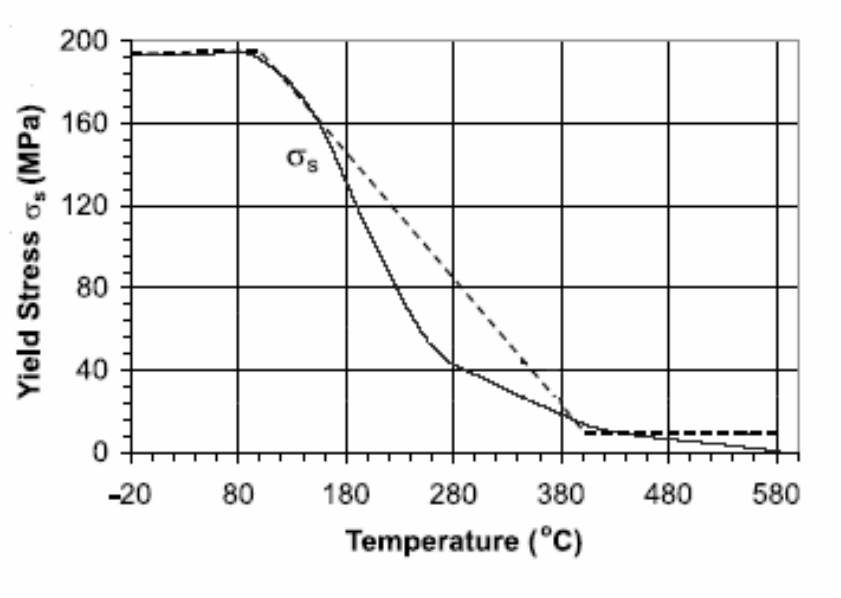

Figure 3-7: Zhu and Chao (2002) yield stress approximation for an Al alloy.

3.3.4 Alternative Material Property Methods

A problem in obtaining temperature dependent material data was that the available properties were below the melting point of the material. Material properties could change significantly with phase changes. Material properties at temperatures above the specified range were to be taken constant with the value at the highest given temperature. This assumption was tested for data that was available for SABS 300WA and Common Steel.

The property values for 300WA were taken to be constant for the temperature range of 1275 – 2000 ℃. This assumption proved to be valid for the thermal conductivity (Figure 3-8) but a significant difference in specific heat was noticed. The difference between the specific heats of the two steels at 2000 ℃ was 155 J/kg.K (24%). At 725 ℃ the specific heats differed with 517 J/kg.K. This was because the latent heat in the SABS 300WA data was taken into consideration, while the Common Steel data considered it separately. From these graphs it was decided to use the thermal properties of Common Steel for SABS 300WA even though there was a slight difference in chemical composition (Table 3-1).

Table 3-1: Chemical composition for 300WA and Common Steel.

	C [%]	Si [%]	Mn [%]	P [%]	S [%]
SABS 300 WA	0.22	0.5	1.6	0.04	0.05
Common Steel	0.17	0.55	1.6	0.04	0.04

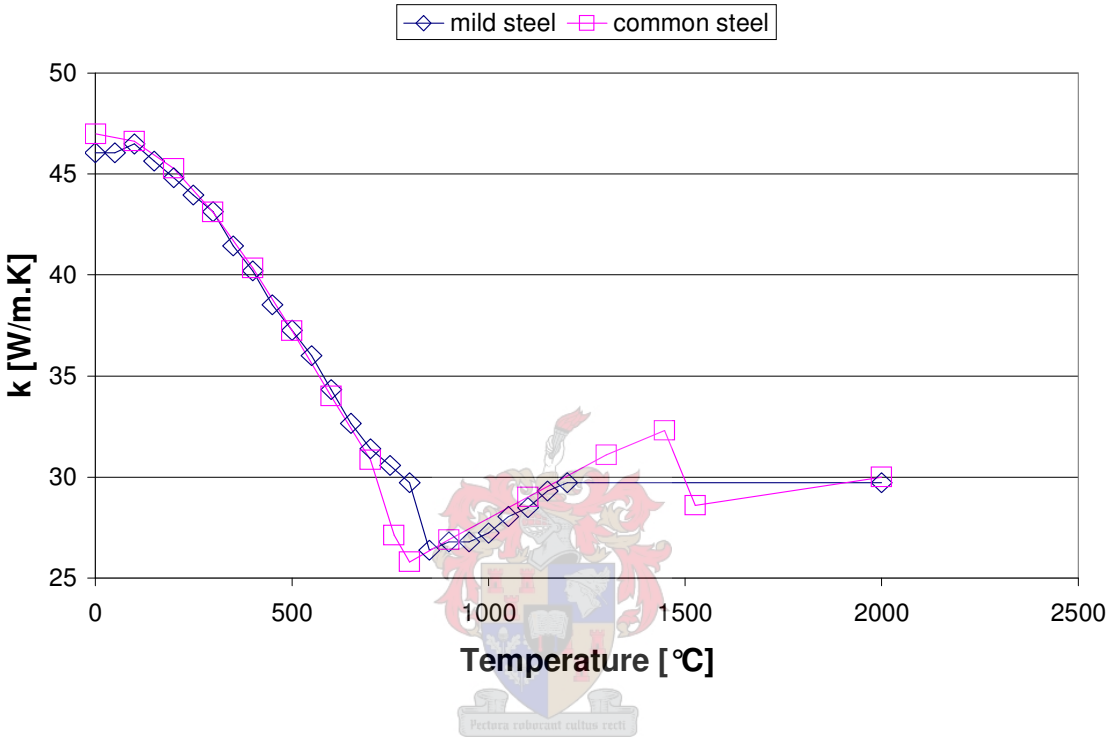

Figure 3-8: Thermal conductivity for 300WA and Common Steel (British Iron and Steel Research Association Metallurgy, 1953).

3.4 Conclusion

A literature study was carried out on the finite element modelling of welding. The use of two-dimensional analyses proved to be accurate within the assumptions made. Heat transfer is restricted to the plane perpendicular to the two-dimensional cross-section analysis while the temperature gradient through the plate thickness in an in-plane 2D analysis is assumed constant. A full three-dimensional model with a sufficiently fine mesh can model the heat flow as accurately as the errors in the material properties, geometry, heat input,

convection and radiation parameters permit. Two-dimensional analyses were performed to sort out general problems that occurred during welding modelling and helped in the design of the 3D modelling.

The modelling assumptions obtained from the literature survey were applied in the modelling in the thesis. It was assumed that the filler and base metal had the same material properties and the un-welded portion was stress free. Radiation heat losses only had an influence at melting point temperatures and were incorporated in combined convection and radiation heat loss boundary conditions.

A double ellipsoidal volume heat flux model proposed by Goldak (1983) was used in the weld modelling. The geometrical parameters used in the model were obtained from measuring the ripples and size of the weld beads in the experiments. The arc efficiency was not known and a value was chosen within the theoretical arc efficiencies available in the literature.

Temperature dependent material properties specified were for thermal conductivity, specific heat, Young's modulus, yield strength and thermal expansion. Temperature dependent material properties were hard to come by and alternative methods were used to obtain these properties. Material property approximations were used or material properties from metals with a similar chemical content were used.

The literature study covered all the aspects of the modelling parameters used in the weld modelling. The effect of material property values on the modelling results can be investigated in future research for various materials.

4 EXPERIMENTS

4.1 Introduction

The objective of this thesis was to create a finite element model of a welding process, but also to compare the modelling results with actual measured results in order to verify if the model was adequate for welding process investigation. Experiments with shielded metal arc welding on flat mild steel plates were carried out to investigate the effect of:

- restraints,
- plate thickness and
- welding current on the deflection of the plates.

The temperature distribution in the plates was also measured to verify the finite element analysis results.

The welding variables in the experiments were investigated with low, medium and high values. The medium values were taken from the standard experiment with the welding of 3 mm thick mild steel plate at a current setting of 90 A and a total of four clamps on the plates. The low and high values were chosen by giving the medium settings higher and lower values. Only one parameter was varied between experiments.

Welding experiments were carried out to investigate the effect on displacement results of changes in welding parameters. The experimental measurements focused on verifying the accuracy of the welding simulation and the ability to predict the distortion magnitude. Adequate information was obtained from the experiments to simulate the same setup within the finite element method (FEM).

4.2 Experimental Set Up

The welding parameters varied in the experiments were the number of clamps on the plates, plate thickness and the welding current used. Low, medium and high values were given for these parameters with the settings used in the standard experiment specified as the medium values. The standard experiment was the welding of a 3 mm thick mild steel plate with a current setting of 90 A and four clamps on the plates (Table 4-1).

Table 4-1: Values of the welding parameters used in the experiments.

	Low	Medium	High
Restraints [Amount of Clamps]	2	4	8
Plate Thickness [mm]	2	3	4
Welding Current [A]	70	90	110

The experiments were carried out on a welding jig that allowed clamping of the plates, gave a rigid support that was not influenced by the welding process and allowed uniform cooling on the top and bottom of the plates. The contact area between the plates and the jig were kept to a minimum to restrict contact heat losses, but still allowed a rigid support for clamping. The jig acted as a heat sink and the regions near the jig/plate interface cooled faster than in the middle of the plate. The contact heat transfer coefficient was not known and had to be determined through modelling.

A linear displacement transducer was used to measure the transient displacement of the plates during the welding and cooling of the plates. The transducer was placed in the middle of the plate on the far edge from the weld (indicated with black dot in Figure 4-3). The transient displacement results during welding and cooling of the plates were insignificantly small and not repeatable. These results were not used for comparison with the finite element analysis results.

The static displacement measurements for the first and last measurements were done with a dial displacement gauge on a high precision measuring table. The surface of the table was taken as the reference plane and all displacements were taken relative to the reference plane. The measurements were taken on an equally spaced 25-point grid marked on the plates (Figure 4-1).

Static displacement measurements were done at five stages of the experiment:

- before clamped to the jig,
- clamped to the jig before welding,
- after welding with all the clamps on the plates,
- after welding with one clamp on the plates and
- after the plates was removed from the jig.

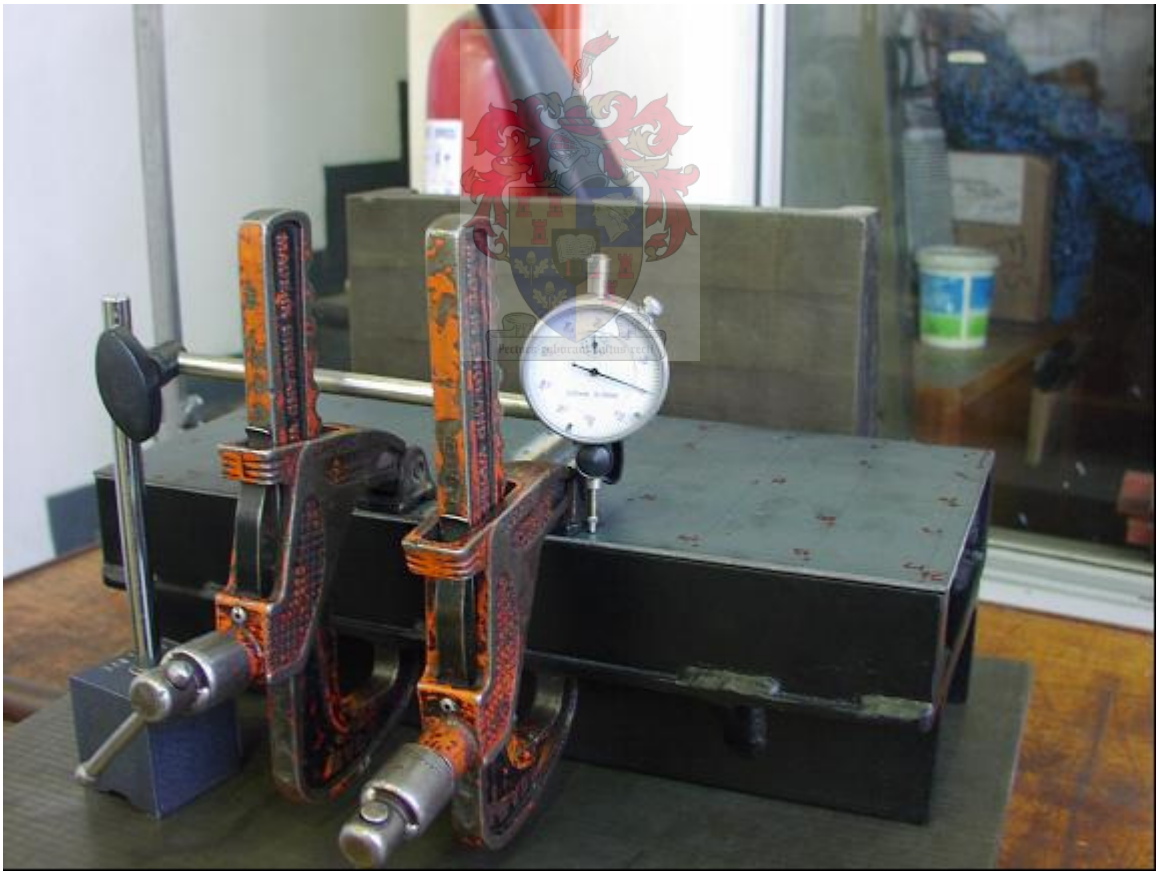

Figure 4-1: Measurement of welded plates with dial gauge on measuring table.

A reference point was used to measure the displacement of the plates on the welding jig. The displacements of the points on the plates were measured relative to the reference point. The point on the measuring grid nearest the last clamp removed from the plate was chosen as the reference point. This clamp was referred to as the reference clamp. Measurements had shown that the removal of the other clamps during the experiment had an insignificant effect on the displacement of the reference point. This proved that the reference point was rigid and was assumed absolute zero throughout the experiment.

The voltage of the welding process was measured over the welding cables and recorded on a data logger. The welding current in the welding cables was measured with a current clamp. These measurements were used to calculate the power and heat input of the welding process.

4.3 Effect of Restraints

4.3.1 Introduction

The amount of restraint on a weldment determines the distortion control and residual stress. The less restrained models give high displacements but low residual stresses. With an increase in restraints, the displacements decrease while the residual stresses increase. The effect of the degree of clamping on the distortions and plastic strains on a welded structure could be seen in Figure 4-2.

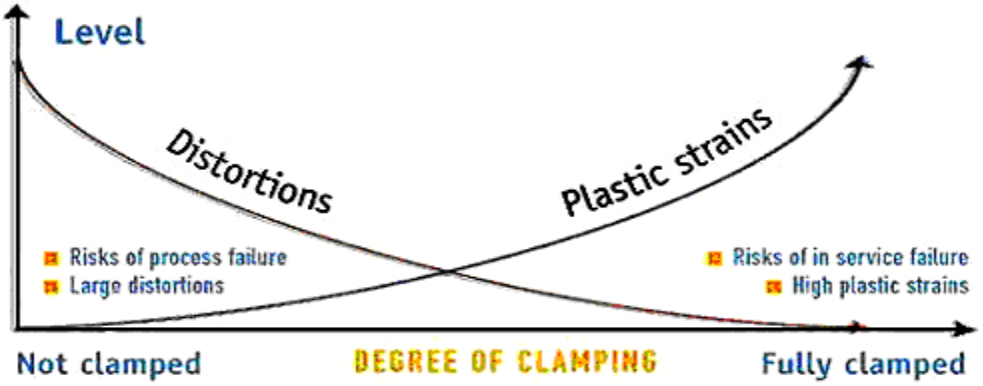

Figure 4-2: Distortion and plastic strain vs. clamping (www.esi-group.com)

The clamping configuration of a weldment will determine the balance between distortions and residual stresses. With optimised welding sequence the distortion of a welded structure can be controlled but the maximum residual stresses due to welding will remain the same (Tsai, et al., 1999). Under conditions of extreme constraint most welds will fail due to cracking. In the case of minimal restraining, distortions of components can lead to large and misaligned gaps, which in turn cause sub-standard welds. The degree of restraint is a function of the type of joint, the rigidity of the structure, the amount of gap between the abutting edges and the plate thickness. Maximum restraint is obtained when a weld of small cross-section joins two rigidly clamped thick plates, whilst minimum restraint occurs in a weld of relatively large cross-section (Lancaster, 1965).

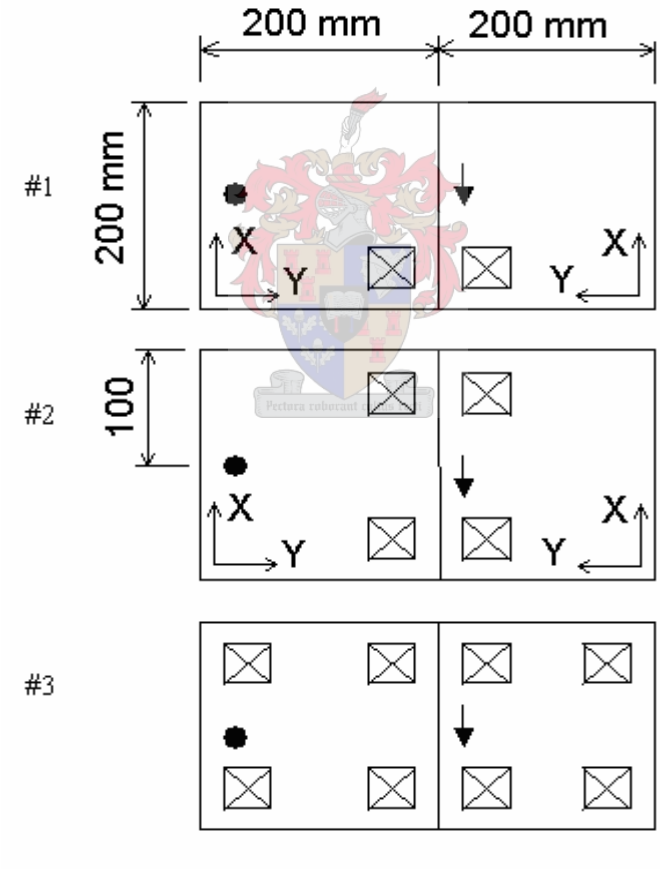

Figure 4-3: Clamping configurations investigated in experiments.

From the abovementioned definition, the 3 mm thick plate weld was considered a minimal restraint weldment. The restraints on the plates were varied with the change in amount of clamps on the plates. Three levels of restraints were investigated: two, four and eight clamps in total on the welded plates. Figure 4-3 shows the clamping configurations and direction of welding.

4.3.2 Results

The welding in the two-clamp experiment (#1 in Figure 4-3) started at the end with no clamps and was welded towards the edge with the clamps. This only prevented movement of the plates at the end of the weld but the plates were free to move at the beginning of the weld. This caused misalignment of the plates and extreme distortion in one plate during welding (Figure 4-4).

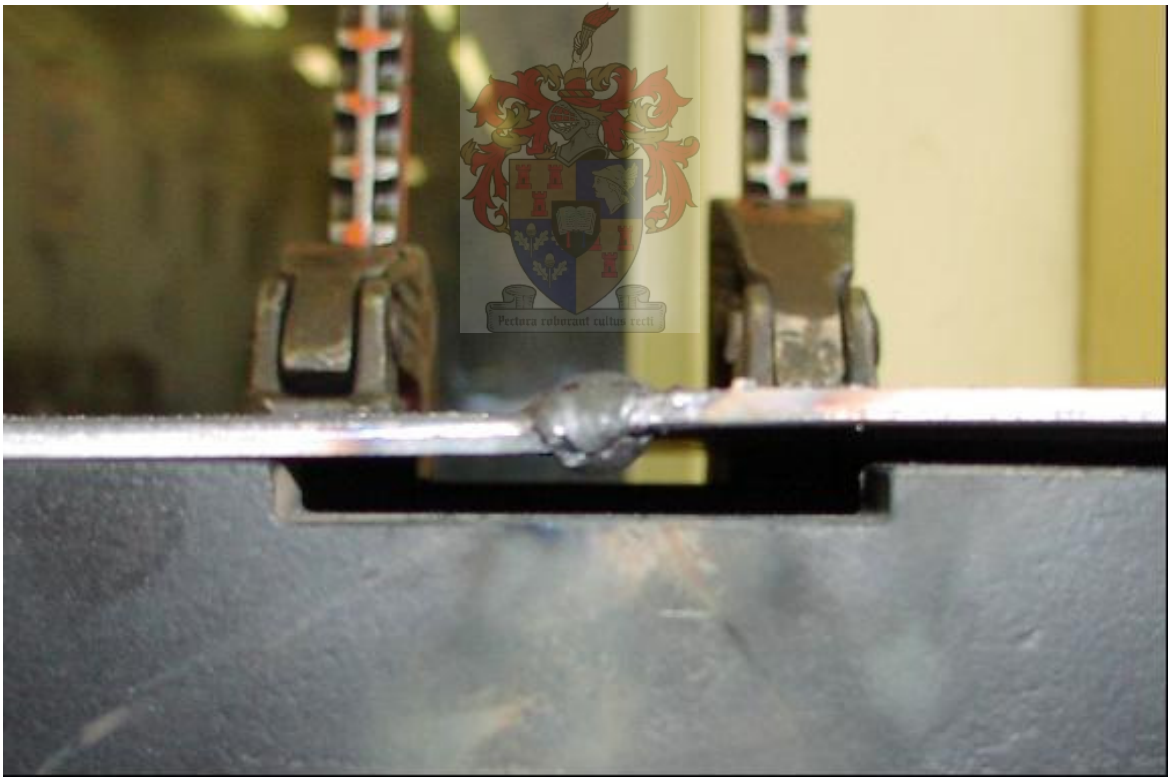

Figure 4-4: Excessive distortion of welded plates due to misalignment.

The large welding distortions that occurred with the plate misalignment could be explained as the contraction forces that formed a couple-moment during contraction. The one plate was subjected to more filler metal than the other, resulting in a larger contraction force in the one plate and created a moment around the weld (Figure 4-5).

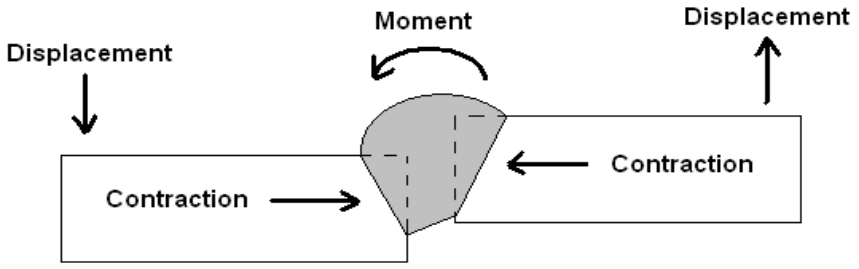

Figure 4-5: Welding distortion theory due to plate misalignment.

The displacement magnitudes for the two-clamp experiment were significantly random but the trends observed were similar. The plates deflected upwards away from the clamps and weldment. The randomness in magnitude of displacement could be attributed to the difficulty in controlling the welding with the plate movement. In the four- and eight-clamp experiments, the misalignment and movement of the plates were controlled.

The displacement measurements of the plates after welding but before the removal of the clamps had shown that the two-clamp experiment deflected the most, while the distortion in the four-clamp and eight-clamp experiments were insignificant (Figure 4-6). The abscissa in Figure 4-6 shows transverse distance with the origin of the graph being the edge furthest from the weld and the 200 mm on the graph axis, the weld centreline.

The plates in the four- and eight-clamp experiments distorted significantly and to a similar extent after the removal of all the clamps with the maximum deflections

at the weld (Figure 4-7). The two-clamp experiment was slightly bended upwards away from the weld. The large distortion of the plates in the four- and eight-clamp experiments showed that high residual stresses were present after welding. With the removal of the clamps there was no resistance to the residual stresses and the plates distorted.

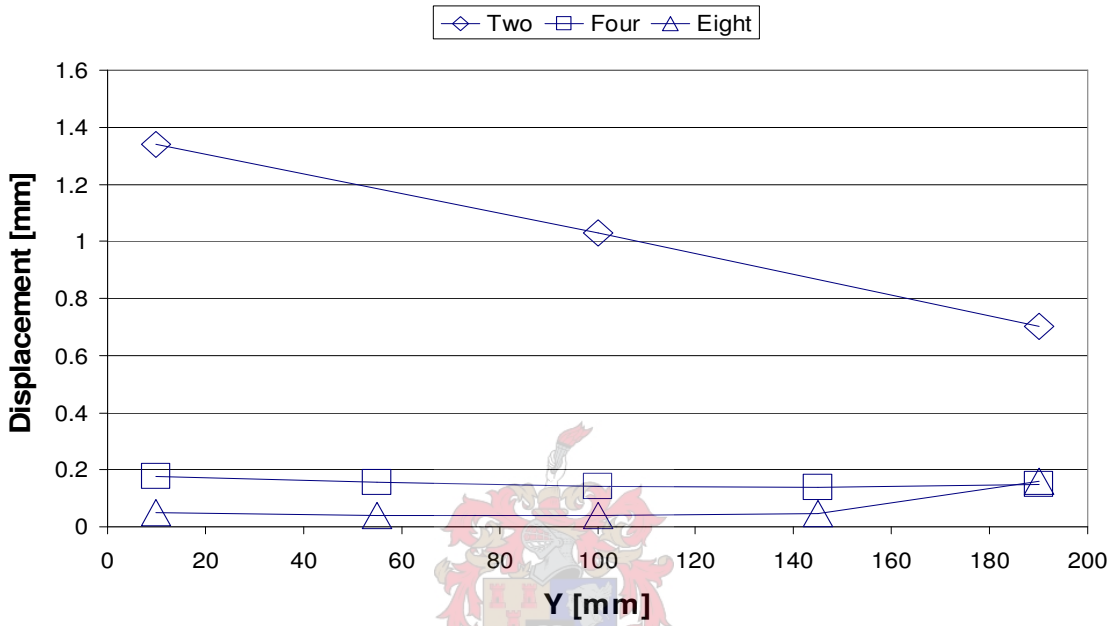

Figure 4-6: Transverse displacement in middle of plate after welding but before the removal of the clamping for different clamp settings.

The difference in distortion between the four- and eight-clamp experiments were insignificant and suggested that the use of more than four clamps on the plates were not necessary for this experiment. The restraints controlled the distortion of the plates during welding but could not control the final distortion after the removal of the clamps.

4.4 Effect of Plate Thickness

4.4.1 Introduction

The effect of plate thickness on plate distortion with constant welding current setting was investigated. The plate thickness had a significant effect on the

magnitude of plate distortion with the thinner plates experiencing the largest distortions. This phenomenon can be explained in terms of the thinner plates being lighter in mass and less in bending stiffness. This means that thinner plates are more likely to welding distortion than thicker plates.

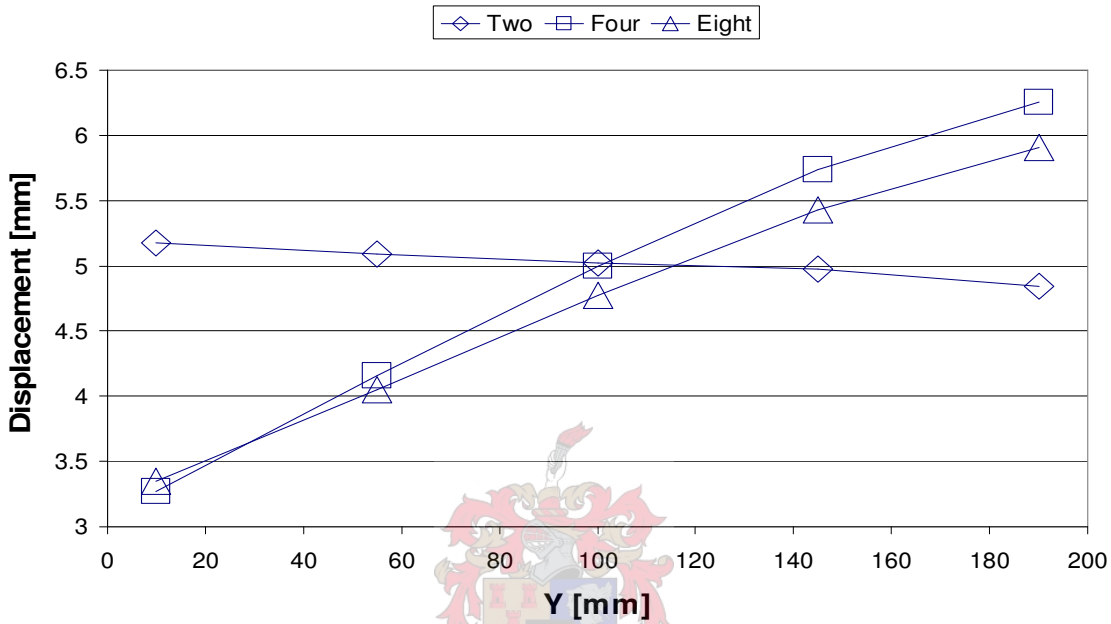

Figure 4-7: Transverse displacement in the middle of the pate after removal of clamps.

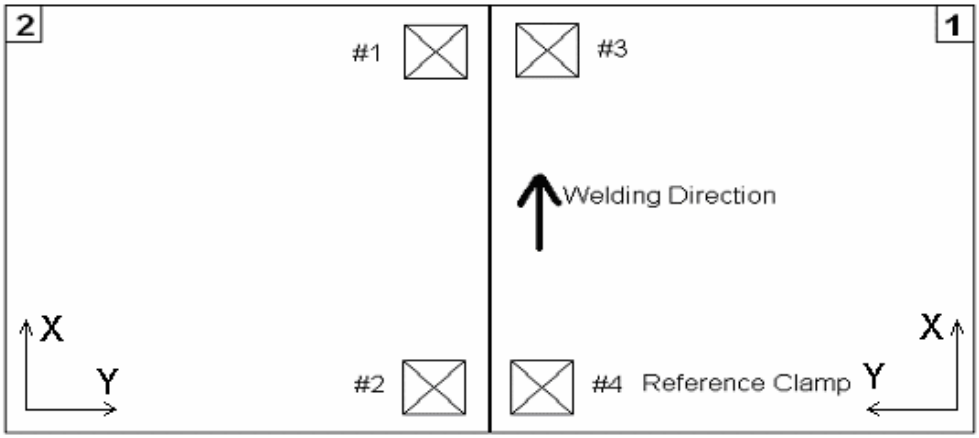

Figure 4-8: Order of the removal of clamps.

The experiment was done on 2, 3 and 4 mm thick mild steel plates. Four clamps in total, two on each plate, were used and a welding current of 90 A was used. The clamps in every experiment were removed in a specified order ending with the reference clamp. The order of removal of the clamps is shown in Figure 4-8. This procedure ensured repeatable experimental results.

4.4.2 Results

To avoid burning through of the plates, the welder increased the welding speed with the thinner plates. The change in welding speed did not have an effect on the current or voltage of the welding, thus the power output remained constant at around 2157 W (Table 4-2). The average welding current and voltage for the experiments were 85.76 A and 25.25 V respectively, giving an error of 4.7% for a current setting of 90 A. The assumption of 25 V for the voltage of the process proved to be an accurate assumption for the 90 A setting on the machine.

The average welding speed for the 2 mm thick plate was 5.53 mm/s, which was significantly faster than the 3.71 and 3.26 mm/s for the 3 and 4 mm thick plates respectively. The overall welding length for the 4 mm plate was shorter due to the fact that the electrode was consumed before the end of the plates.

Table 4-2: Average welding process parameters for different plate thickness.

	Power [W]	Current [A]	Voltage [V]	Time of weld [s]	Weld Length [mm]	Weld Speed [mm/s]
2 mm	2161.33	86.06	25.20	36.25	199.00	5.53
3 mm	2154.36	83.99	25.75	54.02	200.00	3.71
4 mm	2156.68	87.23	24.80	53.92	175.67	3.26
Ave	2157.46	85.76	25.25	48.06	191.56	4.17

Table 4-3: Energy input parameters for different plate thickness.

	Energy [J]	P/v [J/mm]
2 mm	78348.21	390.84
3 mm	116378.53	580.69
4 mm	116288.19	661.56
Ave	103671.64	544.36

The energy input determined the heat input into the weldment. Table 4-3 shows the total energy in Joule and energy per unit length in Joule per millimetre. The total energy was calculated from the product of the power and time of welding (Equation 4-1). The total energy for the 3 and 4 mm (116 kJ) plates were almost the same while significantly less energy was used for the 2 mm thick plate (78 kJ). The welding processes could not be compared on grounds of total energy input because the length of the welds was not the same for all of the experiments.

$$P = VI$$ Equation 4-1

The energy per unit length gave a better indication of the difference in heat input of the welding process and was calculated with the power divided by the welding speed (Equation 4-2). It was assumed that the power remained constant for the experiments and the welding speed were the only variable. An increase in welding speed resulted in less energy per unit length. This meant that the 2 mm thick plate had 41% less heat input than the 4mm thick plates (Table 4-3. Even with less heat input the 2 mm plate distorted more than the thicker plates.

$$E_l = \frac{P}{v}$$ Equation 4-2

Wells developed approximations for the relationship between heat input and the product of the welding speed and weld width divided by the thermal diffusivity of

the metal (cited by Lancaster, 1965). Equation 4-3 shows this relationship for the 2D case where the weldment had fused through the thickness of the plate. It was assumed there was no temperature gradient through the thickness of the plate.

$$\frac{q}{h} = 8kT_m\left(\frac{1}{5} + \frac{vd}{4\alpha}\right) \qquad \text{Equation 4-3}$$

Equation 4-3 shows that for a given plate thickness, h, a minimum rate of heat input is required in order to make a full penetration weld. This was considered the optimum welding heat input requirement for a given plate thickness and base material. Figure 4-9 shows the theoretical heat input as determined with Equation 4-3 compared with the measured heat input in the experiments. From Figure 4-9 it can be seen that the heat input for the 3 mm thick plate was at the optimum value while the 2 mm plate lay above the theoretical value and the 4 mm plate below the line. This meant that the welder used the optimal current settings and welding speed for the 3 mm thick plate. The heat input used for the 2 mm thick plate were above the optimum values and explains the almost burning through of the plates during welding. The graph in Figure 4-9 shows that more heat could be put into the 4 mm plate to obtain a weld through the thickness of the plate.

The comparison of Equation 4-3 with the measured values proved that the human welder operated at optimum conditions and had the ability to adjust the welding process for different welding situations. The heat input values for the standard 3 mm thick plate were repeatable. The spreading of the heat input for the 2 mm thick plate could be attributed to difficulty controlling the welding at high speeds.

The distortions of the welded plates increased with a decrease in plate thickness. The displacement trends for the 2 and 3 mm plates were the same while the 4 mm plates showed little distortion. The maximum displacement recorded for the 2, 3 and 4 mm plates were 7.52, 5.18 and 1.27 mm respectively. All three the maximum displacements were recorded at the coordinates X = 190 mm and Y =

190 mm, the point closest to where the weld was finished (see Figure 4-10). The clamps closest to these maximum points were released first after welding. The 2 and 3 mm plates distorted much more than the 4 mm plate, even though more energy was put into the 4 mm plate.

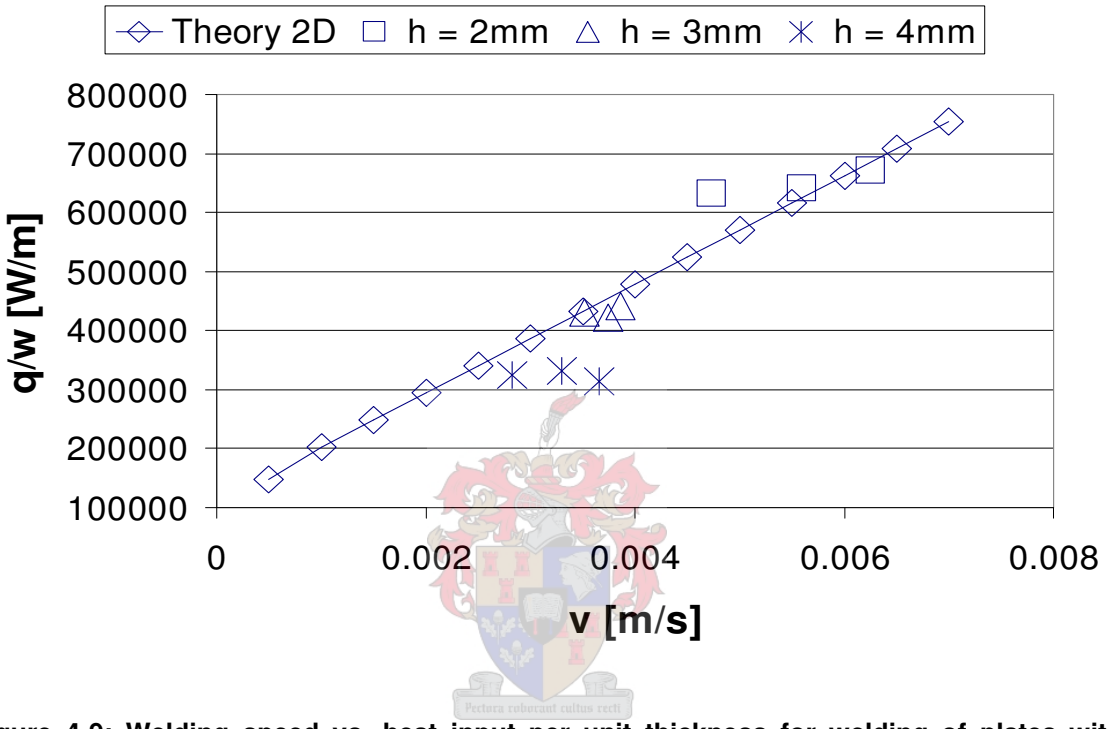

Figure 4-9: Welding speed vs. heat input per unit thickness for welding of plates with different thickness.

The location of the maximum deflection at the edge where the weld finished could be due to the lack of heat dissipation near the edge of the plate. During welding the heat flow away from the weld occurred through conduction of the steel. Near the edge of the plate the amount of material in front of the welding was less, thus a decreasing heat sink effect. This caused the plates to be the hottest at the end of the weld and in turn creating larger distortions.

The plate deflection on a line perpendicular (transverse) to the weld in the middle of the plate is shown in Figure 4-11. The 2 mm thick plate had the greatest deflection near the weldment (Y = 190 mm) while the 4 mm plate had relatively

no displacement. The 3 mm plate experienced moderate deflection compared to the 2 mm plate, with a maximum displacement of 3.15 mm at the weldment.

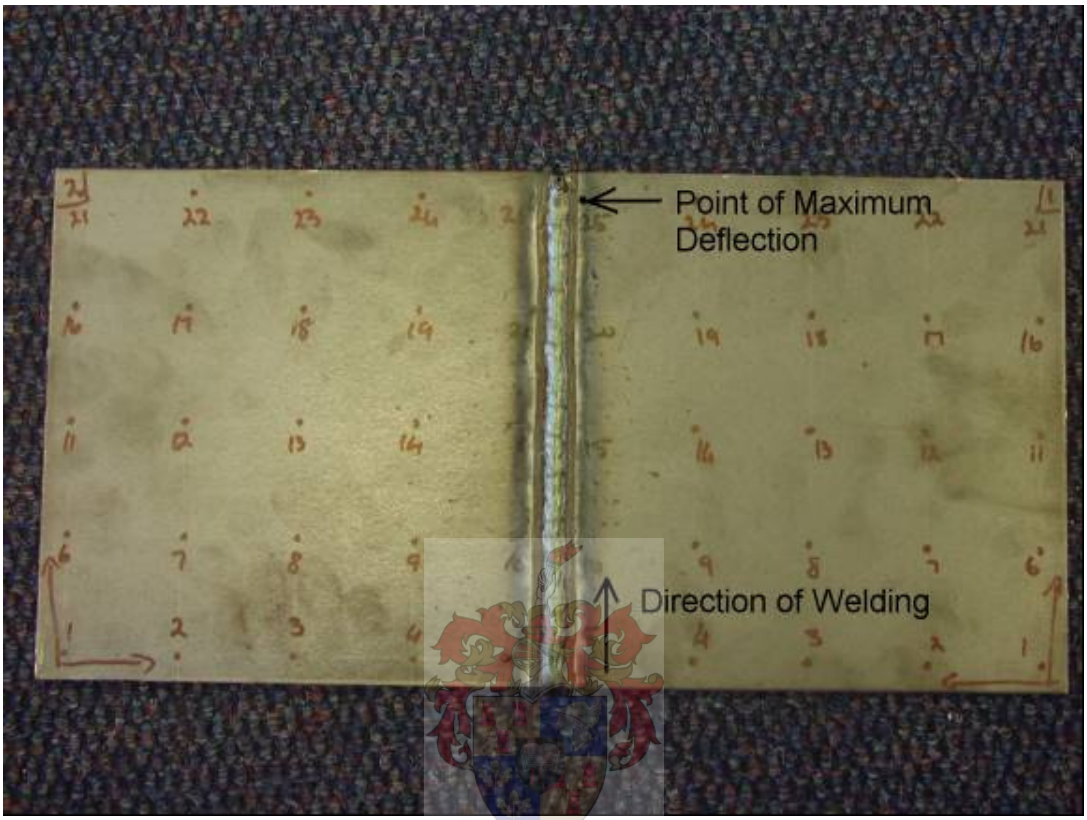

Figure 4-10: Point of maximum deflection for welded plates in the experiments.

The deflection of the plates on a line parallel (longitudinal) to the weldment at a distance of 10 mm from the weld on the side opposite to the reference clamp are shown in Figure 4-12. The deflection of the 2 mm plate showed the familiar longitudinal bending-up of the plates at the edges. This phenomenon occurred due to heat being dissipated at a slower rate at the edges than in the middle of the plate. This effect was observed for the 3 and 4 mm thick plates but to a lesser degree.

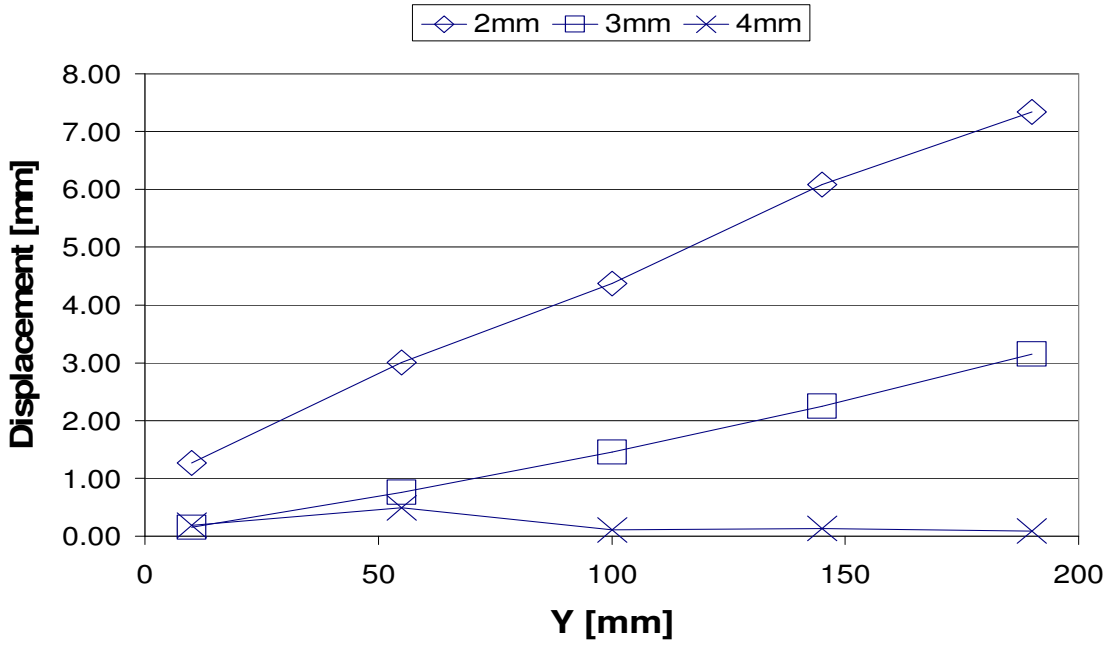

Figure 4-11: Transverse displacement for different thickness after removal of clamps.

The plates deflected the most after the last clamp (reference clamp) had been removed from the plates. During the removal of the other three clamps the plates showed minimal distortion. This plate deflection occurred due to the welding induced residual stress that caused the deflection of the plates when the restrictive forces of the clamps were removed.

The displacements of the plates with only the reference clamp on the plates at the locations as shown in Figure 4-11 and Figure 4-12 are shown in Figure 4-13 and Figure 4-14 respectively. The 2 mm thick plate showed large deflection with only the reference clamp on the plates, while the 3 and 4 mm plates experienced little deflection. In Figure 4-14 the plates deflected the most at the edge of the plate where the first clamp was removed and the deflection decreasing up to the location of the reference clamp (Y = 10 mm).

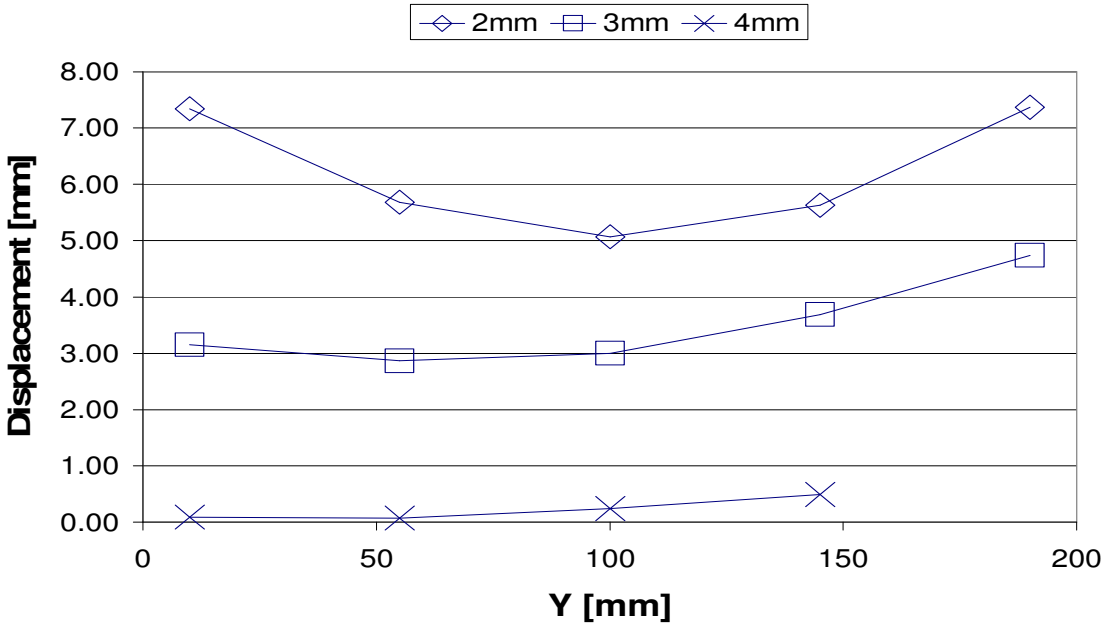

Figure 4-12: Final longitudinal displacement for different plate thickness, after removal of all clamping.

The results from the experiment had shown that the plate thickness had a greater influence on the plate distortion than the energy input per unit length. The 2 and 3 mm thick plates had full penetration welds, while the 4 mm thick plate did not have a full penetration depth. From Equation 4-3 it was seen that the 2 and 3 mm plates were welded at optimal energy input and the 4 mm thick plate below the optimal energy input value.

The excessive distortion of the 2 mm plate could be attributed to two factors. Firstly, the thinner plate had less bending stiffness and less weight to resist the deflection of the plates and secondly the 2 mm thick plates experienced the maximum heat input, without burning through, causing excessive distortion.

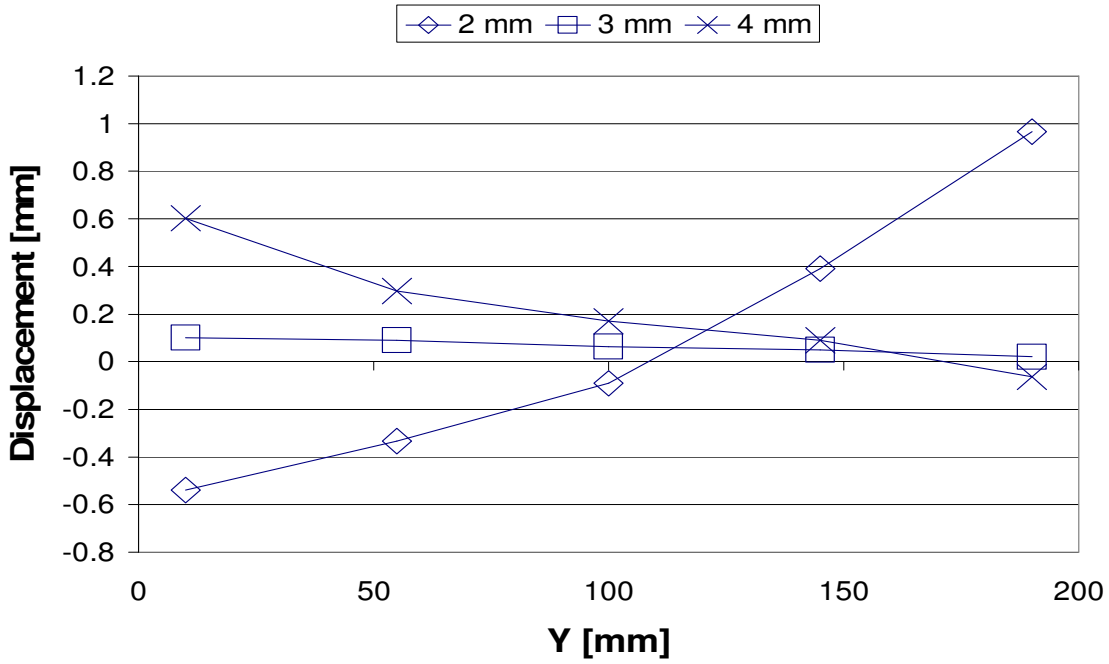

Figure 4-13: Transverse displacement for different plate thickness with only reference clamp on plates.

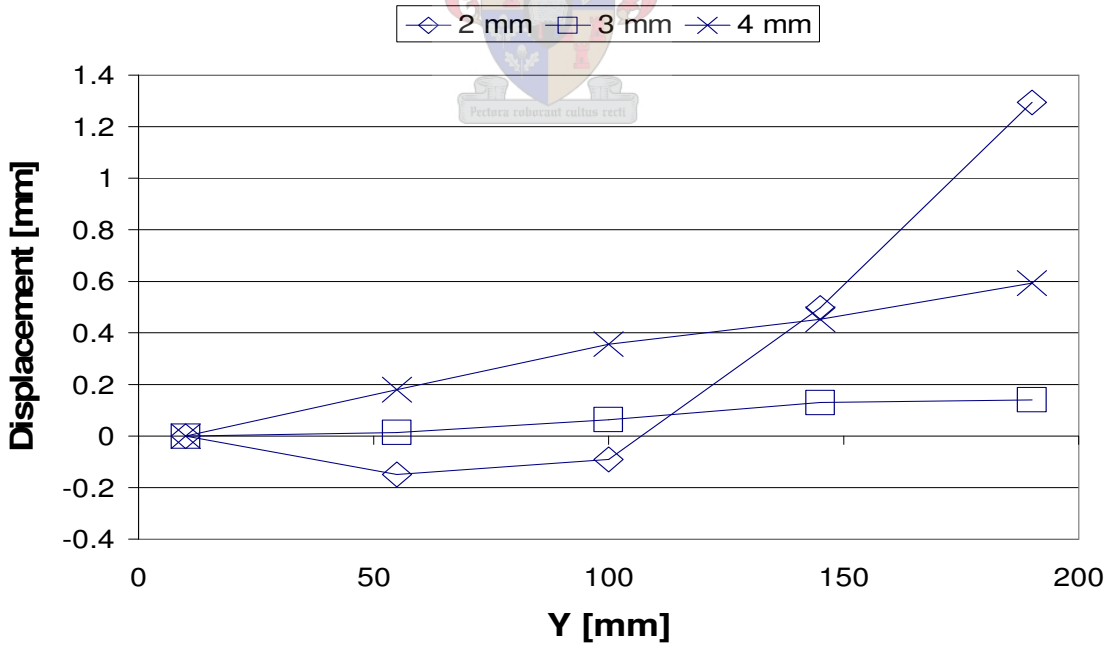

Figure 4-14: Displacement of plates with reference clamp: longitudinal displacement.

4.5 Effect of Current Setting

4.5.1 Introduction

The effect of plate displacement with different electric current settings was investigated on the 3 mm mild steel plates. Welding current settings of 70, 90 and 110 A were investigated. The experiments were compared on final plate displacement, power input and energy per unit length.

The increase of welding current means an increase in power and heat input. The change in welding power was investigated to determine the influence on plate distortion. With an increase of heat input, larger deflections were expected if all other welding parameters remained the same. Since the welder was free to change welding speed with different current settings, the heat input per unit length did not increase with the current, as was expected.

4.5.2 Results

The amount of heat input gave an indication of the expected distortion: more heat input meant more plate distortion. The heat input is increased by increasing the welding current, but the welder succeeded in keeping the energy input constant by changing the welding speed. The average calculated energy per unit length for nine experiments was 556 J/mm (Table 4-5). The average measured current for the 70, 90 and 110 A settings were 70.66, 83.99 and 104.19 A (Table 4-4). The lower measured welding current for the 110 A setting could have been caused by the rapid increase in temperature of the welding electrode since the specified current for the electrode used was 69 – 95 A. An increase in electrode temperature caused an increase in electrical resistance and a drop in current.

Table 4-4: Average welding process parameters for different current settings.

	Power	Current	Voltage	Time	Length	Speed
70 A	1716.89	70.66	24.39	64.54	199	3.10
90 A	2154.36	83.99	25.75	54.02	200	3.71
110 A	3008.62	104.19	28.76	35.62	200	5.64
Ave	2293.29	86.28	26.30	51.39	199.67	4.15

Table 4-5: Average energy input parameters for different current settings.

	Energy [J]	P/v [J/mm]
70 A	110808.08	553.84
90 A	116378.53	580.69
110 A	107167.04	533.44
Ave	111451.22	555.99

The 110 A current setting gave the least plate deflections and the 90 A setting the highest. In the case of the 70 A setting low power was available from the machine and the welder had to decrease the welding speed to obtain a sufficient bond. With the high power input from the 110 A setting the welder increased the welding speed to prevent burning through of the material. This adjustment of the welding speed by the welder had resulted in the 110 A setting to have the lowest heat input per unit length and the 90 A the highest (Table 4-5).

The maximum plate deflections measured for the 70, 90 and 110 A setting was 4.01, 4.74 and 2.49 mm respectively. Figure 4-15 shows the transverse displacement at a distance 190 mm from the start of the weld. The 110 A setting had by far the least deflection while the 70 and 90 A setting had similar displacement results.

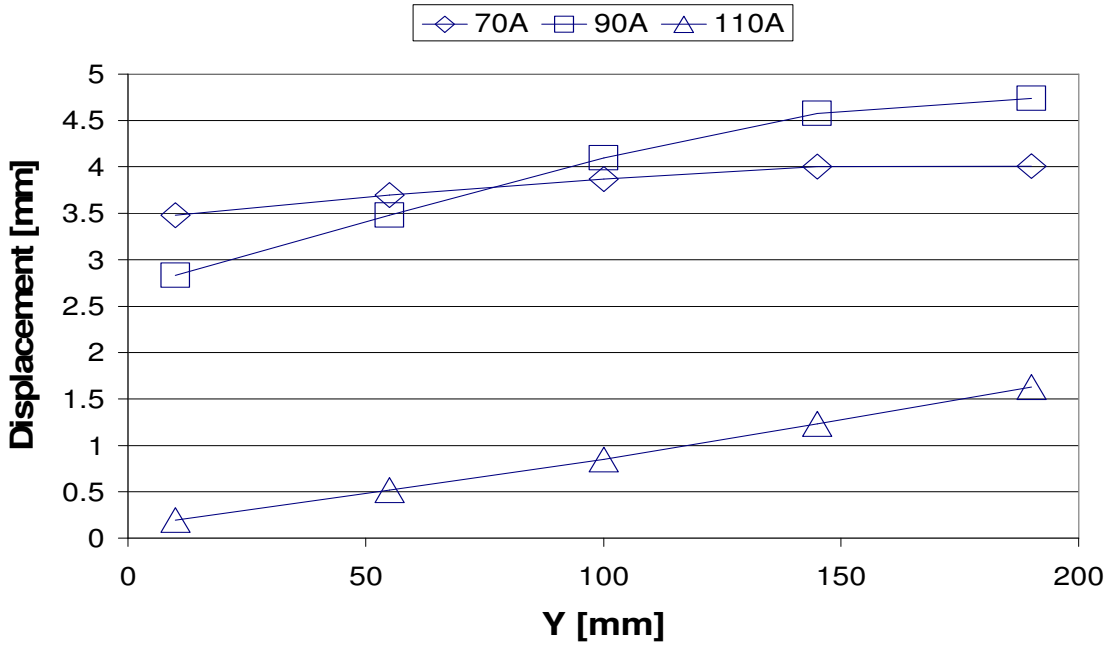

Figure 4-15: Transverse displacement for different current settings after clamp removal.

The maximum displacement for the experiments was close to the weldment at the edge of the plate where the welding stopped. This was similar to the other experiments where the clamping effect and plate thickness were investigated. The deflection of the plate decreased away from the weld.

The longitudinal deflection of the plate at a distance 10 mm from the weld is shown in Figure 4-16. Similar deflection tendencies were observed as with the previous experiments. The plate deflected more at the edge of the plate giving the plate a parabolic shape in the longitudinal direction of the weld. The maximum deflection was at the edge where the welding stopped. The deflection for the 110 A weld was less in magnitude but had a symmetrical parabolic shape.

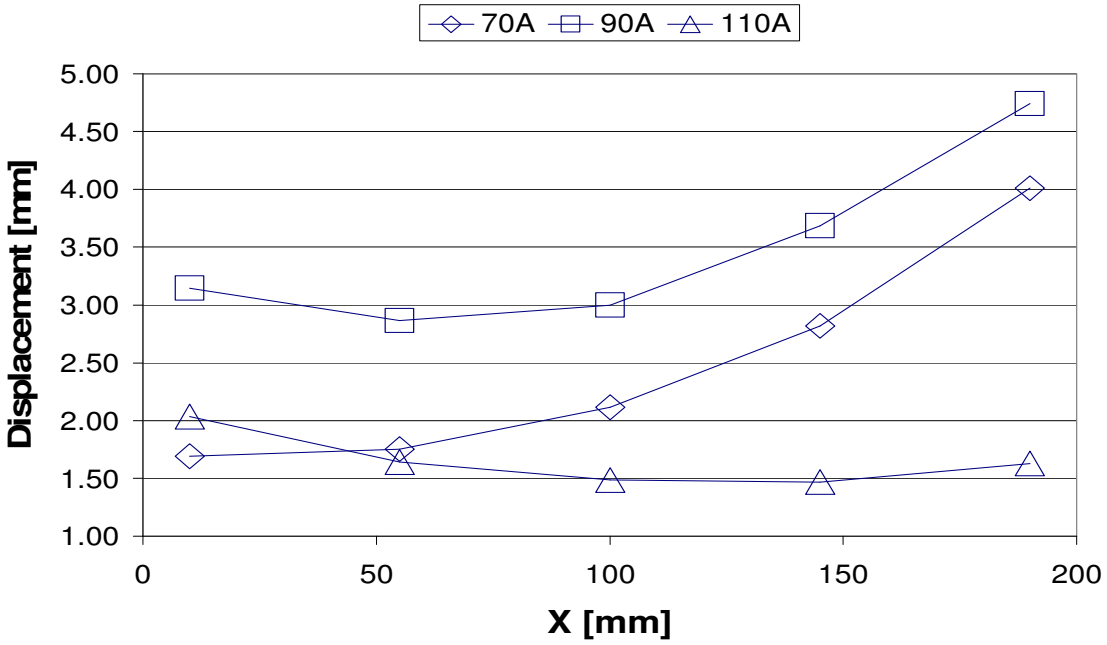

Figure 4-16: Final displacement for different current settings, longitudinal displacement.

The smaller deflections observed for the 110 A current setting could be attributed to lower heat input per unit length caused by higher welding speeds. Full penetration welding was not achieved along the whole length of the plate for the 110 A setting. This could have resulted in smaller contraction forces than for the 90 A settings where full penetration was achieved. The slow welding speed for the 70 A setting resulted in better penetration and heat distribution than the 110 A setting, even though the welding machine were operating at less power (Table 4-4).

The heat input was at its highest for the 90 A setting because the welding electrode could operate normally and the plate thickness was sufficient to absorb the heat input without burning through. The plate deflection was the most for the 90 A setting but the weld strength was the best due to better edge penetration.

4.6 Temperature Measurement

4.6.1 Introduction

The first step in creating a scientific base for the design and analysis of welds is to accurately compute the transient temperature fields. The high temperatures developed by the localised heat source cause significant metallurgical changes in low carbon steels. The measured temperatures were used to determine the temperature distribution in the plates for the experimental set up and to verify the FEM temperature results with the experiments. The experiment was repeated three times with the same settings and conditions to investigate the repeatability of the results.

The thermocouple is the most common method used to measure temperature. This is due to the fact that it is cheap, interchangeable and can measure a wide range of temperatures. A thermocouple consists of two wires of different metals that are joined at one end. A change in the temperature at the connection of the two wires will induce a change in the electromotive force (EMF) between the open ends. As the temperature changes, the EMF will change. Often the thermocouple wires are located inside a metal or ceramic shield that protects it. The most commonly used thermocouple type for measuring high temperatures is the type K. It has one wire of nickel-chromium and one of nickel-aluminium.

Nine K – type thermocouples with a diameter of 0.5 mm wire, spot-welded onto the plates at locations shown in Figure 4-17. The objective of the layout of the thermocouples was to obtain temperature trends in the planes transverse and longitudinal to the weld line. The temperature data was recorded with a HP 34970A data acquisition unit at one-second intervals for every thermocouple.

The thermocouples were placed in rows transverse to the weldment at distances 20, 50 and 150 mm from the weldment and in longitudinal direction at distances 30, 50 and 100 mm from the start of the weld (Figure 4-17). The first row of

thermocouples (X = 30) was close to the welding jig/plate interface. The temperature results from these thermocouples were compared with the other temperatures at the other thermocouples to determine the heat sink effect of the jig.

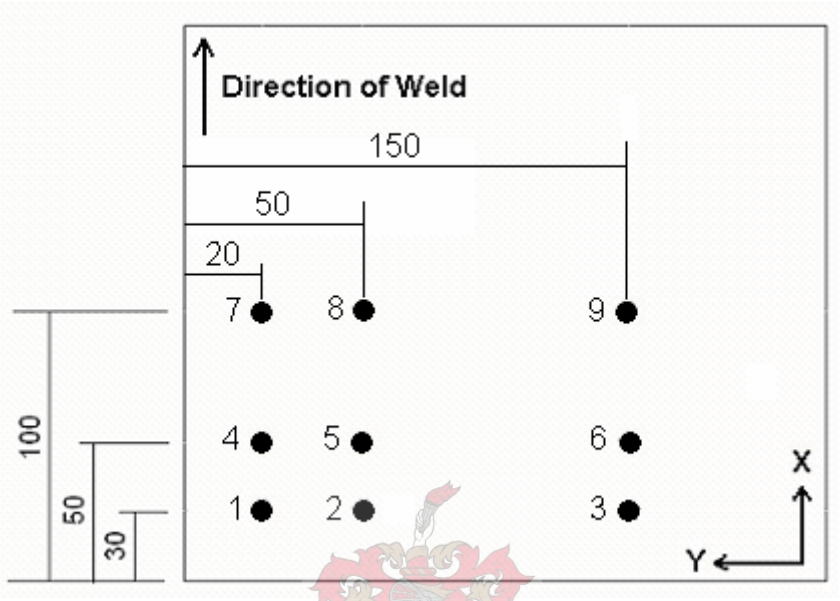

Figure 4-17: Thermocouple locations on welded plates.

The spot welding of thermocouples to a plate proved to be a sufficient bond, but there was a problem with the wires that broke off easily at the spot weld. This was solved by attaching the wires to the plate for a distance with an adhesive bond to prevent a direct pull on the wires at the spot weld.

TIG welding was used to fuse the thermocouple wires in an inert gas environment. The wires were fused into a small lump which was then spot welded to the plate (Figure 4-18). Care was taken to ensure that the wires did not make contact outside the spot weld. The thermocouples were located underneath the plate, at the opposite face of the weld bead to minimize radiation disturbance effects from the arc and the environment. It was assumed that the temperature difference through the thickness of the plate was negligible.

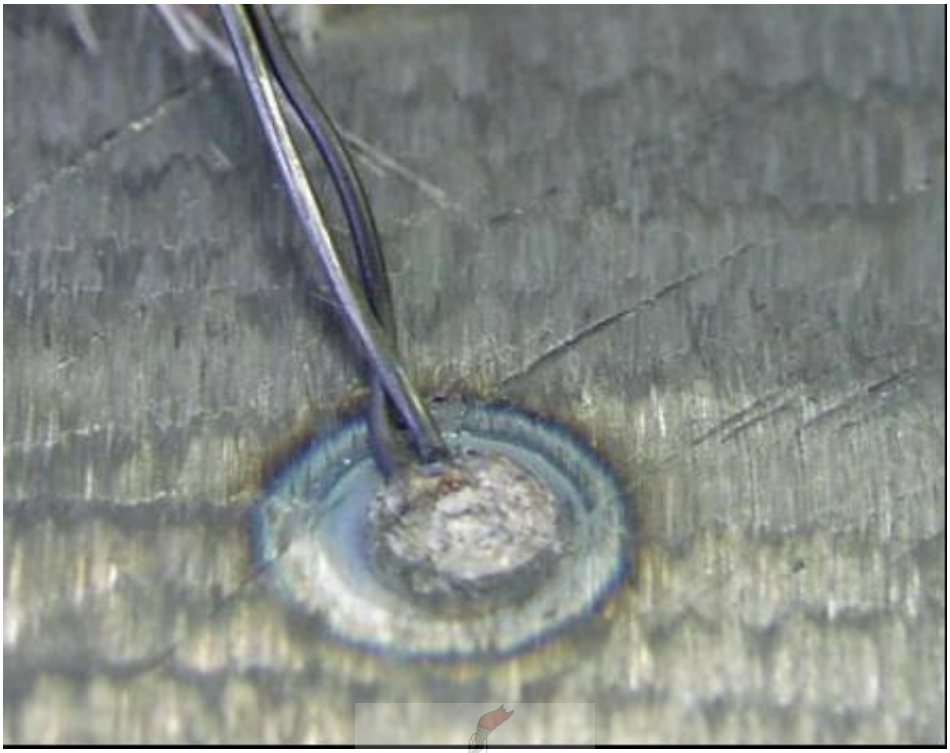

Figure 4-18: Thermocouple spot-welded to mild steel plate.

4.6.2 Results

A thermocouple measures the temperature at the first contact between the two wires (Dally, Riley & McConnell, 1993). The contact point of the thermocouple wires was inside the spot weld and the distance of the spot weld to the centre of the weld was measured. High spatial temperature gradients existed near the weld and it was therefore important that the placement of the thermocouples had to be accurate and repeatable for the three experiments.

The measured distances from the centre of the weld to the contact point of the thermocouple is shown in Table 4-6. The average error in distance of the measuring point relative to the specified point for the thermocouple was 1.6 mm. The average error for the thermocouples 20 mm from the weld was 1.3 mm. This was an acceptable tolerance level and it was assumed that the thermocouples measured temperatures at the same distances from the weld in the three experiments. The true distance of the thermocouples were used in the modelling.

Table 4-6: Distance of thermocouple measuring point to centre of weld.

	Distance of thermocouple contact from centre of weld								
Point	1	2	3	4	5	6	7	8	9
Specified Distance	20	50	150	20	50	150	20	50	150
Experiment									
#1	18	48	148.5	18	47	148	17	46	148
#2	21	53	149	21	51	152	20	50	151
#3	22	52	152	20	51	153	21	49	151
Average	20.3	51.0	149.8	19.7	49.7	151.0	19.3	48.3	150.0

The highest temperature variation was measured at the thermocouples located at X = 100 mm, the centreline of the plate perpendicular to the weld. The thermocouples close to the jig/plate interface (X = 30 and 50 mm) recorded lower temperatures. The welding rig acted as a heat sink, which lead to faster cooling of the plate near the welding rig. A difference of 41.4 °C was measured for the maximum temperatures at the thermocouples 20 mm from the weld at 30 and 100 mm from the initial weld position (Figure 4-19). At 50 mm from the weldment the difference of ΔT = 54 °C was bigger than at 20 mm from the weld.

The maximum temperatures measured at the thermocouples compared significantly well with the analytical solution proposed by Rosenthal. The temperatures from the analytical solution were higher because convective and radiation heat losses are not taken into consideration and constant material properties were assumed.

The temperatures were the highest at the centre of the plate, furthest away from the jig. In the second experiment the temperatures close to the jig, X = 30 and 50 mm, were higher than for the first and third experiment. The clamps were not fastened as tight in the other experiments and the contact heat

transfer coefficient between the plate and jig was thus lower, resulting in higher temperatures. The clamping force was not measured and was initially not considered important in the temperature measurement experiment. From the experiments it was clear that the contact pressure due to clamping had a significant effect on the temperature distribution.

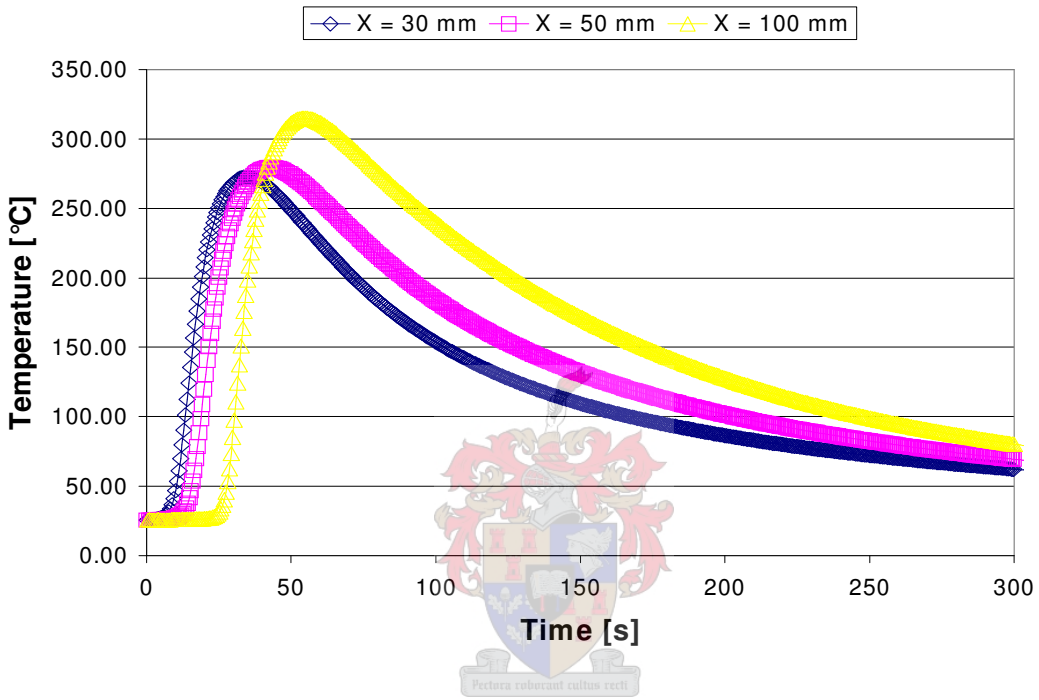

Figure 4-19: Maximum temperatures of thermocouples at distance 20 mm from weld.

The average percentage in maximum temperature difference between the thermocouples in the three experiments was 3.04%. Little difference in results could be seen for the temperature distribution graphs at a distance 20 mm from the weld in the middle of the plate (Figure 4-21). The repeatability of the temperature measurements for the three experiments was excellent and could be used for verification with FEM results.

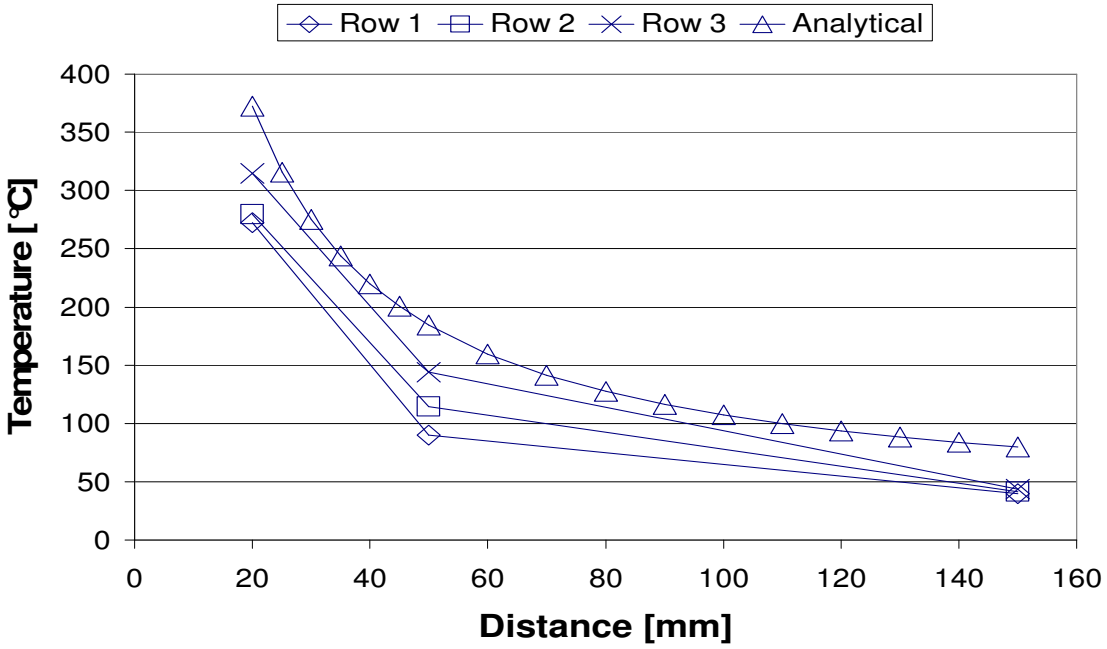

Figure 4-20: Comparison of maximum temperatures in transverse line with analytical solution.

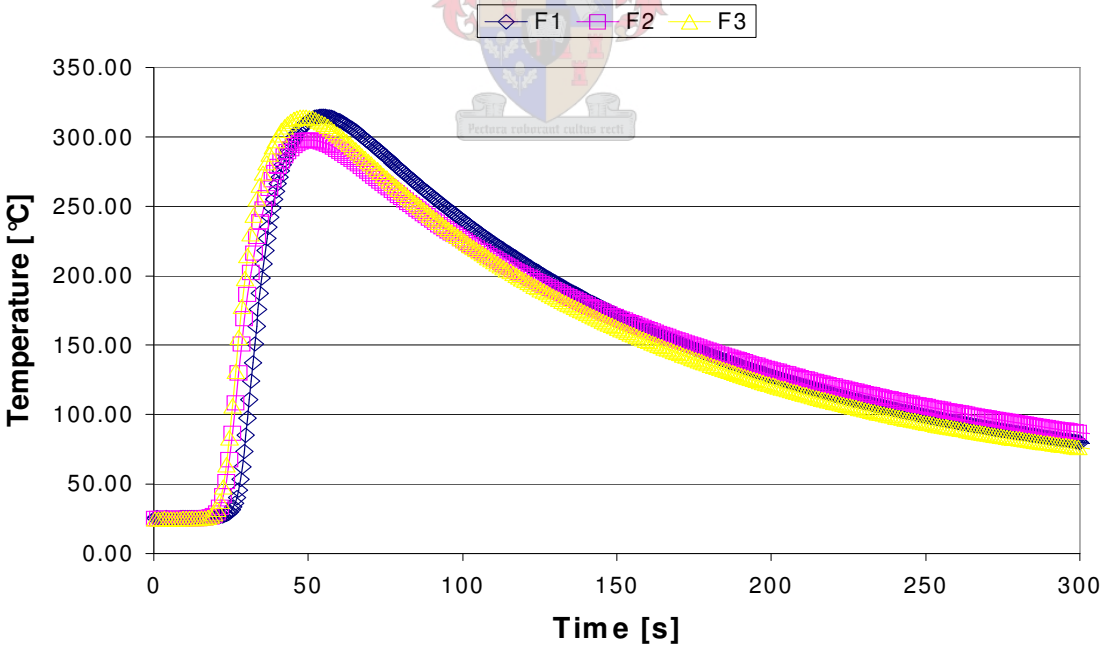

Figure 4-21: Temperature distribution at distance 20 mm from weld in centre of plate for three different experiments.

4.7 Conclusion on Experiments

Experiments were carried out to investigate the effect of changes in welding parameters on the distortion of the welded plates. The parameters investigated were;

- the number of restraints on the clamps,
- the plate thickness and
- the welding current.

Low, medium and high values were given to these parameters. The median values were taken from a standard experiment that was created and values lower and higher were appointed for the other experiments.

The effect of restraints was investigated for two, four and eight clamps on the plates. The lack of restraint in the two-clamp experiment caused the plates to be misaligned. This caused excessive distortion in one plate during welding. The plates did not distort significantly more after the removal of the clamps.

In the four and eight clamp experiments no significant displacements was measured after welding with all the clamps still on the plates and distorted after the removal of the clamps. This indicated that residual stresses were building up in the plates and caused the plates to distort after the removal of the restraining forces.

The plate thickness had significant effect on the distortion of the plates. The maximum displacement for the 2, 3 and 4 mm thick plates were 7.52, 5.18 and 1.27 mm respectively. The welder avoided burning through of the material with the 2 mm thick plates by increasing the welding speed, thus decreasing the heat input per unit length. The welding speed used for different plate thickness coincided with theoretical equations.

An increase in welding current increases the power input of the welding process. The power input of the welding process did not affect the heat input per unit

length. The welder maintained a constant heat input per unit length by increasing the welding speed with an increase in welding current. The maximum displacements for the 70, 90 and 110 A current settings were 4.01, 4.74 and 2.49 mm respectively.

5 MODELLING OF WELDING EXPERIMENTS

5.1 Introduction

Finite element analysis (FEA) has been used by many authors to predict welding distortions and temperature distributions in different types of joints and materials (Deo, et al., 2002, Michelaris, et al., 1996, Moshaiov, et al., 1990). Prediction is difficult due to the complex variations of temperature, thermal contraction and expansion and variation of material properties with temperature. Furthermore, modelling of the weld process must account for the specialized effects of the moving weld arc and material deposit.

Finite element (FE) models of the welding experiments were carried out to verify the validity of the numerical results. The numerical and experimental results were verified on temperature and plate displacement results. The finite element method was used to obtain results that were not measured in the experiments like stresses and strains, giving insight into the welding process that cannot be seen in the workshop.

The main modelling parameters investigated were the material properties, element mesh density, weld modelling tool options and analysis options. In the analysis options the time step size, convergence tolerances and job options were significant in the analysis. The application of the modelling parameters is discussed in this chapter. The use of thermal analysis, structural analysis with temperature history definition and coupled thermo-mechanical analysis were performed in this thesis. Modelling techniques were investigated to obtain an effective finite element model for welding simulation.

5.2 Weld Modelling in MSC.Marc

The FEM solver MSC.Marc with the pre- and postprocessors MSC.Patran and MSC.Mentat were used in this research. MSC.Marc is a non-linear commercial FEM software package that has the capabilities to perform welding simulations. Special model definition options for the simulation of welding are available in MSC.Marc/Mentat.

Welding is a thermal process with specialized boundary conditions. These boundary conditions are specified through the definition of the weld flux in conjunction with the specification of the weld path and filler metal options. The pre-defined moving heat source tools include, but not limited to, the Goldak double ellipsoidal heat source model. Filler metal deposition is defined via element activation/de-activation.

Additional items to facilitate welding analysis in MSC.Marc are time stepping, convergence checking and adaptive meshing. Adaptive time stepping was used in the weld models where the increment time was estimated through the allowable temperature change per increment. Convergence tolerances were relaxed to decrease modelling time but without threatening the accuracy of the results. Non-linear temperature dependent material properties and latent heat effects were specified.

5.3 Weld Model Preparation

5.3.1 Geometry and Element Meshing

As with any finite element analysis, the first step was the modelling of the geometry and element mesh. This was done in MSC.Patran due to its user-friendly and powerful geometry and meshing tools. An input file was created in MSC.Patran and imported into MSC.Mentat. MSC.Patran was not fully

compatible with all the capabilities of MSC.Marc while MSC.Mentat is the original pre- and postprocessor for MSC.Marc.

Four node shell elements with the option of quadratic temperature distribution through the thickness of the elements were used. The elements had the option of three integration points through the thickness of the element, which was considered to give an accurate estimation of the temperature distribution through the plate thickness. These elements were suitable for thermal and coupled thermal-structural analysis.

As a rule, elements behave best when it were of a compact regular shape (Cook, R.D., 1995), thus the elements were kept rectangular throughout the model. The element aspect ratio was kept below 5:1 in the weld region and increased towards the far edge of the plate to an aspect ratio of 10:1.

The size of the elements in the welding region was determined through guidelines that Goldak had proposed for accurate representation of the heat source model. The Gaussian ellipsoidal model required approximately four quadratic elements along each axis to capture the inflection of the Gaussian distribution (Goldak, et al., 1986). An element size of 2 x 1 mm was used in the weld zone which satisfied the guidelines proposed by Goldak. This captured more accurate temperature results without an analysis time penalty. The geometrical heat source values for the standard experiment were 5, 3, 2.5 and 10 mm for the width, depth, forward length and backward length respectively resulting in 2.5 and 6.25 elements in the width and length of the heat source.

5.3.2 Material Properties

The metal most widely used in welded fabrication is carbon steel containing up to about 0.3% carbon (mild steel). This material undergoes only minor hardening in the heat-affected zone of fusion welds and normally is welded without any pre- or

post welding heat treatment. Mild steel is easily available, cheap and can be welded by most of the welding processes. This steel was chosen for these experiments due to its relatively problematic free weldability.

The material properties were discussed in Chapter 3.5. The temperature dependent material properties specified in the model were conductivity, specific heat, elastic modulus, yield strength and thermal expansion coefficient. Latent heat of solidification can be specified in the material specification options list. Various authors specified the latent heat of fusion for low carbon steel as 260 kJ/kg (Goldak, et al., 1986). The mass density remained constant at all times with a value of 7850 kg/m^3. The melting range for mild steel was taken as 1432 – 1526 ℃.

Non-linear temperature dependent material properties were specified in the model. The models were improved systematically from constant properties to temperature dependent properties, improved conduction for weld pool convection and latent heat effects. The use of temperature dependent material properties in the structural analysis required smaller time steps, due to the low Young's modulus at high temperature.

5.3.3 Boundary Conditions

The loads and boundary conditions in a model are everything that operates in the immediate environment that is not explicitly modelled. The loads and constraints specified in the thesis were divided into two groups: thermal and structural boundary conditions. The thermal boundary conditions were the heat source, initial temperature, thermal contact, weld filler initial temperature and convection/radiation heat losses. The structural conditions were the restraints put on the plates by the welding jig and clamps and the restrictions in the plane of symmetry. In the uncoupled structural analysis the thermal history was applied as a state variable.

5.3.3.1 Thermal Boundary Conditions

The most important thermal boundary condition specified in the welding analysis was the applied heat source. The double ellipsoidal heat flux volume was discussed in Chapter 3.1.5 and will not be explained in detail in this section. No guide for the sizing of the heat source model existed and values were chosen until the correct molten zone size was produced. It was found that to get a correct weld pool size, smaller dimensions had to be used. This is due primarily to the interaction between the heat source power, which is Gaussian along the longitudinal weld arc axis, and the volume specified by the double ellipsoid dimensions (Francis, 2002).

The heat source parameters were determined by measuring the rippling effects of the weld beads. In the absence of sufficient measurements the distance in front of the heat source was taken equal to one-half the bead width and the distance behind the heat source equal to twice the width (Goldak, et al., 1984). The heat source parameters used in the modelling for the different experiments are shown in Table 5-1. The welding speeds and power input were the average calculated values from the experiments. The value of the arc efficiency was taken as η_{arc} = 0.5 from the literature (Groover, 1999). Small changes in the arc efficiency had a negligible effect on the temperature distribution since the filler metal was specified with an initial melting point temperature of 1480 °C.

Table 5-1: Experimentally determined heat source parameters.

		Width	Depth	Front length	Back length	Speed	Power	arc efficiency
Clamps	Two	7	3	3.5	14	3.67	2174	0.7
	Four	7	3	3.5	14	3.71	2155.4	0.7
	Eight	7	3	3.5	14	3.31	2264	0.7
Plate Thickness	2 mm	6	2	3	12	5.53	2161.3	0.7
	3 mm	7	3	3.5	14	3.71	2155.4	0.7
	4 mm	8	4	4	16	3.26	2156.7	0.7
Current	70 A	7	3	3	14	3.1	1716.89	0.7
	90 A	7	3	3.5	14	3.71	2154.36	0.7
	110 A	6	3	3	12	5.64	3008.62	0.65

The theory on the combined convection and radiation heat transfer coefficient was explained in Chapter 3.3.7 and Appendix A. This data was specified via a face film boundary condition and applied to all the free surfaces of the plate.

The heat sinking effect of the welding jig had a significant effect in the temperature results. In the thermal analysis heat transfer coefficients were specified between the plate and welding jig. The contact heat transfer coefficient was taken as 7500 W/m².℃ and the near contact heat transfer coefficient as 1000 W/m².℃. The ambient temperature and initial temperature was taken as 25 ℃.

5.3.3.2 Structural Boundary Conditions

The major boundary conditions specified for the structural analysis were the welding jig contact and the clamps. The contact area of the welding jig and clamps were modelled as rigid bodies. The jig was kept rigid for the whole duration of the analysis, while the clamps were removed just before the end of the model. Symmetrical boundaries conditions were applied at the centre of the weld line to prevent movement perpendicular through the weld centreline (X - translation fixed) and movement along (longitudinal and up-/downwards) the weld centreline (Y - and Z - translation fixed).

In the uncoupled structural analysis the thermal history was specified as a state variable. The state variable used the thermal history obtained in the thermal analysis and mapped in on every node for the structural analysis.

5.3.4 Element Activation/De-Activation

MSC.Marc uses the element activation/de-activation option for the dynamic creation of filler elements and the generation of associated boundary conditions.

Two methods are supported for the creation of the filler elements: the quiet element method and the deactivated element method.

In the quiet element method the filler elements are initially used with scaled down material properties with a default factor of 10^{-5}. When the filler elements are physically created by the moving heat source, all stresses and strains in the elements are reset to zero and used with regular material properties. The drawback of the quiet element method is that it is prone to ill conditioning due to large discrepancy in the material stiffness.

In the deactivated element method, filler elements are initially deactivated in the analysis and are not shown on the post file. The elements are physically created when all the nodes are inside the “box” of the heat source model. This method does not suffer from ill conditioning problems but can cause distorted filler elements when used in large deformation welding analysis. The deactivated filler elements were used in the coupled analysis and the quiet element method was used in the uncoupled analysis.

5.3.5 Coupled and Uncoupled Analysis

The uncoupled analysis approach was used instead of the coupled thermo-structural analysis. The coupled analysis proved to be resource intensive and time consuming. By separating the thermal and structural analysis, better control and monitoring of the analysis was achieved. It was assumed that the deformations in the structural analysis had no influence on the temperature distribution. The thermal analysis of the welding process was performed with thermal contact of the welding jig taken into consideration. The jig and the plate were modelled as rigid bodies with heat transfer capabilities.

The temperature results from the thermal analysis were applied as a boundary condition in the structural analysis. All analyses were done for 600 s at which

time the plate temperature had cooled down close to ambient temperature. After 600 s the clamps on the plates were removed, to simulate the plate deformation during the removal of the clamps.

5.4 Numerical Results

The modelling results did not compare accurately with the experimental results, but similar trends were found in the FEM results. The displacement results were compared directly with the experimental results, while each model was compared on grounds of temperature distribution and vertical displacement.

5.4.1 Thermal Results

5.4.1.1 Effect of Different Plate Thickness

Even though the input power for the welding of different plate thickness was constant, the time of weld differed greatly. This caused different heat input into the steel plates. From the FEM results it was clear that the different welding speeds affected the maximum temperatures and cooling of the plates.

With the slower welding speeds for the 3 and 4 mm thick plates, more heat was put into the plates. This meant higher peak temperatures, which had several of affects on the welded structure. This included a larger heat affected zone (HAZ) and longer time of cooling to room temperature. The thicker plates have more material and thus more heat storage capacity, thus keeping the heat longer.

Steel plates of different thickness welded at the same welding parameters had difference in temperature distribution and cooling time of the plates. The thicker plates could absorb more heat for a sufficient bond, thus causing higher peak temperatures and longer cooling of the plates. After 600 s, there was a significant difference between the plate temperatures for different plate thickness (Figure 5-1). This indicated that with an increase in plate thickness there is an increase in production “recycling time”, due to slower plate cooling.

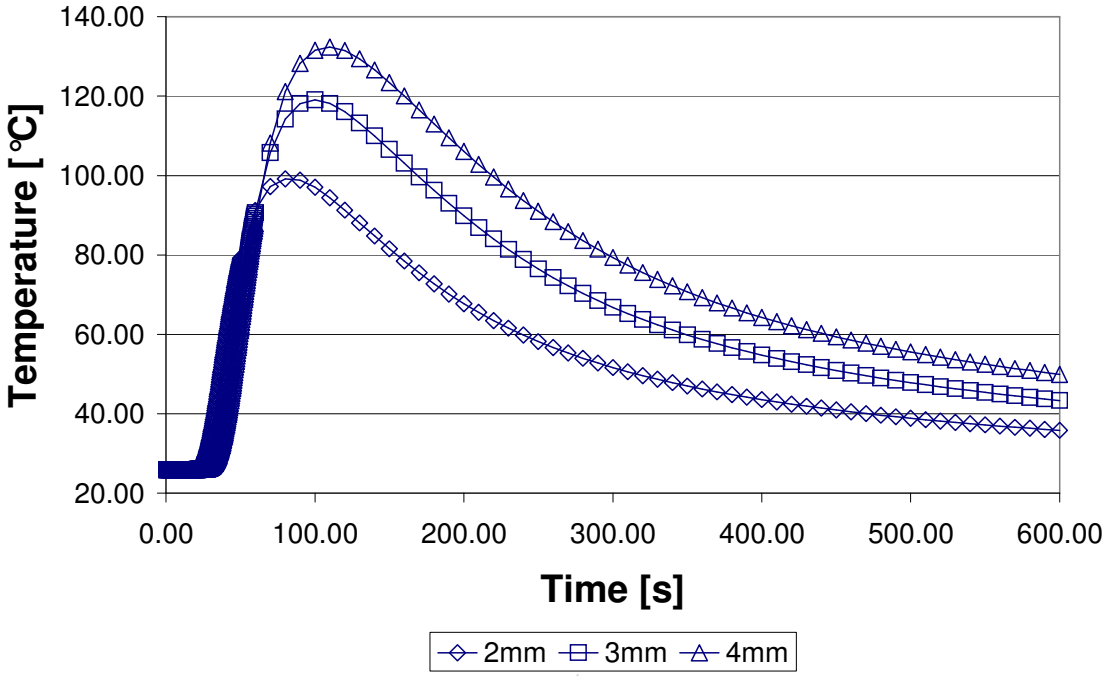

Figure 5-1: Temperature distribution for different thickness, 50 mm from weld.

5.4.1.2 Effect of Different Current Settings

The FEM results for different welding current settings have shown that the highest temperature distribution was in the 70 A welding process. The slower welding speed for the 70 A welding resulted in an increase in energy per unit length (see Equation 4-2). The 110 A welding current setting gave the lowest temperature distribution.

Although the 70 A current setting gave the highest temperatures, it did not give the overall maximum plate displacement in the experiments. The plates welded with the 90 A setting gave the largest displacement while the 110 A the least. The displacement for the 70 A setting was in between. The structural results will be discussed in Section 5.4.2.

Unlike the temperature results for different plate thickness, the cooling of the plates were the same, which indicated that the plate thickness is an important

factor in the cooling of the plates. The cooling of the plates were almost the same because in all three experiments the plates had the same stored heat capacity.

Steel plates of the same thickness welded at different welding current settings have the same cooling time. The only difference was in the time of the weld itself: the higher the current, the faster the welding speed. The difference in temperature of the steel plates after 600 s did not differ greatly, thus concluding that a difference in welding current do not have a significant effect on the “recycling time” of a welded structure, except for the time of the weld itself.

5.4.2 Structural Results

The thermal results were applied as boundary conditions in the structural analysis. Shell elements with quadratic temperature distribution between the nodes were used in the structural analysis. The assumptions discussed in the Section 3.2.4 were applied structural analysis.

It was assumed that the temperature distribution in the welded plates was symmetrical and only one plate was modelled. Only the displacement results were verified with experimental results, while the stress results gave insight to the residual stress distribution in the welded plates. The displacement results were investigated by using the same 25-point measuring grid used in the experiments. The displacements were compared on lines parallel (longitudinal) and perpendicular (transverse) to the weldment.

The welding process was modelled over a period of 600 seconds with the clamps attached to the plates. From 600 to 610 seconds the contact surfaces of the clamps were gradually released to simulate the removal of the clamps. The most distortion of the plates occurred during the removal of the clamps.

Assumptions made in experiments and models regarding the environmental effects could have attributed to results that did not validate accurately with the experimental results. The effects of assumptions made in the modelling were not investigated in this study, since it fell outside the scope of this thesis.

5.4.2.1 Effect of Different Plate Thickness

The displacement results of the welding analysis of 2, 3 and 4 mm thick mild steel plates gave good comparison with the displacement tendencies observed in the welding experiments but not as accurate in the magnitude of the plate displacement. The experimental results were only used as a base of comparison and were taken as absolute.

With the use of shell elements, the plate thickness could be changed without changing the model. This did imply that the contact tolerances specified in the models had to be adjusted accordingly with the change in plate thickness. The welding heat input parameters were also specified with values obtained from the experiments.

The thinner plates underwent the most distortion as was observed in the experiments. The 4 mm plate showed the least distortion (0.06 mm) and the 2 mm thick plate showed overall the most deflection (1.96 mm), although the maximum vertical displacement was found in the 3 mm thick plate model (2.61 mm). Figure 5-2 shows the plate displacement perpendicular to the weldment in the middle of the plate (X = 100 mm). In the graph the centre of the weldment is at Y = 200 mm.

The maximum recorded vertical displacement (Z-direction) for the 3 mm FEM model could be attributed to the contact tolerances in the model. With the releasing of the clamps in the model, the shell elements can still “cling” onto the contact surfaces moving away, before the deformable body and contact surface

separates. This can happen for only a split second in the model but the deformation can be significant to the results.

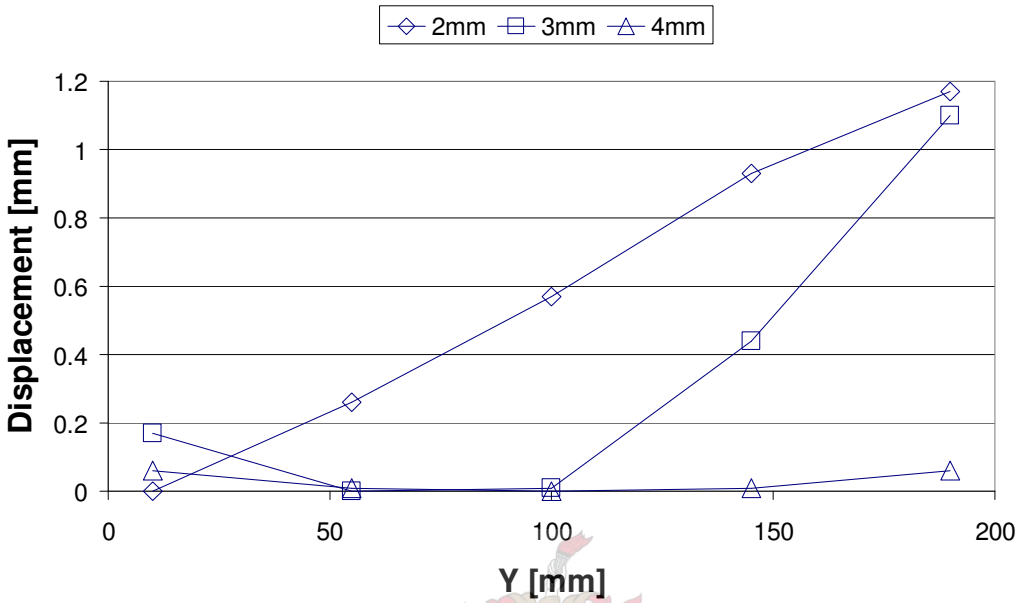

Figure 5-2: Transverse displacement for different thickness after clamp removal (FEM).

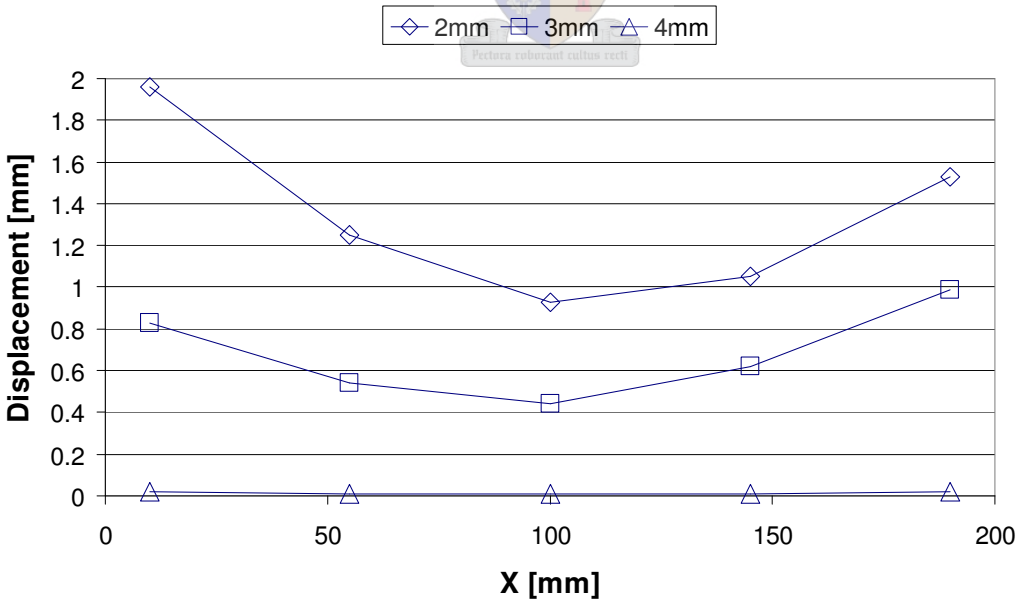

Figure 5-3: Longitudinal displacement for different thickness after clamp removal (FEM).

5.4.1.2 Effect of Different Welding Current

The use of different welding currents implied the use of different magnitude heat sources in a welding process. The variables for the models with different welding currents were the welding power, weld pool dimensions and welding speed. These variables were measured in the welding experiments and applied to the models.

The volume weld heat source parameters were adapted till weldpool dimensions were obtained that was the same as in the experiments. These dimensions were smaller than the weld pools in the experiments (Table 5-2). This effect could be attributed to the Goldak double ellipsoidal heat source volume that has a Gaussian distribution within the specified volume. Goldak (1986) argued that these dimensional distribution functions could be criticized as “fudge factors”, but they do enable accurate temperature fields to be computed. The quadratic temperature distribution used in the shell elements could also prevent Gaussian distributed temperature within the weldpool elements.

Table 5-2: Volume heat source dimension used in FEA for different weld current settings.

	a [mm]	b [mm]	c_f [mm]	c_r [mm]	P [W]	v [mm/s]	η
70A	3.5	3	2.225	6	858.5	3.1	0.7
90A	3.5	3	2.225	6	1077.7	3.71	0.7
110A	3	3	2	4	1504.31	5.64	0.5

Figure 5-4 shows the weld pool size obtained in the 70 A model. The effect of the “quiet” element method used to represent the weld filler metal could be observed in front of the molten zone in Figure 5-4. There is no temperature rise in the elements in front of the heat source because the material properties of the elements were reduced by a factor of 1e-5. These elements were activated when they were within the boundaries of the specified volume heat source.

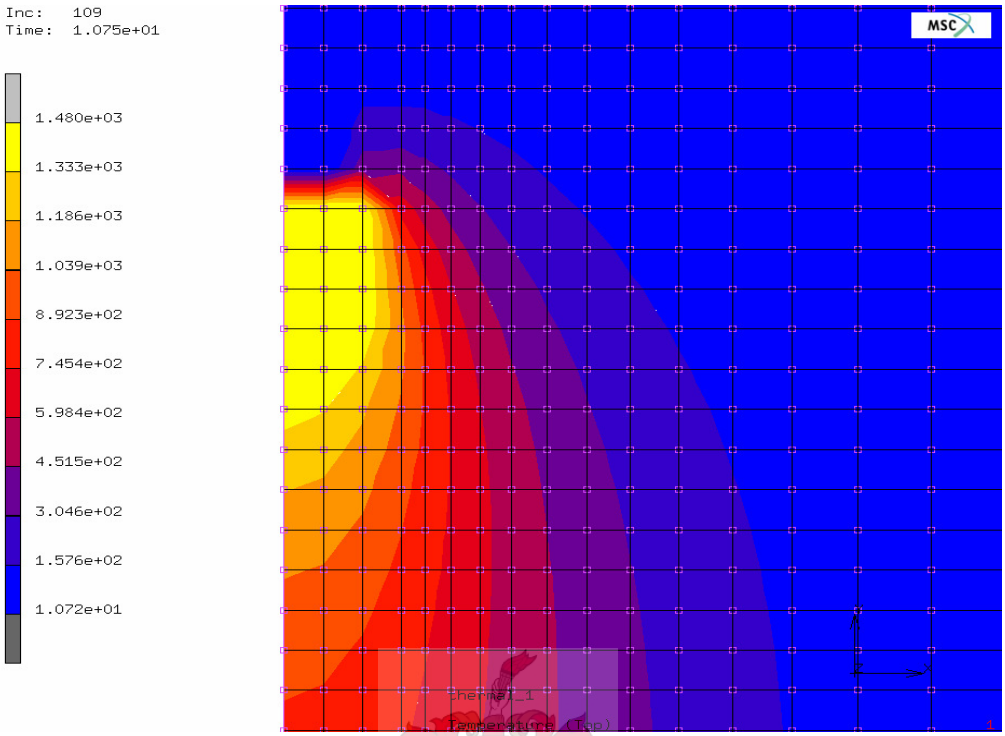

Figure 5-4: Weld pool size in FEA for 70 A model.

The maximum displacement for all models was near the weld. The 70 A model showed the highest maximum displacement (2.69 mm), followed by the 90 A model (2.61 mm) and the 110 A model (2.18 mm). This coincides with the experimental results. Even though the maximum vertical displacement was in the 70 A model, the overall highest displacement was observed for the 110 A model.

In the 110 A experiment the weld was not the whole length of the plates because the welding electrode was finished before it reached the end of the plates. In the model it was assumed that the welding was over the total length of the plates.

The transverse displacement results showed slight upward displacement of the plates on the open side of the plate for the 70 and 90 A models. In the 110 A model, large displacement at the open side of the plate was observed. This effect was not observed in the experimental results and could not be explained by the author. The transverse and longitudinal displacement for the 70 A model verified

best with the experimental results for plate 2. The difference in displacement results for the two plates in the experiments could be attributed to inaccuracies in the experiments. This was discussed in more detail in Chapter 4.

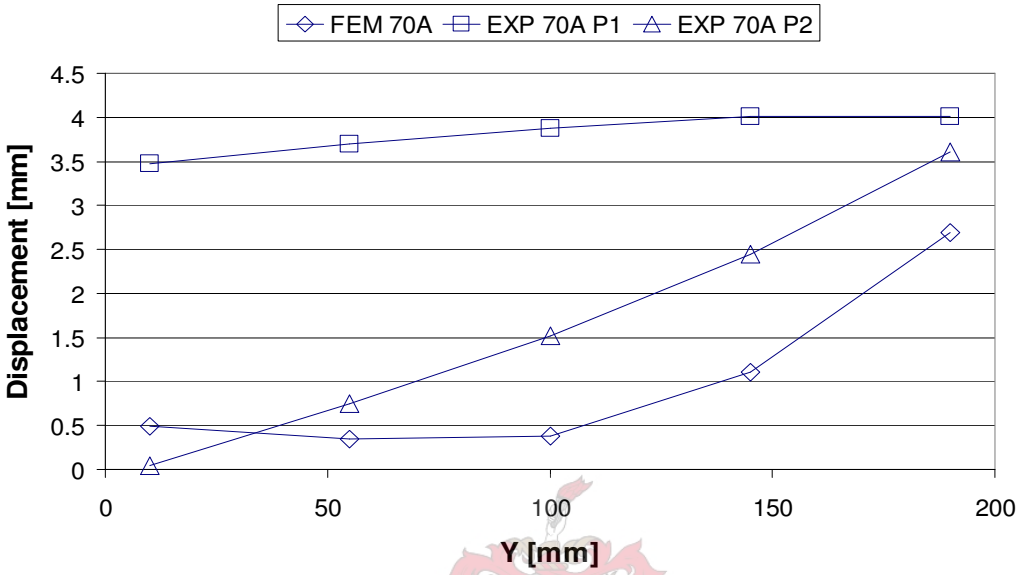

Figure 5-5: Transverse displacement for 70A welding.

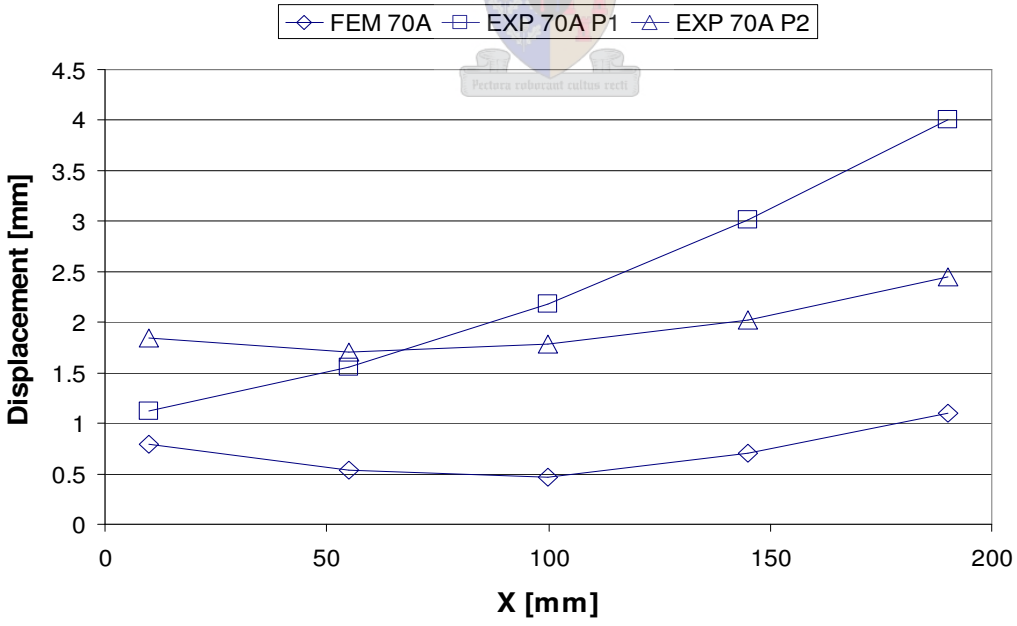

Figure 5-6: Longitudinal displacement for 70A welding, 55mm from weld.

5.4.3 Experiment vs. FEM

The models did not converge to within an overall 80 % accuracy of the experimental displacement results but did reveal agreement of tends. The points of agreement between the experiments and FEA are discussed in this section.

With the verification of the experimental and modelling results, it was noticed that everything from the experiments could not be modelled explicitly. This could have led to inaccurate results. The design of the experiments was very robust and more attention could have been focused on the retrieval of information. The measuring technique used in the experiments was very robust and was used because it was less time consuming.

The maximum displacements were observed close to the weld while the distortion became less away from the weld. In lines parallel to the weldment (longitudinal displacement) the plates bended upwards at the edges, resulting in a parabolic shape of the plate (Figure 5-3 and Figure 5-6). In the 2 and 3 mm cases (EXP) the maximum displacements was in the corner of the plate where the welding finished while the in the 4 mm case the maximum displacement were in the middle of the plate at the weldment.

The prediction of the location of the point of maximum displacement gave an indication of the accuracy of the distortion modelling of the welded plates. The most common point of maximum displacement in the experiments was measured at the point closest to where the welding finished. Only the 3 mm model agreed with the experiment. The 2 mm model predicted the maximum displacement at the start of the welding and the 4 mm model in the middle of the plate on the open side of the plate.

All three models investigating the effect of different welding current predicted the maximum displacement of the plate correctly. These models also showed the overall best agreement with welding tends.

In general, both the experiments and FEA agreed in parabolic shaped plates parallel to the line of welding and the maximum displacement at the welding. These results proved that the basic assumptions used in the models were correct and laid a foundation for weld modelling.

6 CONCLUSION

The scope and objectives of the thesis to qualify for the MSc.Eng. degree included:

- the development of a welding simulation using the finite element method,
- the verification of numerical results with those obtained in experiments and
- the identification of the crucial parameters in weld modelling.

These objectives were successfully accomplished.

A literature survey was done on the welding process and prediction of welding results in general. The survey was focused on temperature estimation, numerical and analytical, and welding induced distortions. Guidelines proposed and used by previous researchers were selected according to the specifications and requirements of the model or weld. The use of two-dimensional in-plane weld modelling had been accepted by various researchers as accurate representations of the real welding process (Goldak, et al., 1986 and Deo, et al., 2002). Based on the comments made by these researchers, the use of shell elements for welding analysis was justified.

The use of temperature dependent material properties had been proved to be crucial in the estimation of the temperature distribution of the plates. The greatest limitation to computational weld mechanics was obtaining accurate temperature dependent material properties (Goldak, et al., 1986). In cases where material properties at elevated temperatures were not known, the properties of materials with similar chemical content were used. Guidelines proposed for the calculation of properties at elevated temperatures was also used (Zhu, et al., 2002).

Mild steel (SABS 1431 300WA) was used in the thesis because it was cheap, had a good weldability and it was the most widely used metal in welding.

Shielded metal arc welding was used in the experiments. It was proved from the experiments that the human welder gave repeatable results and welded at optimal conditions. The parameters measured in the experiments were used as input for the FE models. These parameters included the weld bead length, welding speed and power input. The geometrical heat source parameters used in the double ellipsoidal was taken from measurements of the weld bead. These parameters were oversized with a factor less than 1.5 to obtain correct weld pool size in the analysis.

The temperature results from the FE model were compared with the experimental temperature results. The model parameters were changed within the limits of the guidelines proposed by previous researchers until the results were in acceptable tolerance of the experimental results. The element size, material properties, volume weld flux, heat loss boundary conditions and analysis options like the initial time step was experimented within the model until satisfactory results were obtained.

Three-dimensional coupled analysis with contact as done and found to be time consuming. The analysis was uncoupled and the nodal temperature history from the thermal analysis was specified as a boundary condition in the structural analysis. The three-dimensional analysis proved to be also time consuming and inefficient. The welding was modelled with shell elements to save on computation time.

The displacement magnitudes from the FEA models did not compare significantly with the experiments, but the distortion tendencies observed in the experiments were reflected in the models. The models were not valid to make accurate distortion prediction but were sufficient to be used in welding feasibility case studies and research.

6.1 Recommendations

The effect of the welding induced deformations was only investigated at local area of the welding. Studies on the effects of welding on a complex structure can to be investigated to determine the overall effect of the welding procedure on the structure. This study will require the modelling of different weld geometries.

The available temperature dependent material properties were restricted and innovative measures were taken to obtain these data. The thermo-physical properties of mild steel at elevated temperatures can be investigated. The metallurgical transformations of the steel during welding can be modelled to determine the size and properties of the HAZ.

The simulation of other manufacturing processes like machining, forging, sheet metal working and casting can be investigated. Little measurable financial impact exists for modelling of manufacturing processes where the key elements of successful modelling can be reviewed and to quantify the cost savings.

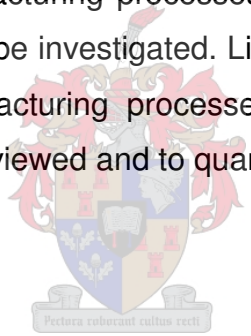

REFERENCES

Adak, M., Mandal, N.R., 2003, Thermo-Mechanical Analysis of Plates Undergoing Line Heating Pseudolinear Equivalent Constant Rigidity System, Transactions – Society of Naval Architects and Marine Engineers, v 111, p 353 – 361.

Adams, V., Askenazi, A., 1999, Building Better Products with Finite Element Analysis, Onword Press, USA.

Audronis, M., Bendikas, J., 1983, The Welding Deformations of Chrome-Nickel Stainless Steels, Material Science, Vol. 9, No. 2, p 169 – 173.

Bonifaz, E.A., 2000, Finite Element Analysis of Heat Flow in Single-Pass Arc Welds, Welding Journal, v 79, p 121s – 125s.

Britsih Iron and Steel Research Association Metallurgy, 1953, Physical Constants of Some Commercial Steels at Elevated Temperatures, London Butterworth Scientific Publications.

Callister, W.D., 1997, Material Science and Engineering: An Introduction, John Wiley and Sons, Inc., New York, USA.

Cook, R.D., 1995, Finite Element Modelling for Stress Analysis, John Wiley and Sons, Inc., USA.

Dally, T.W., Riley, W.F., McConnell, K.G., 1993, Instrumentation for Engineering Measurements, Second Edition, Wiley, New York, 1993.

Deo, M.V., Michaleris, P., Sun, J., 2002, Prediction of Buckling Distortion of Welded Structures, Science and Technology of Welding and Joining.

Eagar, T.W., Tsai, N.S., 1983, Temperature Fields Produced by Travelling Distributed Heat Sources, Welding Journal, v62, n12, p346 – 355.

Ericsson, M., 2003, Simulation of Robotic TIG-Welding, Department of Technology, University of Trolhattan, Sweden.

Faure, W.C., Welding, Fabrication and Metal Work, Welding and Fabrication, Bloemfontein, South Africa.

Francis, J.D., 2002, Welding Simulations of Aluminium Alloy Joints by Finite Element Analysis, Master's Thesis, Virginia Polytechnic Institute and State University, Viginia, USA.

Fuersbach, P.W., Eisler, G.R., 2002, Determination of Material Properties for Welding Models by Means of Arc Weld Experiments, 6th International Trends Research, Pine Mountain, Georgia, USA.

Goldak, J., Chakravarti, A., Bibby, M., 1984, A New Finite Element Model for Welding Heat Sources, Metallurgical Transactions B, Vol. 15B, p 299 – 305.

Goldak, J., Bibby, M., Moore, J., House, R., Patel, B., 1986, Computer Modeling of Heat Flow in Welds, Metallurgical Transactions B, Volume 17B, p 587 – 600.

Groover, M.P., 1999, Fundamentals of Modern Manufacturing – Materials, Processes and Systems, John Wiley and Sons, Inc, New York.

Hutton, D., Fundamentals of Finite Element Analysis, McGraw-Hill, New York, 2004.

Jang, C.D., Lee, C.H., 2003, Prediction of Welding Deformation of Ship Hull Blocks, Proceedings of International Workshop on Frontier Technology in Ship and Ocean Engineering.

Jung, G.H., Tsai, C.L., 2004, Fundamental Studies on the Effect of Distortion Control Plans on Angular Distortion in Fillet Welded T-Joints, Welding Journal, pp 213 – 223.

Kadivar, M.H., Jafarpur, K., Baradaran, G.H., 2000, Optimizing Welding Sequence with Generic Algorithm, Computational Mechanics, v26, p 514 – 519.

Lancaster, J.F., 1965, The Metallurgy of Welding, Brazing and Soldering, George Allen and Unwin Ltd, London.

Louhenkilpi, S., Markku, U., Kytonen, H., Vapalathi, S., 2003, Effect of Thermophysical Material Data on Heat Transfer in Continuous Casting, Modelling of Casting, Welding and Advanced Solidification Processes, pp 733 – 740.

Lourens, C., 2002, Wondermetal is poised to make inroads into the vehicle sector, Industrial Reporter Business Day.

Luo, Y., Ishiyama, M., Murakawa, H., 1999, Welding Deformations of Plates with Longitudinal Curvature, Transactions of Joining and Welding Research Institute, Osaka, Japan, Vol. 28, No. 2.

Michaleris, P. and A. DeBiccari, 1996, Prediction of Welding Distortion, Welding Journal, 76(4): 172s-180s

Michelaris, P., Feng, Z., Campbell, G., 1997, Evaluation of 2D and 3D FEA Models for Predicting Residual Stress and Distortion, ASME PVP – Approximate

Methods in the Design and Analysis of Pressure Vessels and Piping Components, 347, pp. 91 – 102.

Michaleris, P., Deo, M.V., 2002, Experimental Verification of Distortion Analysis of Welded Stiffeners, Journal of Ship Production, 18(4):2 16-225.

Mills, A.F., 1995, Heat and Mass Transfer, Richard D. Irwin, Inc, USA.

Moshaiov, A., Eagar, T.W., 1990, Modelling of Distortion in Complex Structures, Automation in the Design and Manufacture of Large Marine Systems, C. Chryssostomidis ed., Hemisphere Publishing Corporation, New York.

Msc.Software Corporation, 2005, Msc.Marc Volume A: Theory and User Information, Version 2005.

MSC.Software Corporation, 2003, MSC.Marc Introductory Course.

NAAMSA, 2003, New Vehicle Manufacturing Industry Data, www.naamsa.co.za,.

Phillips, A.L., 1968, Welding Handbook, Section One: Fundamentals of Welding, American Welding Society, New York.

Pilipenko, A., 2001, Computer Simulation of Residual Stress and Distortion of Thick Plates in Multi-Electrode Submerged Arc Welding. Their Mitigation Techniques, Department of Machine Design and Materials Technology, Norwegian University of Science and Technology, Norway

Tsai, C.L., Park, S.C., Cheng, W.T., 1999, Welding Distortion of a Thin-Plate Panel Structure, Welding Journal, pp 156 – 165.

Tsai, N.S., Eagar, T.W., 1985, Distribution of the Heat and Current Fluxes in Gas Tungsten Arcs, Metallurgical Transactions B, v16B, pp 841 – 846.

Weaver, M.A., 1999, Determination of Weld Loads and Throat Requirements Using Finite Element Analysis with Shell Element Models – A Comparison with Classical Analysis, Welding Journal, v78, n4, p 116s – 126s.

Wu, A., Syngellakis, S., Mellor, B.G., 2001, Finite Element Analysis of Residual Stresses in a Butt Weld, Proceedings of the Seventh Postgraduate Conference in Engineering Materials, p 37 – 38.

Zhu, X.K., Chao, Y.J., 2002, The Effect of Temperature-Dependent Material Properties on Welding Simulation, Computers and Structures, Vol 80, pp 967 – 976.

APPENDIX A

A.1 Calculation of Natural Convection

Fluid motion past a surface increases the rate of heat transfer between the surface and the fluid. A flowing fluid transports thermal energy by virtue of its motion. As the air velocity increases, the isotherms move close together. Isotherms are lines of constant temperature. Fourier's law is not only valid in a stationary solid, but it also applies in a moving fluid. Fourier's law of heat conduction states that in a homogeneous substance, the local heat flux is proportional to the negative of the local temperature gradient (Mills, 1995):

$$q_s = -k\frac{\partial T}{\partial y}\bigg|_{y=0} \qquad \text{Equation A-1}$$

As the isotherms move closer together and the temperature gradient normal to the cylinder surface increases, so does the resulting heat conduction. The fluid in contact with the cylinder is stationary due to viscous action and heat can be transferred from the surface in the fluid by conduction only. The local heat transfer rate is given by Equation A-2 (Mills, 1995).

Newton's law of cooling defined the convective heat transfer coefficient by the relation:

$$q_s = h_c(T_s - T_e) \qquad \text{Equation A-2}$$

Combining Equations A-1 and A-2 give the convective heat transfer coefficient:

$$h_c = \frac{-k\left(\frac{\partial T}{\partial y}\right)\Big|_{y=0}}{T_s - T_e} \qquad \text{Equation A-3}$$

The effect of increasing the fluid velocity is to steepen the temperature gradient at the surface, thereby increasing the heat transfer coefficient.

Natural convection, also known as free or buoyant convection occurs when density differences due to heat differences take place and the earth's gravitational force produces a buoyancy force. Velocities associated with natural convection are relatively small, not much more than 2 m/s. Convective heat transfer coefficients tends to be low in the order of 5 W/m².℃ (Mills, 1995).

For convective heat transfer dimensionless groups of pertinent variables are used to organise experimental data for convective heat transfer coefficients. The welded plates were assumed to be a heated plate facing up. The dimensionless numbers needed to calculate the heat transfer coefficients were the Nusselt and Rayleigh numbers. The Nusselt number, Nu, can be viewed as dimensionless heat transfer coefficient in Equation A-4 and the Rayleigh number, Ra, was given by Equation A-5.

$$Nu = \frac{h_c L}{k} \qquad \text{Equation A-4}$$

$$Ra = \frac{\beta \Delta T g L^3}{\nu \alpha} \qquad \text{Equation A-5}$$

The convection input data in Patran/Marc in the convection load/BC's menu defines the film coefficient on faces of solid elements. The film coefficient is defined as the convection coefficient for convective boundary conditions in Patran. It can be entered either as a real constant or a reference to an existing field definition. The film coefficient is user specified and is available from a number of sources. Equation A-6 was for $Ra_L > 10^7$, turbulent thermals rise irregularly above the plate and result in a Nusselt number independent of plate

size or shape. The Rayleigh number for the case of a welded plate was calculated to be in the order of 10^{10}.

$$Nu_L = 0.14 Ra_L^{1/3}; \qquad 2\times10^7 < Ra_L < 3\times10^{10} \qquad \text{Equation A-6}$$

The heat transfer coefficient can be defined as a function of temperature by substituting Equations A-4 and A-5 into Equation A-6 and the equation for h_c for free convection from a horizontal plate was given in Equation A-7.

$$h_c = \frac{0.14\, k\left(\frac{\Delta\rho}{\rho}\right)^{1/3}}{\left(\frac{\nu\alpha}{g}\right)^{1/3}} \qquad \text{Equation A-7}$$

The heat transfer coefficient was specified in terms of the fluid's physical properties. Tables with temperature dependent data of these physical properties were available (Mills, A.F., 1995) and the heat transfer coefficient as a function of temperature is shown in Figure 2. These values may be conservative compared to similar data found in the literature survey (Francis, J.D., 2002). Pilipenko used a value of 30 W/m².K for the convective heat transfer coefficient which was much higher than the values shown in Figure 2 (Pilipenko, A., 2001). The values in Figure 2 were used in the simulation of the convective heat losses in the FE modelling.

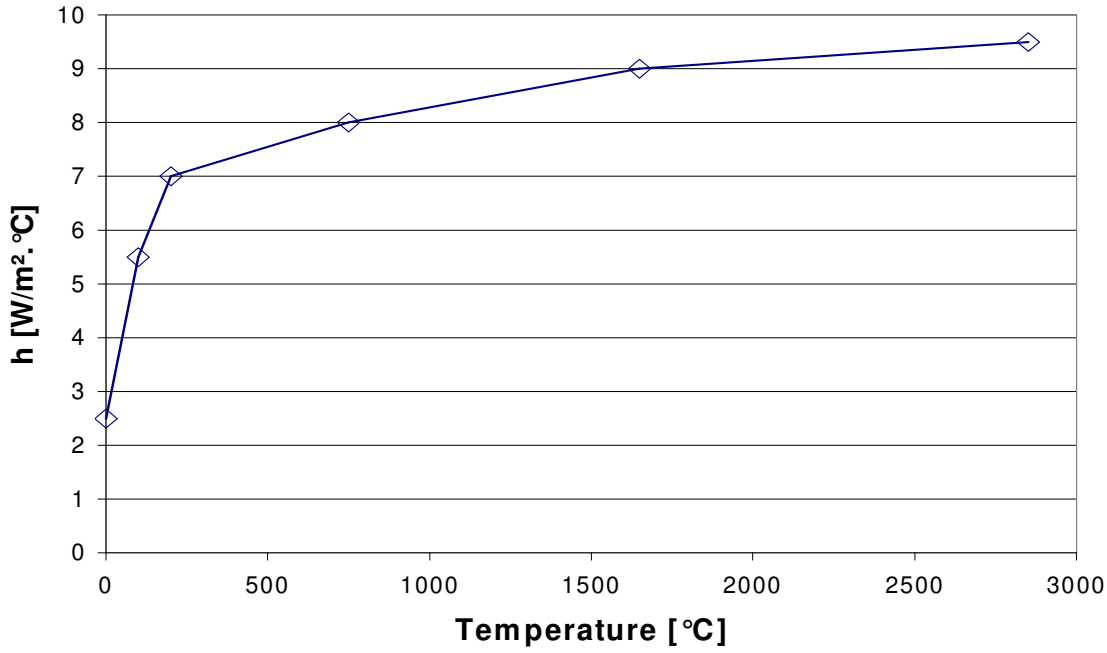

Figure A-1: Convective heat transfer coefficient of heated horizontal plate.

APPENDIX B EXPERIMENTAL RESULTS

B.1 Effect of Restraints

B.1.1 Final Plate Transverse Displacement for Plate 1

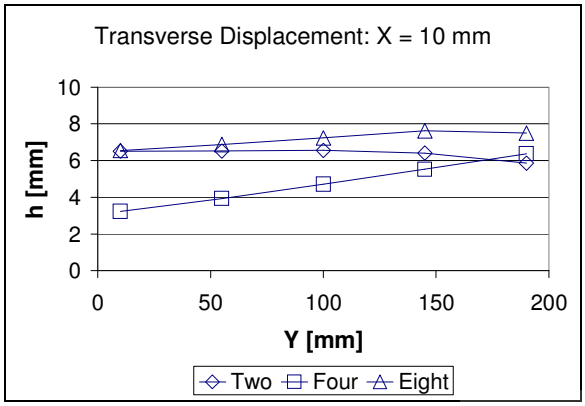

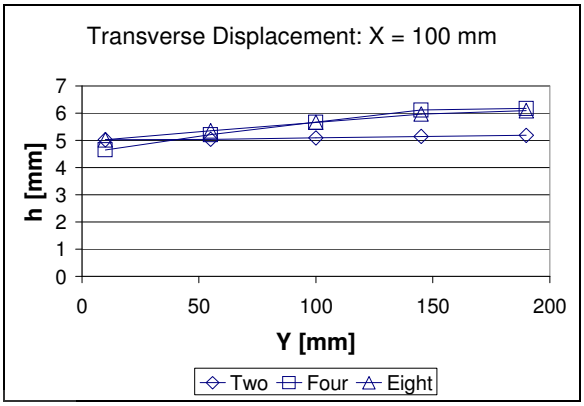

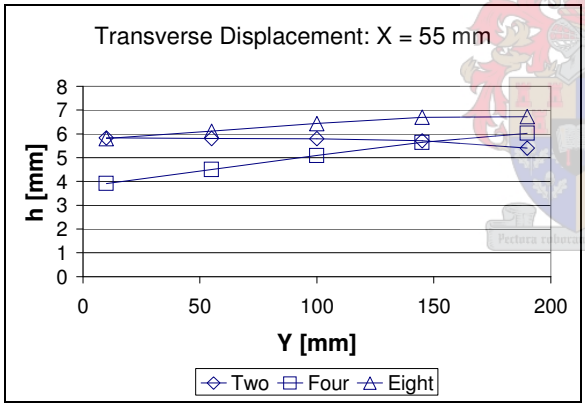

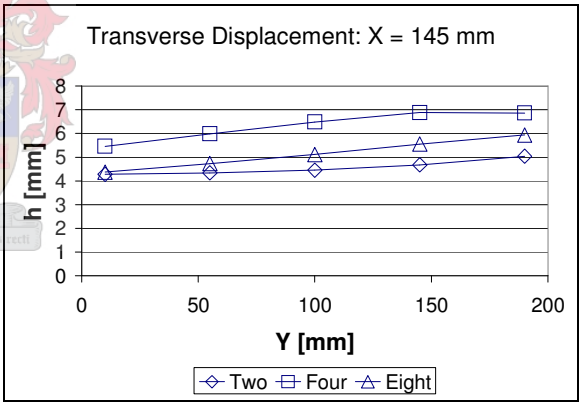

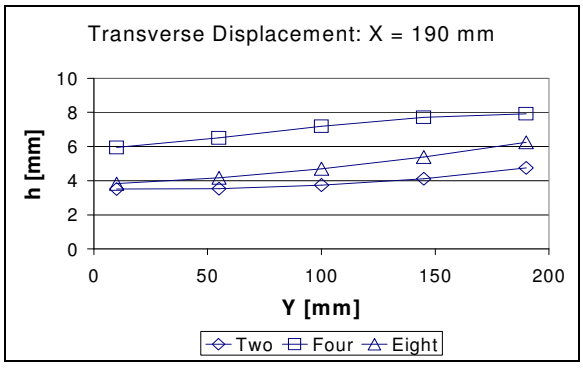

B.1.2 Final Plate Longitudinal Displacement for Plate 1

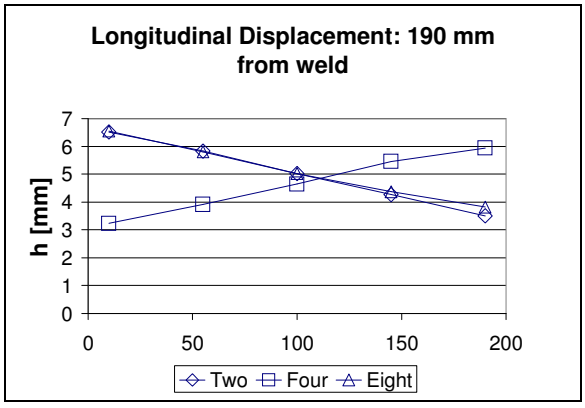

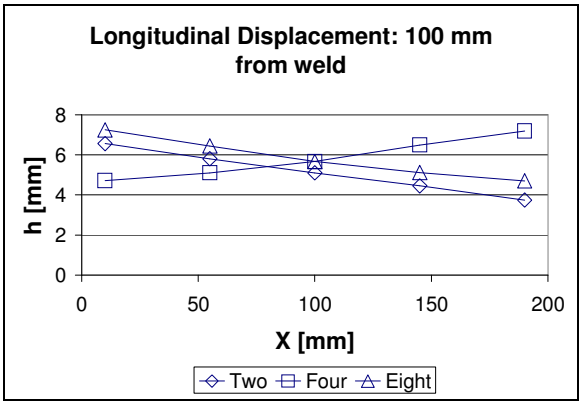

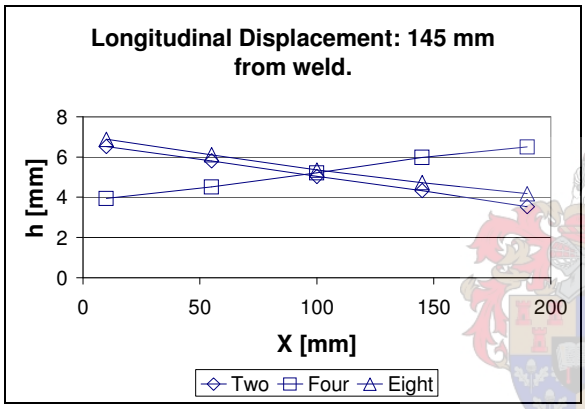

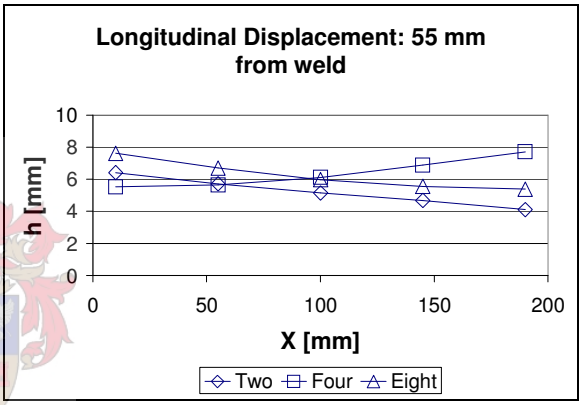

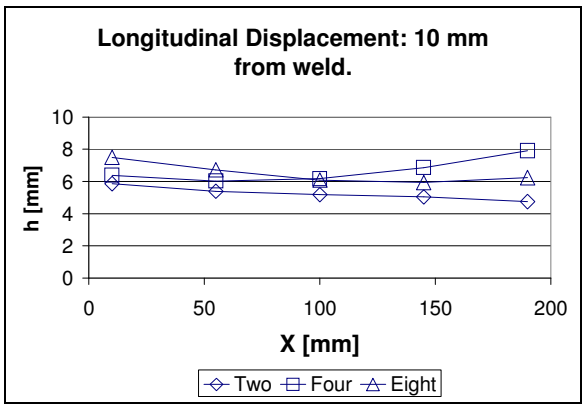

B.1.3 Final Plate Transverse Displacement for Plate 2

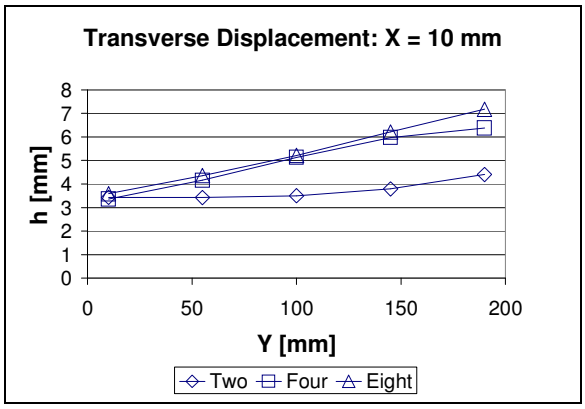

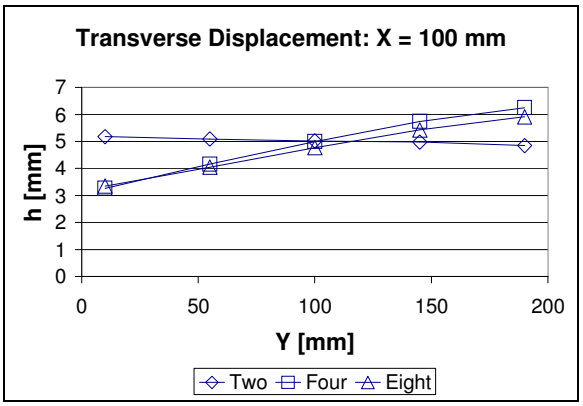

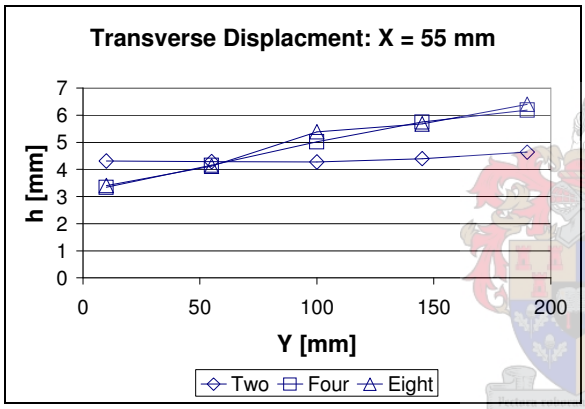

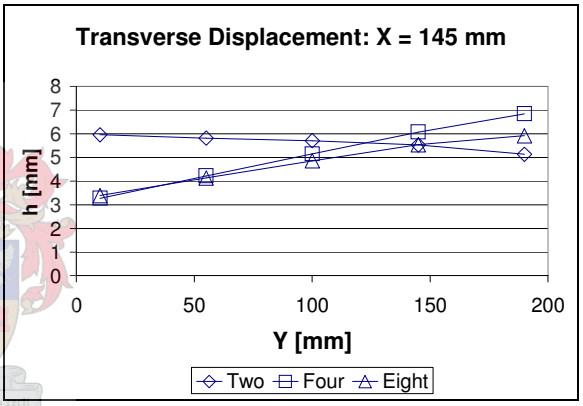

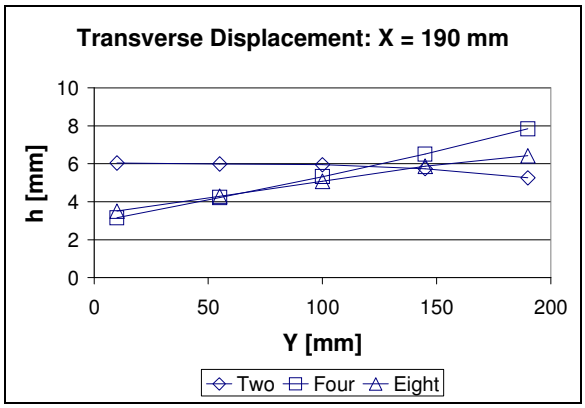

B.1.4 Final Plate Longitudinal Displacement for Plate 2

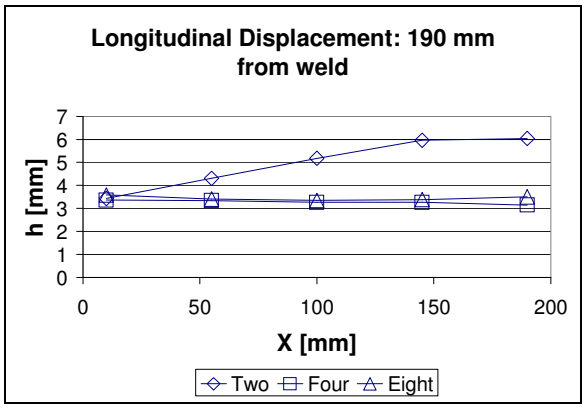

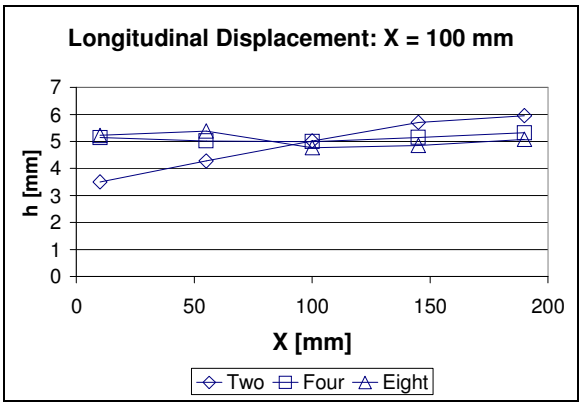

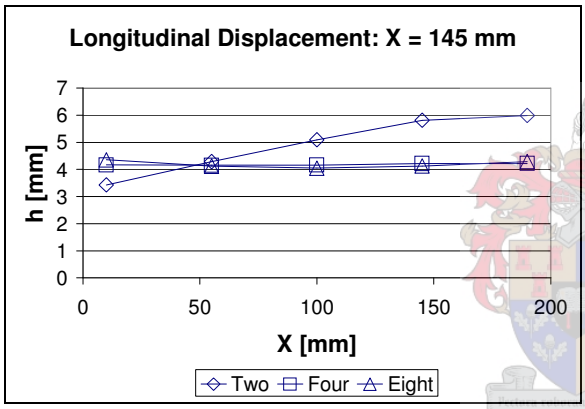

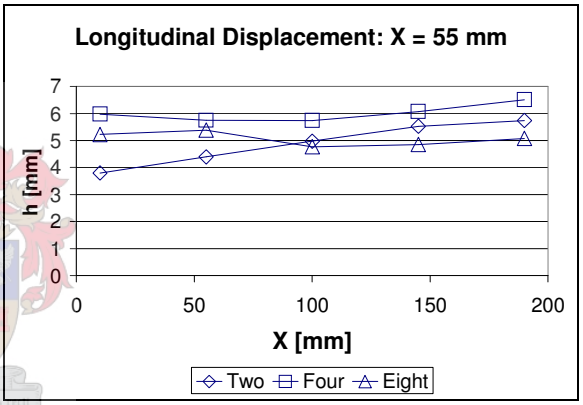

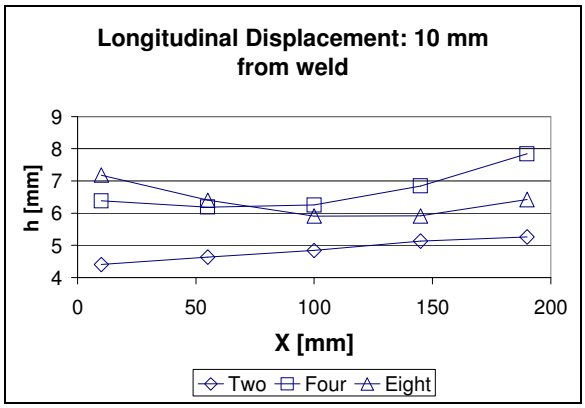

B.2 Effects of Plate Thickness

B.2.1 Final Plate Transverse Displacement for Plate 1

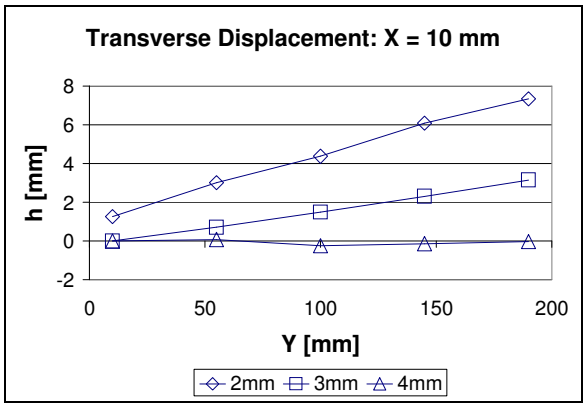

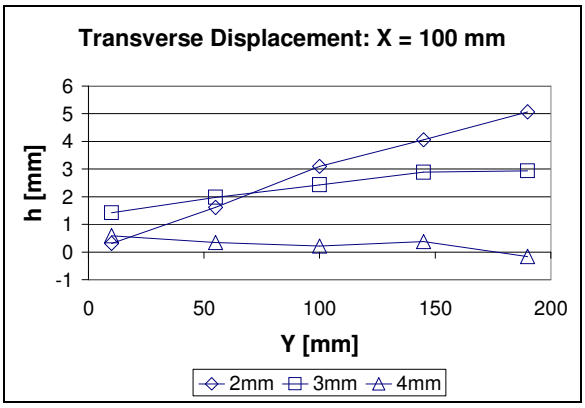

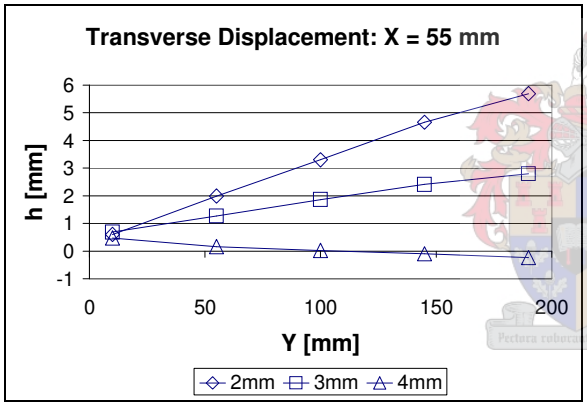

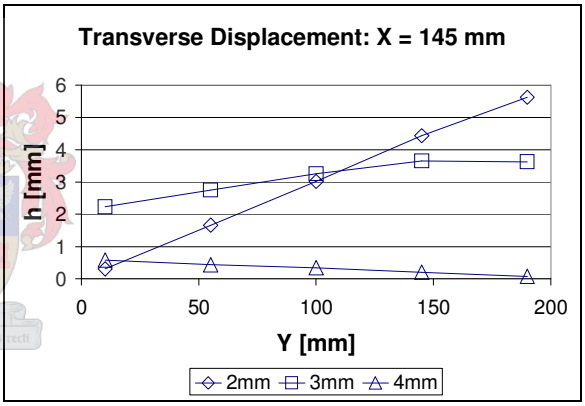

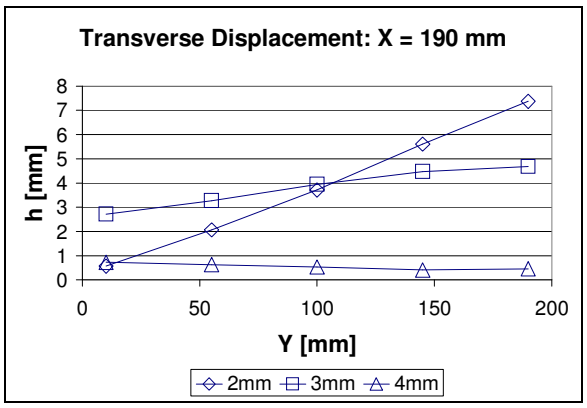

B.2.2 Final Plate Longitudinal Displacement for Plate 1

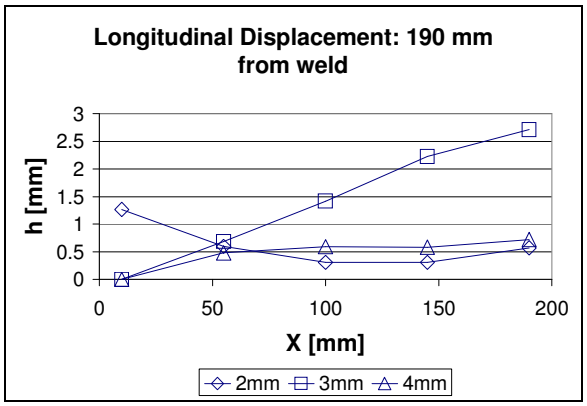

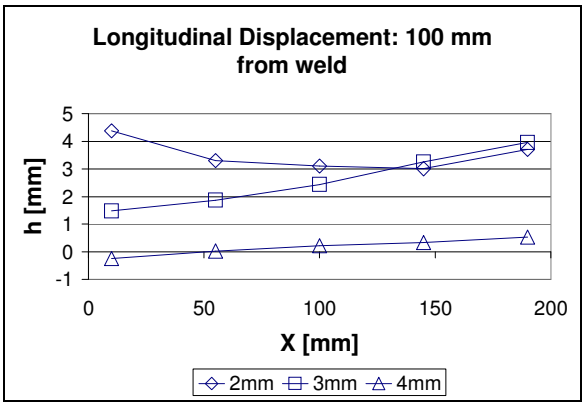

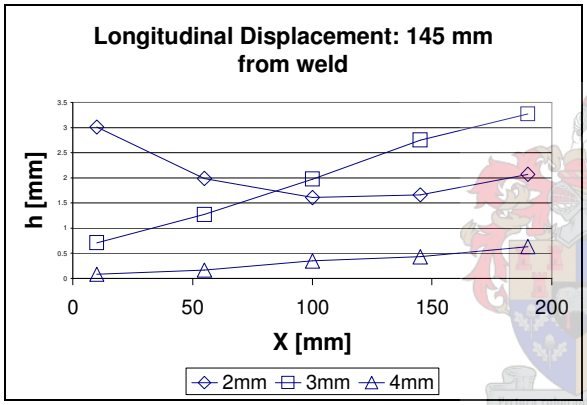

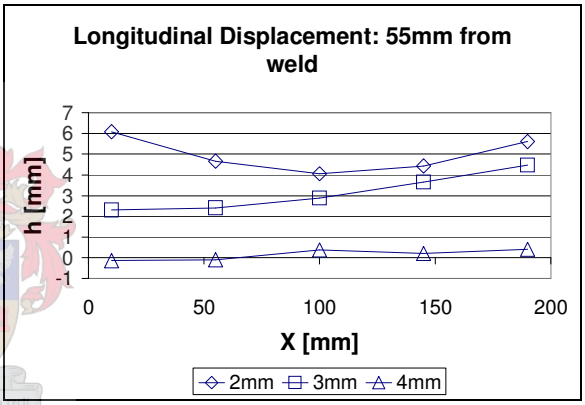

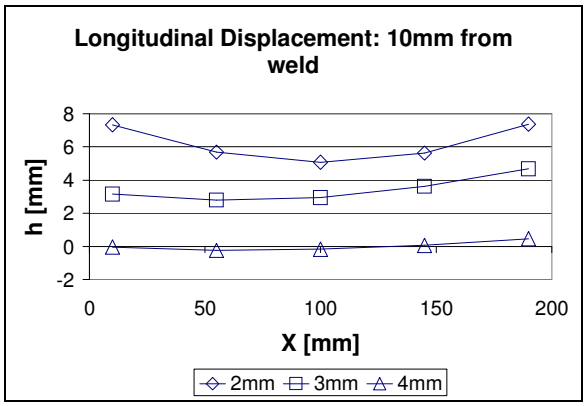

B.2.3 Final Plate Transverse Displacement for Plate 2

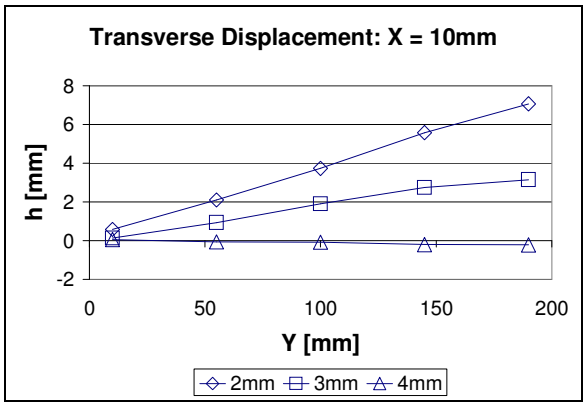

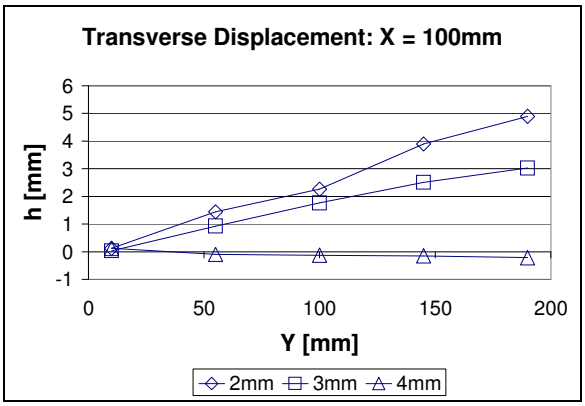

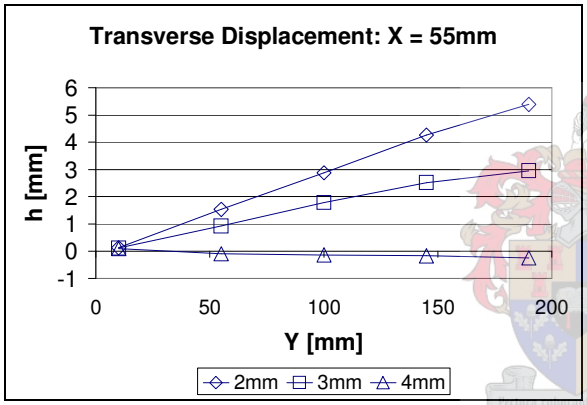

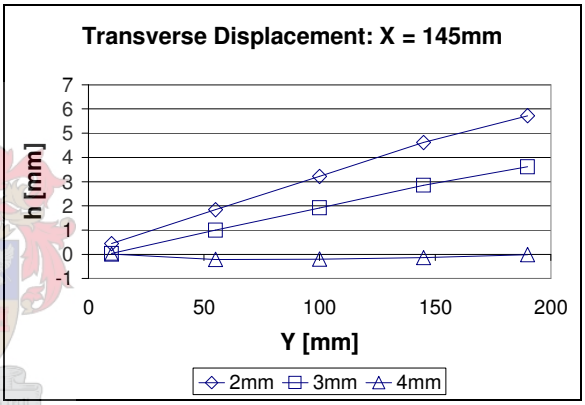

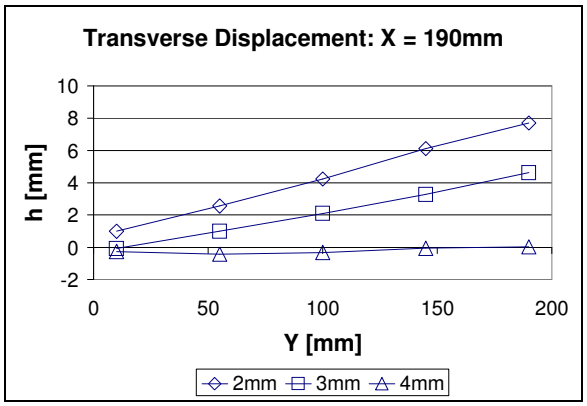

B.2.4 Final Plate Longitudinal Displacement for Plate 2

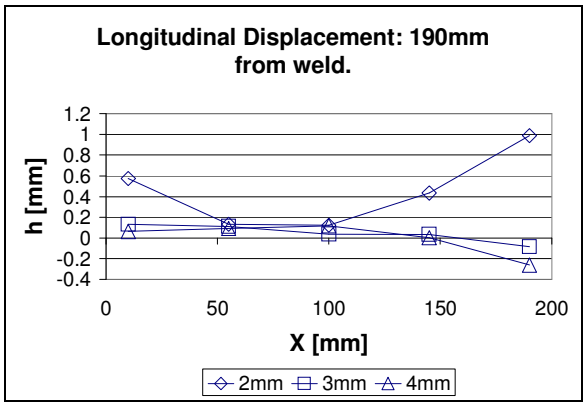

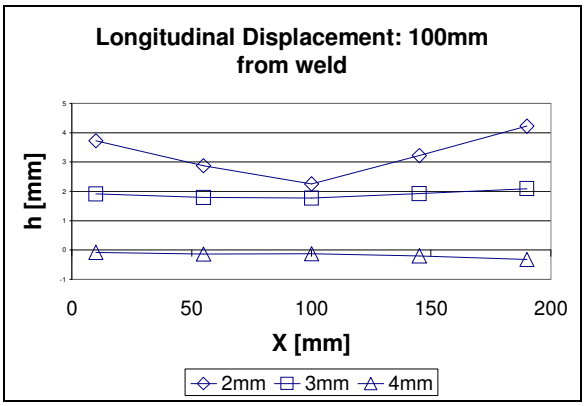

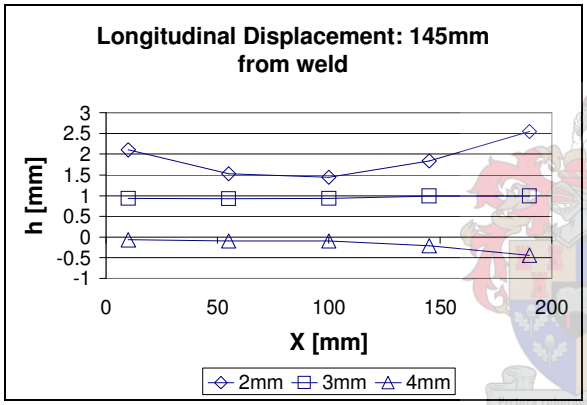

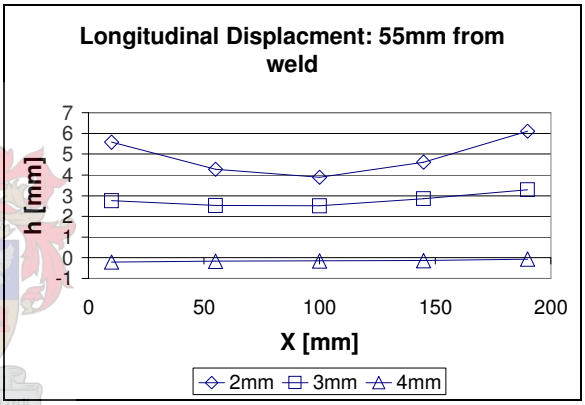

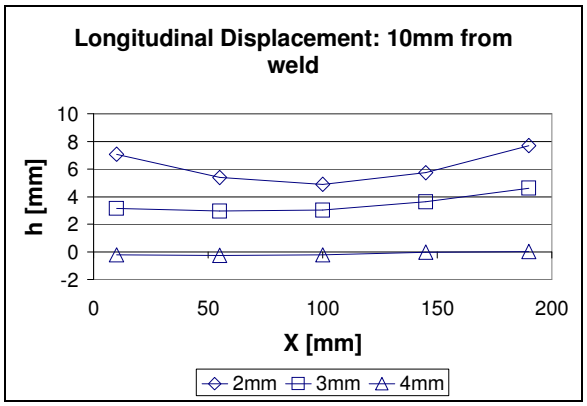

B.3 Effect of Heat Input

B.3.1 Final Plate Transverse Displacement for Plate 1

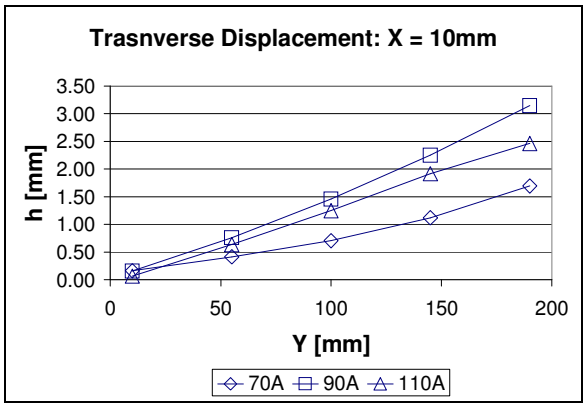

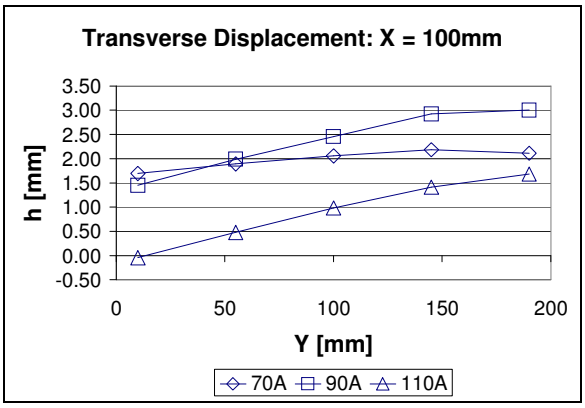

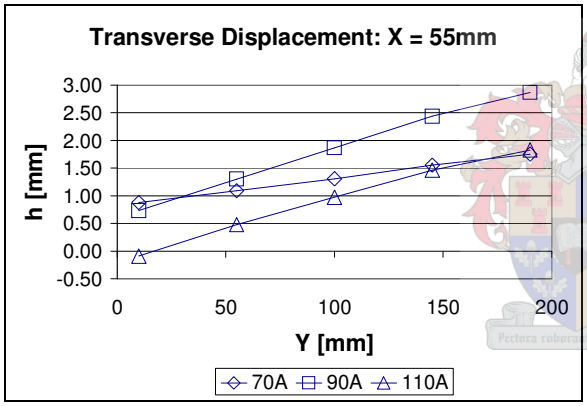

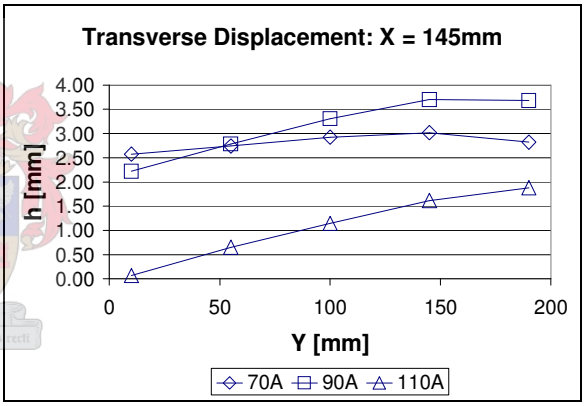

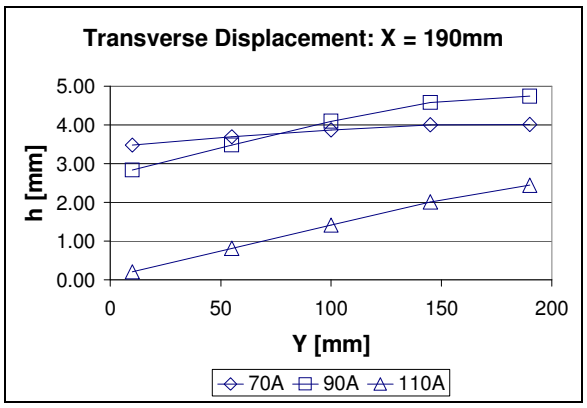

B.3.2 Final Plate Longitudinal Displacement for Plate 1

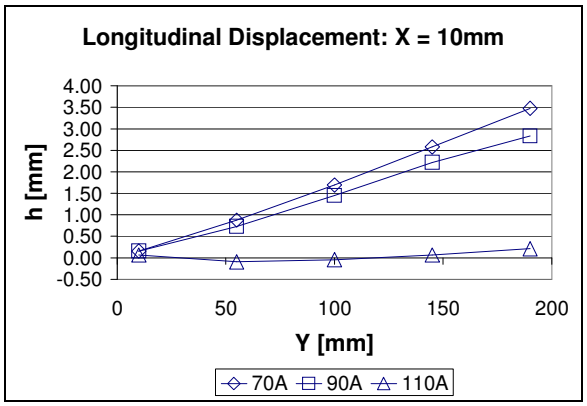

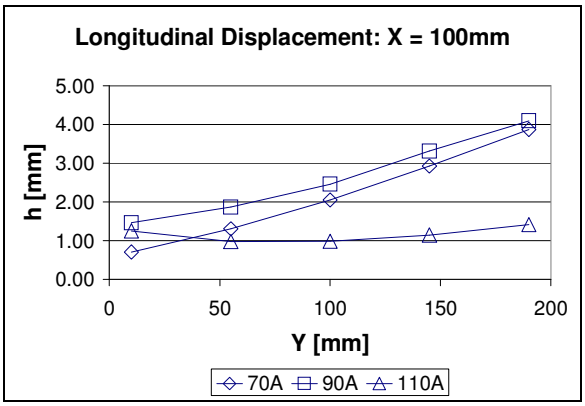

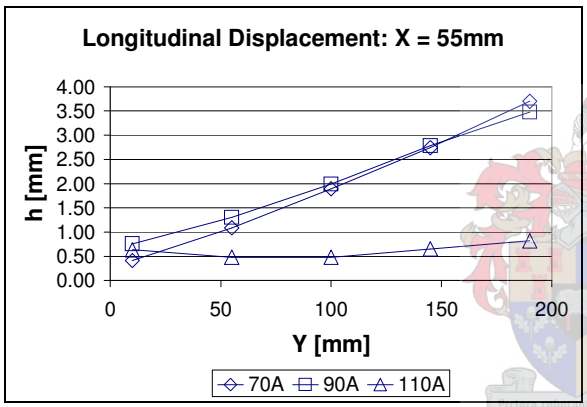

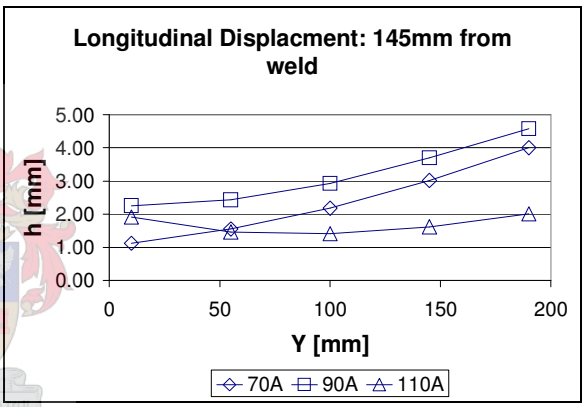

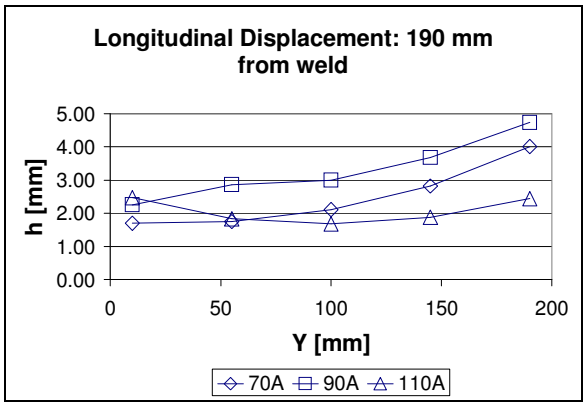

B.3.3 Final Plate Transverse Displacement for Plate 2

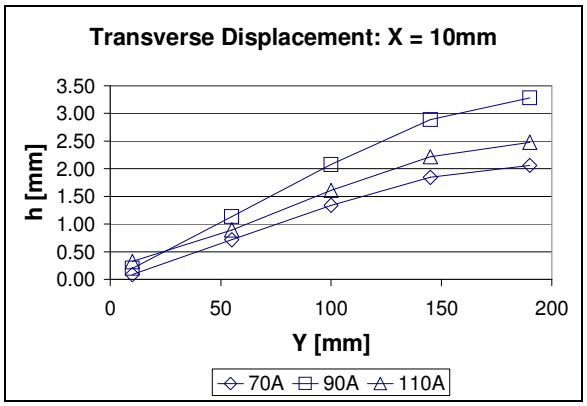

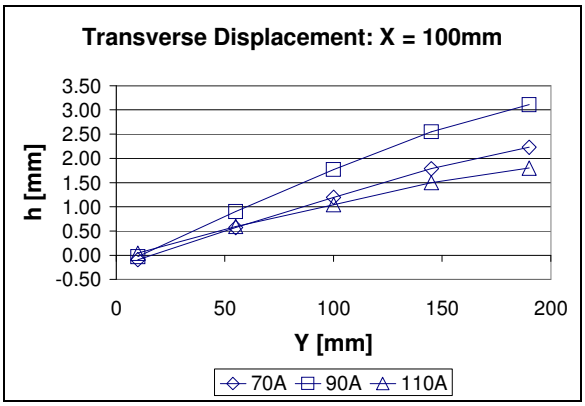

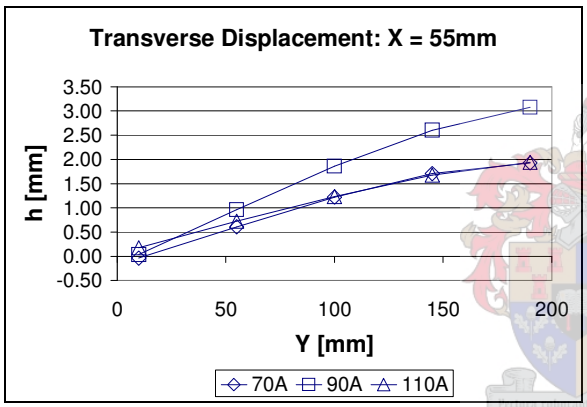

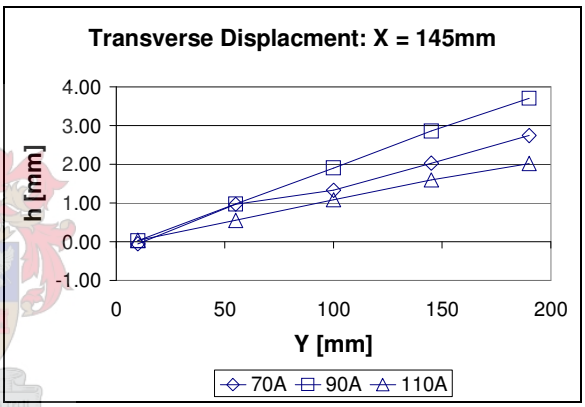

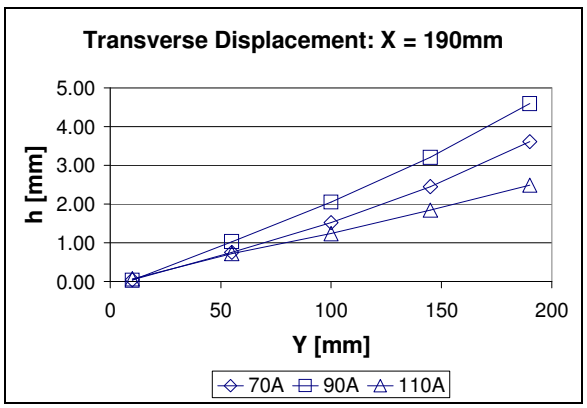

B.3.4 Final Plate Longitudinal Displacement for Plate 2

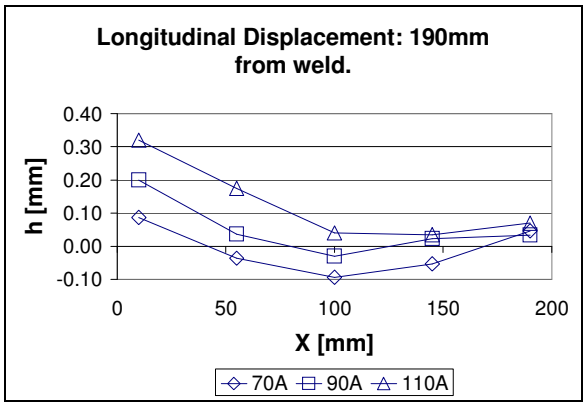

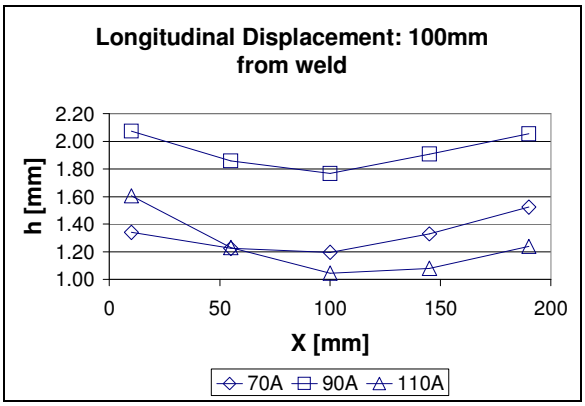

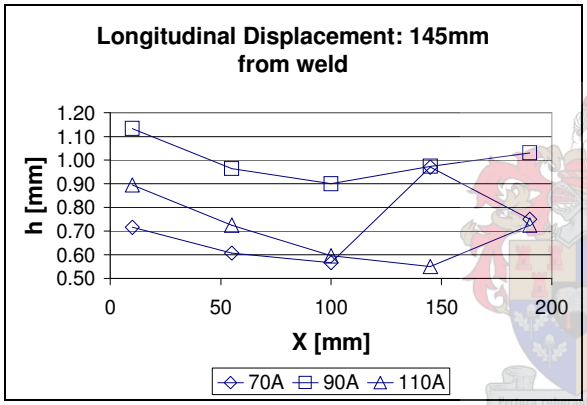

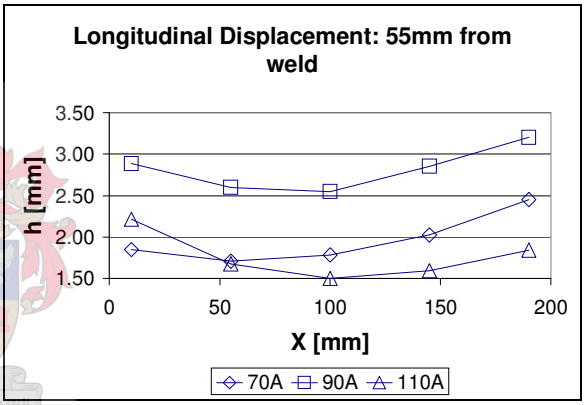

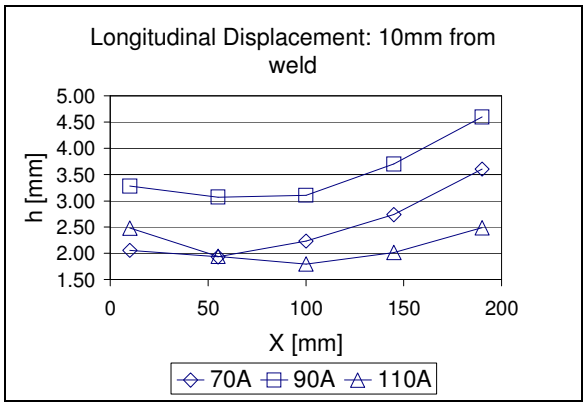

APPENDIX C EXPERIMENTAL TEMPERATURE RESULTS

C.1.1 Temperatures 30 mm from beginning of the weld

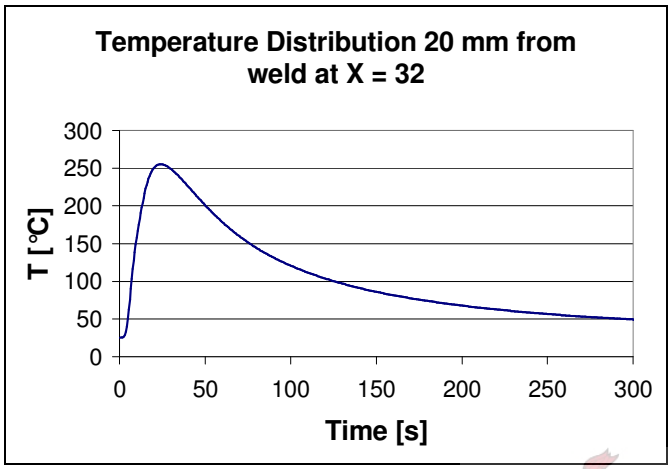

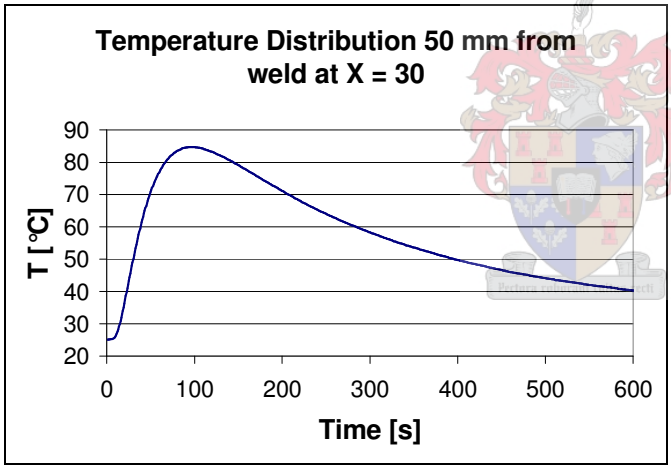

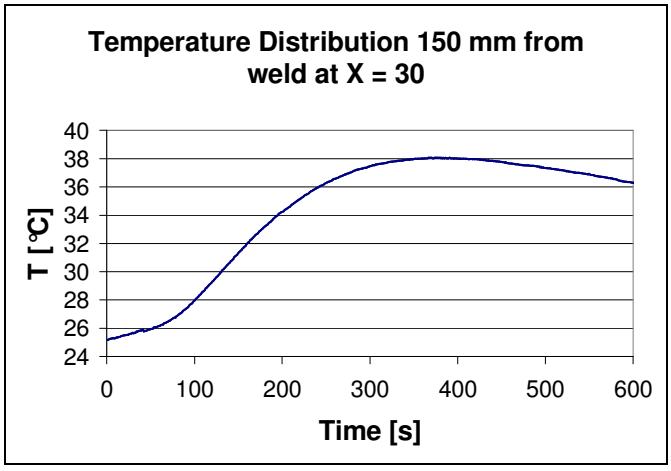

C.1.2 Temperatures at 50 mm from the beginning of the weld

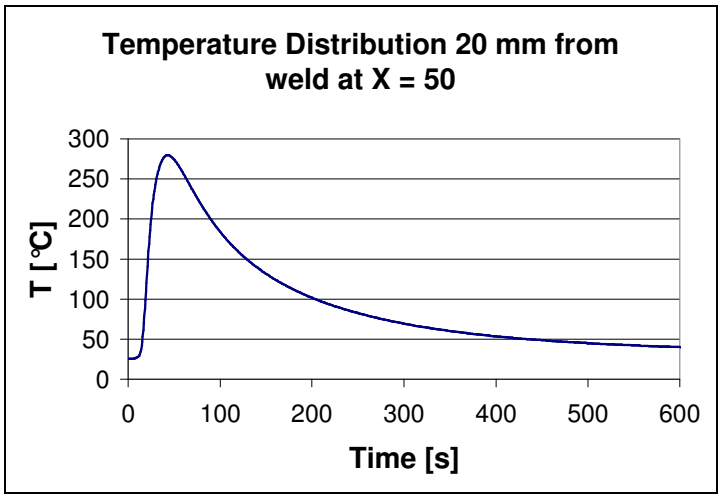

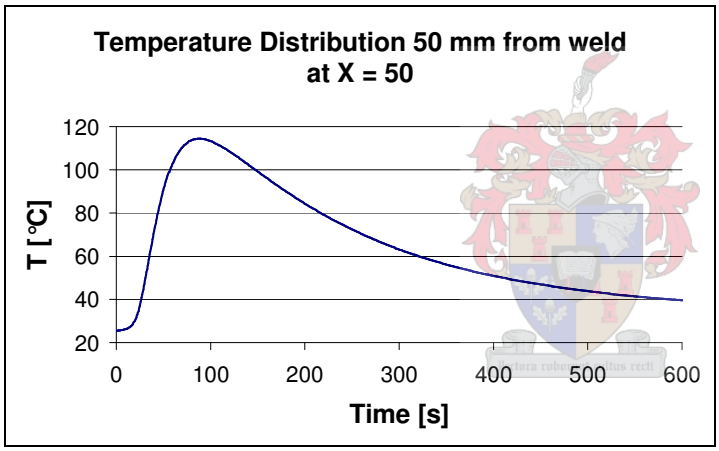

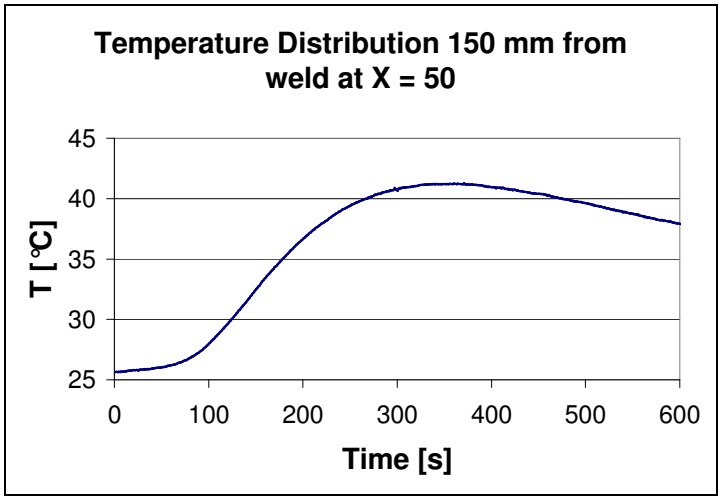

C.1.3 Temperatures at 100 mm from beginning of weld

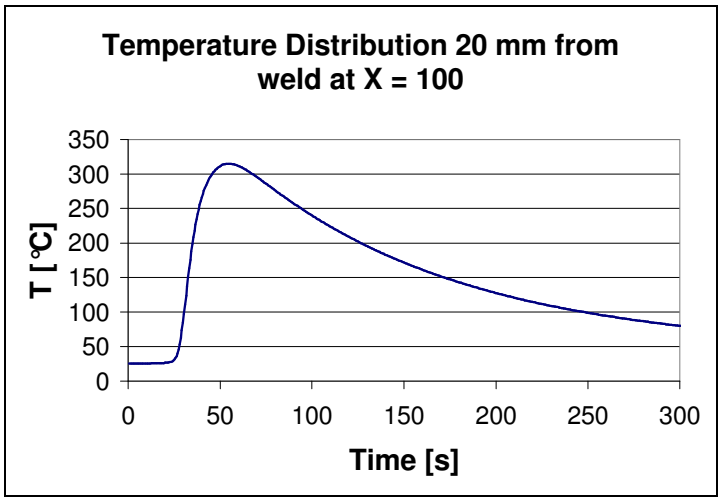

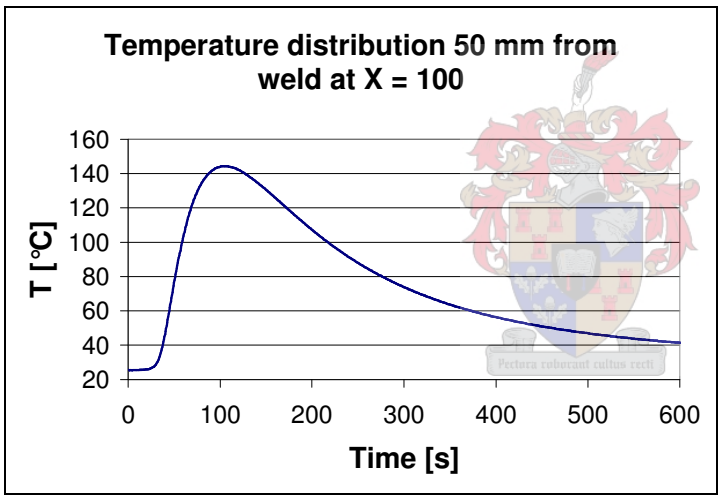

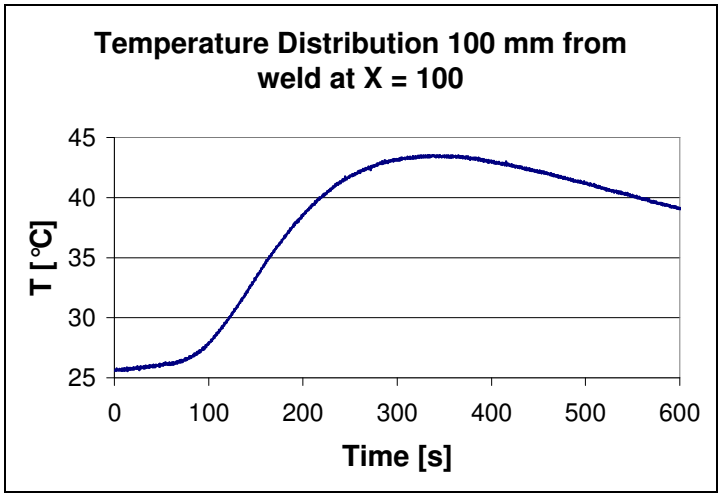

C.1.4 Temperature Distribution 20 mm From Weld